Investigation of Local Field Effect on the Spontaneous Emission Lifetimes of Rare-earths Doped in a Binary Glass Matrix of $PbO-B_2O_3$

A Thesis submitted for the degree of

DOCTOR OF PHILOSOPHY

by

G. Manoj Kumar

School of Physics

University of Hyderabad

Hyderabad - 500 046

India

February 2005

To my Parents

DECLARATION

I hereby declare that the matter embodied in this thesis entitled "Investigation of Local Field Effect on the Spontaneous Emission Lifetimes of Rare-earths Doped in a Binary Glass Matrix of $PbO-B_2O_3$" is the result of investigations carried out by me in the School of Physics, University of Hyderabad, Hyderabad, India, under the direct supervision of Prof. D. Narayana Rao.

Place: Hyderabad

Date: **(G. Manoj Kumar)**

Acknowledgements

I dedicate this thesis to my parents, without whose constant moral support and encouragement, this day would not have been possible. At the outset, I would like to thank all those who have directly or indirectly helped me at various stages of my stay at the university.

I am very greatful to my research guide who has given me an opportunity to work in his group. It is here I have learned my precious lessons on – how to and most importantly how not do an experiment! I am indebted to him for introducing me to the subject of local field.

I wish to thank Prof. G. S. Agarwal for his constant encouragement and suggestions.

I wish to thank Prof. S.P. Tewari, Prof. S. Dutta Gupta and Prof. Sunandana for their constant support and inspiring discussions. Special thanks are due to Dr. Suneel Singh for many discussions I had with him to clarify the fundamentals of optics.

I thank the Dean, School of Physics, for making available all the facilities required for the experiments. I also thank all the non-teaching staff for their co-operation.

I would like to thank Dr. Ravikanth for teaching me how to prepare glasses.

I would like to thank Dr. Vittal, Osmania University for extending his lab facility. My sincere thanks to Mr. Koteswara Rao for his unconditional help.

I thank all my senior lab-mates Drs – Venu, Prem, Ramana, Palash, Ashoka, Prakash, Sonika, Subbalakshmi, Raghu and Sastri. Thanks are due to my senior colleagues Azher, Hari, Loganathan, Nagesh, Phani, Subhajit, and Sudhakar for their support throughout. I would like to thank my labmates/friends Srinivas, Rajani, Joseph, Harsha, Shivakiran, Chaitanya, Venkatram, Santhosh, Philip, Sharath, Prakash, Shatabdi and Abhijit for their constant support and making my stay a memorable one. I also wish to thank my classmates Charan, Chari, Ranjani and Ravi and my juniors Rajneesh, Chaitnya, Rizwan, Sudershan, Santosh and Chandra Shekar.

My special thanks to my teacher Ravi Sharma sir who has been the inspiration behind my interest to learn Physics.

*****

Table of Contents

Chapter 1

Introduction and Motivation 1-11

1.1 Introduction 1
1.2 Modification of lifetimes 2
1.3 Local fields in transparent dielectric 3
1.4 Local fields in absorbing dielectric 4
1.5 Motivation for the thesis work 5
1.6 Choice of the materials 6
1.7 Organization of the thesis 7
1.8 References 9

Chapter 2

Spectroscopy of Rare-Earths in Glasses 12-26

2.1 Rare-earths 12
2.2 Glass 13
2.3 Energy levels in lanthanides 15
2.4 Judd - Ofelt theory 18
2.5 Linewidth and the lifetime 20
2.6 Nonradiative relaxation 22
2.7 Applications of rare-earths 23
2.8 References 24

Chapter 3

Sample Preparation and Experimental Techniques 27-54

Section I:

3.1 Lead Borate glass 27
3.2 Glass preparation 28
3.3 Characterization of sample 30
3.3.1 X -ray Diffraction 32
3.3.2 Differential Scanning Calerometry 32
3.3.3 FTIR 33
3.3.4 Refractive index 34
3.3.5 Absorption 35
3.3.6 Fluorescence 36

Section II:

3.4 Spectral Interferometry 41
3.5 Experimental set- up 41
3.6 Reflection spectrum 47
3.7 A Novel algorithm 50
3.8 References 52

Chapter 4
Lifetimes in Transparent Dielectric 55-75
4.1 Introduction 55
4.1.1 Virtual cavity 56
4.1.2 Real cavity 57
4.2 Lifetimes and local field 59
4.3 Examples of local field effect 61
4.4 Lifetimes in europium 62
4.5 Lifetimes in terbium 68
4.6 Conclusion 73
4.7 References 74

Chapter 5
Lifetimes in Absorbing Dielectric 76-101
5.1 Energy transfer in rare-earths 76
5.2 Eu^{3+}- Nd^{3+} system 84
5.3 Concentration quenching in Sm^{3+} 93
5.4 Conclusion 99
5.5 References 99

Chapter 6
Conclusions and Future Scope 102

List of publications 106

Chapter 1
Introduction and Motivation

1.1 Introduction

The ability to control the spectral properties of atoms and ions is of vital importance in the fabrication of the photonics based devices. This enables one to fabricate the devices with accurate control of the performance characteristics. Rare-earths in general and rare-earth doped glasses in particular have been at the forefront of the telecommunications revolution. The components of the modern telecommunication based on the optical fibers include lasers, amplifiers, infrared to visible converters and detectors. The spectral properties, fluorescence widths and the lifetimes, play a crucial role in the choice of materials for the fabrication of these devices. Apart from the presence of the large number of energy levels, the long lifetimes of these levels make rare-earths an attractive choice as the lasing ions. The fabrication of lasers and amplifiers suitable for the high-density transmission of information needs large fluorescence spectral widths to increase the number of channels. Therefore, an understanding of the various physical processes that influence the spectral properties is of great importance.

Spontaneous emission has played a very important role in establishing the concepts of the modern quantum theory. Einstein demonstrated that an excited atom must undergo spontaneous emission if the radiation and the matter are to achieve thermal equilibrium [1]. Spontaneous emission is often regarded as being an unavoidable consequence of the coupling between the matter and space and is thought to be as induced by the vacuum fluctuations. In the framework of the quantum optics, where both the atom and the radiation field are quantized, spontaneous emission is viewed as the interaction between the excited atom with the ground state of the field. The spontaneous emission rate of atom in free space is given as

$$A_0 = \frac{\mu^2 \omega^3}{3\pi\eta\varepsilon_0 c^3} \qquad (1)$$

where μ is the dipole moment, ω is the transition frequency and ε_o is the free space permittivity.

1.2 Modification of lifetimes

The picture of spontaneous emission is so fundamental that it is often believed to be to an inherent property of the atom that cannot be altered. However, changing its environment can modify spontaneous emission rate of an atom. This was first noted by Purcell [2]. According to Fermi's golden rule, the spontaneous emission rate depends on the electronic wavefunctions of the states involved and also on the optical density of the states and the electromagnetic field strength at the position of the atom. The changes to the rate can be achieved either by changing the density of the states or the strength of the field at the position of the atom. Experimentally, this can be achieved by bringing the atom near a suitable surface, putting it in a cavity or embedding it in a dielectric host. The earliest experiments on the modification of the spontaneous emission rates were performed by bringing the atom close to a metallic surface. This was the system used by Drexhage [3,4] in the first experimental verification of the modification of the spontaneous emission rates. They examined the lifetimes of Eu^{3+} ion in front of a metallic surface as a function of the distance between the atom and the metallic surface. Here, the atom is assumed to be a dipole oscillator which responds to its own field reflected from the mirror. The retardation of the reflected field plays an important role. If the reflected field returns to the dipole in phase, then the spontaneous emission rate is enhanced, and if it returns out of phase, the rates are suppressed. Apart from the metallic surface [5,6], other investigations carried are with semi conducting structures [7] or the dielectric surfaces [8] in similar type of experiments. In an alternate approach, modification of the spontaneous emission rates were achieved by placing the atom in a resonator – inhibited and enhanced spontaneous emission of Rydberg atoms in confocal resonators [9,10], inhibited spontaneous emission in a penning trap [11],

and suppression of blackbody radiation in Rydberg atoms [12]. The experiments on the modifications to the lifetimes were also performed at optical wavelengths – Yb atoms coupled to a degenarate confocal resonator [13], Barium placed near the center of a concentric confocal resonator [14], using flowing dye [15], quantum wells [16], Eu^{3+} in microcavity [17] and Er^{3+} in Si/SiO_2 microcavity [18].

1.3 Local Fields in Transparent dielectric

However, from an application point of view, the atoms placed in a bulk dielectric, like polymer thin films or the glass are of importance. The experiments in bulk dielectric include measurements on Eu^{3+} in thin films [19,20], Sulphorhodamine and Europium complexes in solutions [21,22], which have all shown inhibition or enhancement of the lifetimes.

The subject of the spontaneous emission in a dielectric has been studied both theoretically [23-27] and experimentally. The analysis of the lifetimes in a dielectric assumes a cavity around the emitter. Two different types of models for the cavity have been used in the literature [28,29]– one, the cavity is filled with the same dielectric as that of the surroundings and other where it is empty. The former is known as the virtual cavity and the latter the real cavity. The dimensions of the cavity are assumed to be larger than the size of the emitter and small compared to the wavelengths involved. The applied field polarizes the dielectric around the emitter and this polarization produces a field at the atom, known as the reaction field. The sum of the applied field and the reaction field is known as the local field. The local field is related to the applied field (E) through the refractive index of the dielectric [30, 31] as

$$E_{local} = l(n)E \qquad (2)$$

where E_{local} is the electric field in the dielectric and l is the correction introduced because of the local field. According the Fermi's golden rule, the spontaneous

emission probability is proportional to the square of the electric field at the position of the atom.

$$A = \frac{2\pi}{\eta}\left|P_{fi}\right|^2 \rho(\omega) \qquad (3)$$

where P_{fi} is the dipole operator at the position of the atom and $\rho(\omega)$ is the photon density of states. This implies that the lifetime in a dielectric is related to the free space lifetime through the refractive index. The nature of this dependence is different for the real and the virtual cavities. In general, the refractive index is a wavelength dependent quantity. Since emission occurs over a wide spectral region, the knowledge of the refractive index as a function of wavelength is essential. The lifetime of an emitter in a dielectric, taking into account the local field effect, can be given as [32,33]

$$\tau(n) = n^{-1} l^{-2} \tau(0) \qquad (4)$$

Judd and Ofelt [34,35] theory that estimates the various spectroscopic quantities of rare-earth ions using the absorption spectrum uses the virtual cavity model to take into account the local field. Recently, there have been studies involving the measurement of the lifetimes of Eu^{3+} in liquids [36] and gases [37], which showed that the real cavity model is more relevant. While the studies on the lifetimes of Eu^{3+} in nanocrystals surrounded by various liquids [38] showed the virtual cavity model to be appropriate for their system. However, there have been no systematic efforts in a solid matrix until now.

1.4 Local Fields in Absorbing dielectric

When the dielectric is absorbing, i.e. the dielectric resonance is near to the transition frequency of the emitting ion, it has been shown that the lifetime critically depend on the radius of the cavity [39,40]. The absorption of the dielectric leads to nonradiative decay of the excited states and thereby reducing the lifetimes [39-45]. In many real situations, the radiating ion would be surrounded by an absorbing medium. Such a situation may arise from self-

absorption, impurities, codopants etc. In general, an excited atom may decay radiatively or nonradiatively. The nonradiative decays reduce the fluorescence intensity as well as the lifetimes. In an absorbing dielectric, the lifetimes very sensitively depend on the radius of cavity, allowing one to investigate its magnitude. In such situations, refractive index is no longer real and one has to take into account the complex nature of the refractive index of the medium. In an absorbing dielectric, the lifetimes are a function of both the real and imaginary parts of the refractive index and the radius of the cavity. The radius dependent terms are responsible for the nonradiative decay. The coupling between the decaying atom and that of dielectric or the impurity responsible for the absorption, in general, may be mediated by various multipolar interactions. The simplest way to achieve the absorption is to co-dope an element such that its absorption overlaps the emission of the ion being studied. Large body of experimental literature exists on the codoped systems in terms of the Dexter-Foster theory [46,47] but none on the rates given in terms of the quantum optics.

1.5 Motivation for the thesis work

The motivation for this thesis work emanates from the question as to which cavity model is more appropriate for the description of the lifetimes in a dielectric. While the Lorentz virtual cavity model is used very frequently by researchers, some of the recent experimental works on the lifetimes in liquids [37] and gases [38] as a function of the refractive index showed that the real cavity model is more pertinent. This question has not been addressed very extensively – there have been no studies in this direction on the all important solid matrix. In a general situation, the atom would also undergo nonradiative relaxations and it has been shown that in such a situation, the radius of the cavity plays an important role in determining the lifetime. The knowledge of the radius around the emitter helps in estimating the lifetime with the knowledge of the refractive index and hence the lifetime can be tailored according to the need. This thesis attempts to study the fluorescence lifetimes of rare-earth doped in glasses to address the question of the nature of the cavity around the emitter and to

estimate the radius of the cavity. Hence the present study is of a great interest, both form a fundamental as well as technological application viewpoint. On the fundamental level, it helps in better understanding of the phenomenon involving interactions of the atoms with the radiation and on the application front, the photonics based devices can be designed with much better control on the performance.

1.6 Choice of the materials

The choice of the dielectric host and the emitters is very crucial for the study of this phenomenon. In order to address the question of the nature the cavity the contributions from the nonradiative rates should be minimal and ideally absent. Nonradiative transfers quench the fluorescence and the quantum yeild decreases. The quenching of fluorescence can be either because of the interaction of the radiating atom with the dielectric or because of the interaction among the radiating atoms themselves. Rare-earths are a class of materials, which are strongly fluorescing. Of all the rare-earths, Eu^{3+} and Tb^{3+} are an ideal choice for this experiment as these two are free from the concentration quenching effects - that is, the lifetimes do not depend on the concentration of emitters. Also, the lifetimes are in the order of a millisecond making it easier for the experimental observation. In order to observe the variation in the lifetimes, the variation of refractive index should be sufficiently large. The refractive index of the most of the glasses fall in the range of 1.4 to 2.5 and are an attractive choice. It is also important that while the refractive index is changed the environment around the atom should not alter much. This can be achieved by choosing a binary glass system. The refractive index of a binary glass can be varied by the relative compositional variation. Lead Borate system can give a good variation of the refractive index. For the study on the radius of the cavity, absorption can be introduced by introducing another ion. Rare-earths have a large number of levels in the energy spectrum and it is easier to find two ions with matching energy levels. Nd^{3+} has the closest matching level with Eu^{3+} and has been chosen for this study. This thesis attempts to address the question of the nature of the cavity and

the determination of the magnitude of the radius of the cavity by studying the lifetimes of rare-earths doped in Lead-Borate glass.

1.7 Organization of the thesis

Chapter 2 gives a brief description of the rare-earths and discusses about the various interactions that give rise to its energy level structure. It also describes the selection rules for the transitions in rare-earths. The procedure used for the calculation of the various spectroscopic properties using the Judd-Ofelt theory is given. Some examples of the applications of the rare-earth and rare-earth doped glasses are also given.

Chapter 3 is divided into two sections. The first Section deals with the preparation of the glasses used for the work in this thesis. The glass is characterized for its amorphous nature using the X-Ray Diffraction technique. Various other techniques used for the characterization of the glass, such as the refractive index, infrared spectra and Differential Scanning Calorimetry is also described. The techniques used for the characterization of the doped rare-earth-absorption and fluorescence is discussed. Details of the experimental setup for the measurement of the lifetime are discussed. The second section shows our attempts to measure the refractive index dispersion using white light Michelson Interferometer and the reflection techniques. A novel algorithm is also discussed for the measurement of the refractive index dispersion.

Chapter 4 addresses the question of the nature of the cavity. The lifetimes of Eu^{3+} and Tb^{3+} are studied as a function of the (real) refractive index. The change in the refractive index is achieved by varying the relative composition of the PbO and B_2O_3. Both in Eu^{3+} and Tb^{3+}, because of the large energy gap between the fluorescing level and the highest ground states, the probability of nonradiative transfers is negligible. The fluorescence intensity measurements show a linear increase with the concentration of the dopant showing the absence of the concentration quenching. The lifetimes do not alter with the concentration

of the dopant. The measured lifetimes are purely radiative and change in the lifetimes with refractive index is a consequence of the local field. The lifetimes as a function of the real refractive index are fitted using the equations for two different local filed models - the real and virtual. The variation of the lifetimes follows the real cavity model [48].

Chapter 5 extends the results of the chapter 4 by introducing absorption into the medium. Presence of the absorption leads to nonradiative decay of the excited state and lifetimes decrease as a result. Two different systems are chosen for this study. In the first system, the effect of Nd^{3+} on the lifetimes of Eu^{3+} is studied. At a constant concentration of Eu^{3+}, the concentration of Nd^{3+} is varied. The fluorescence intensity and the lifetimes of Eu^{3+} decrease with the increase of the Nd^{3+} as a result of the resonance energy transfer from Eu^{3+} to Nd^{3+} [49]. In the second system, the effect of cross relaxation on the lifetimes of Sm^{3+} is studied. Here, the concentration of the Sm^{3+} ions leads the quenching of the fluorescence known as the concentration quenching. The lifetime of Sm^{3+} decreases with the increase of its concentration. The quantum yields are calculated based on the measured lifetimes and the lifetimes calculated based on the Judd-Ofelt theory. The results are analyzed using the theoretical equation [40] that contains both the real and imaginary parts of the refractive index and the radius of the cavity. The data is fitted to obtain the magnitude of the radius of the cavity. The parameter related to the radius has been found to be of the order of 1-1.5 nm.

Chapter 6 concludes the results of the thesis. This chapter also presents a brief description of the future perspectives.

1.8 References

1. A. Einstein, Z. Phys. **18**, 121 (1917).
2. E. M. Purcell, Phys. Rev. **69**, 681 (1946).
3. K. H. Drexhage, J. Lumin. **1-2**, 693 (1970).
4. H. Drexhage, in *Progress in Optics*, edited by E. Wolf (North - Hollond, Amsterdam, 1974), **12**, p. 165.
5. R. M. Amos and W. L. Barnes, Phys. Rev. B **55**, 7249 (1997).
6. P.T. Worthing, R. M. Amos and W. L. Barnes, Phys. Rev. A **59**, 865 (1999).
7. E. Yablonovitch, T. J. Gmitter and R. Bhatt, Phys. Rev. Lett. **61**, 2546 (1988).
8. E. Snoeks, A. Lagendijk and A. Polman, Phys. Rev. Lett. **74**, 2459 (1995).
9. D. Kleppner, Phys. Rev. Lett. **47**, 233 (1981).
10. R. G. Hulet, E. S. Hilfer and D. Kleppner, Phys. Rev. Lett. **55**, 2137 (1985).
11. G. Garbielse and H. Dehmelt, Phys. Rev. Lett. **55**, 67 (1985).
12. A. G. Vaidyanathan, W. P. Spencer and D. Kleppner, Phys. Rev. Lett. **47**, 1592 (1981).
13. D. J. Heinzen, J. J. Childs, J. E. Thomas, and M. S. Feld, Phys. Rev. Lett. **58**, 1320 (1987).
14. D. J. Heinzen and M. S. Feld, Phys. Rev. Lett. **59,** 2623 (1987).
15. F. De. Martini, G. Innocenti, G. R. Jacobovitz, and P. Mataloni, Phys. Rev. Lett. **59**, 2955 (1987).
16. Y. Yamamoto, S. Machida, Y. Horikoshi K. Igeta and G. Bjork, Opt. Commun. **80**, 337 (1991).
17. F. De. Martini, M. Marrocco, P. Mataloni, L. Crescentini, and R. Loudon, Phys. Rev.A **43**, 2480 (1991).
18. A. M. Vredenberg, N. E. J. Hunt, E. F. Schubert, D. C. Jacobson, J. M. Poate and G. J. Zydijk, Phys. Rev. Lett. **71,** 517 (1993).
19. G. L. J. A Rikken, Phys. Rev. A **51**, 4906 (1995).
20. G. L. J. A Rikken, Physica B **204**, 353 (1995).

21. P. Lavallard, M. Rosenbauer and T. Gacoin, Phys. Rev. A **54**, 5450 (1996).
22. F. J. P. Schuurmans and Ad Lagendijk, J. Chem. Phys. **113**, 3310 (2000).
23. G. S. Agarwal, Phys. Rev. A **12** 1475 (1975).
24. G. Nienhuis and C. Th. J. Alkemade, Physica, **81C**, 181 (1976).
25. J. Knoester and S. Mukamel, Phys. Rev. A **40**,7065 (1989).
26. V. Malyshev and E. C. Jarque, J. Opt. Soc. Am. B **14**, 1167 (1997).
27. G. S. Agarwal, Opt. Exp. **1**, 44 (1997).
28. L. Onsager, J. Am. Chem. Soc. **58**,1486 (1936).
29. C. J. F. Bottcher, *Theory of Electric Polarisation* (Elsevier, Amsterdam, 1973).
30. R. J. Glauber and M. Lewenstein, Phys. Rev. A **43,** 467 (1991).
31. P.W. Milonni, J. Mod. Opt. **42**, 1991 (1995).
32. M. E. Crenshaw and C. M. Bowden, Phys. Rev. Lett. **85**, 1851 (2000).
33. O. Keller, *Progress in Optics*, (North-Holland, Amsterdam, 1997) Vol. XXXVII, p.257.
34. B. R. Judd, Phys. Rev. **127**, 750 (1962).
35. G. S. Ofelt, J. Chem. Phys. **37**, 511 (1962).
36. G. L. J. A. Rikken and Y. A. R. R. Kessener, Phys. Rev. Lett. **74,** 880 (1995).
37. F. J. P. Schuurmans, D. T. N. de Lang, G.H. Wegdam, R. Sprik, and Ad Lagendijk, Phys. Rev. Lett. **80,** 5077 (1998).
38. R. S. Meltzer, S. P. Feofilov, B. Tissue and H. B. Yuan, Phys. Rev. B **60**, 14012 (1999).
39. S. Scheel, L. Knoll and D. G. Welsh, Phys. Rev. A **60**, 1590 (1999).
40. S. Scheel, L. Knoll and D. G. Welsh, Phys. Rev. A **60**, 4094 (1999).
41. S. M. Barnett, B. Hunter and R. Loudon, Phys. Rev. Lett. **68**, 3698 (1992).
42. S. Tiong and P. Kumar, J. Opt. Soc. Am. B **10**, 1620 (1993).
43. G. Jezeliunas and D. L. Andrews, Phys. Rev. B **49**, 8751 (1994).
44. S. M. Barnett, B. Hunter R. Loudon and R. Matloob, J. Phys. B **29**, 3763 (1996).

45. G. Jezeliunas, Phys. Rev. A **53**, 3543 (1996).
46. D. L. Dexter, Luminescence of Crystals, Molecules and Solutions ed. By F. Williams (Plenum press, New York 1973).
47. Th. Foster, Ann. Phys. **2**, 55 (1948).
48. G. Manoj Kumar, D. Narayana Rao, and G. S. Agarwal, Phys. Rev. Lett. **91,** 203903 (2003).
49. G. Manoj Kumar, D. Narayana Rao, and G. S. Agarwal, To appear in Opt. Lett.

Chapter 2

Spectroscopy of Rare-earths in Glasses

This chapter discusses briefly about rare-earths and outlines the mechanisms responsible for their energy spectrum. It also describes the selection rules for the transitions in rare-earths. The equations used for the calculation of spectroscopic properties of the f - f transitions in rare-earths using Judd-Oflet theory are described.

2.1 Rare-earths

The elements in the periodic table with the atomic number from 57 to 71 are known as the lanthanides. They belong to the broader class of elements known as the rare-earths, which also includes the actinides. The electronic configuration of the neutral lanthanides possess the common feature of a Xe configuration with three outer electrons $5d6s^2$ and n electrons in the 4f shell, with $n \leq 14$. Lanthanides are chiefly trivalent and when ionized, the outer electrons $5d6s^2$ are removed and the triply ionized elements have the configuration [Xe] $4f^n$. Though other valance states are also known but they are much less stable. The closed 5s and 5p shells effectively shield the 4f shell. The ligand field of the glass has only very weak influence on the electronic cloud of the lanthanide ion, which makes their spectroscopic properties very similar to that of their corresponding element. As one progresses along this series, the average radius of the 4f shell slowly decreases. This phenomenon is known as lanthanide contraction. The observed absorption and fluorescence is because of the intraconfigurational f-f transitions. The excited state lifetimes of rare-earths in glasses can be as long as 10ms and can have high fluorescence efficiencies. These two properties make these ions a good choice for the present studies.

2. 2 Glass

Glass belongs to the class of amorphous materials. This is a state of matter that possesses most of the macroscopic and thermodynamic properties of the solid state, while displaying the structural disorder and isotropic behavior of a liquid. It is also referred to as super cooled liquid. It lacks the periodic arrange-

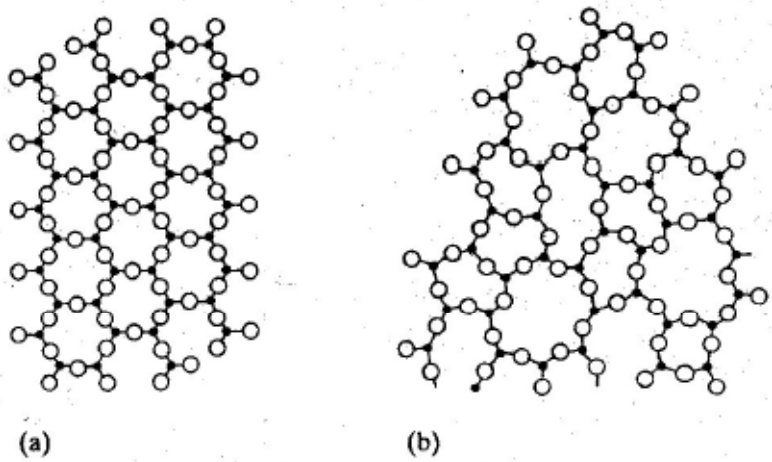

Figure 2.1 *(a) Schematic two-dimensional representation of the structure of hypothetical crystalline compound* A_2O_3 *and (b) the glassy form.*

-ment of constituent atoms. In a crystal, the atoms are arranged in a periodic pattern that repeats upto infinity. Figure 2.1 is a schematic representation of the atoms in a compound of the type A_2O_3 in a crystal and glass respectively. According to the International Union of Crystallography, a crystal is a solid that gives a discrete [1] X-ray diffraction diagram. The discrete pattern is a result of the long range ordering of the atoms. The glass is considerably less ordered and the X-ray diffraction pattern is not discrete and shows a broad hump as shown in figure 2.2 (for a common glass slide). This broad hump is a result of the short range order. For a truly amorphous material i.e. where there is no amount of short range order present, the X-ray diffraction should not have this hump and it would be a straight line even at the lower angles of incidence.

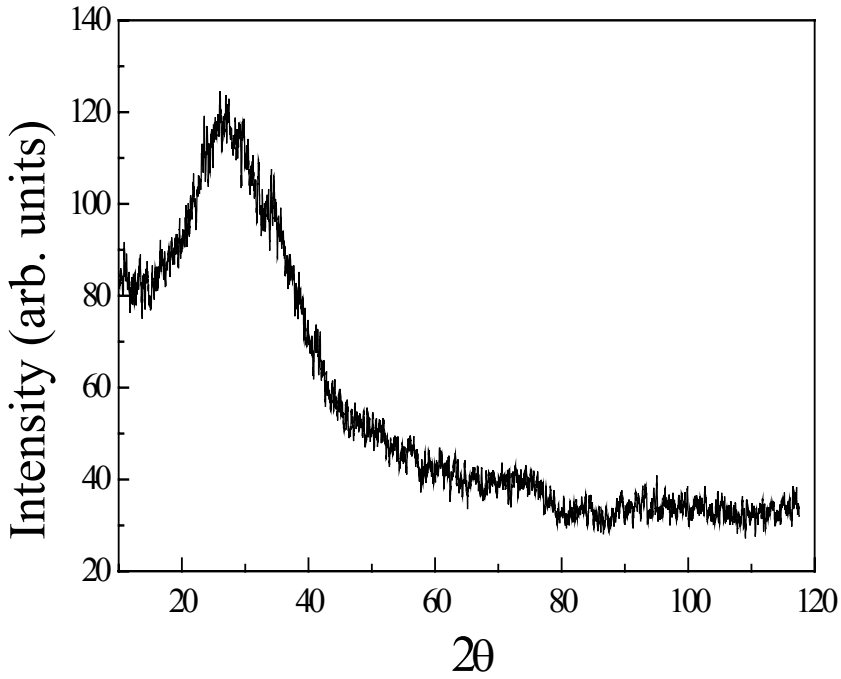

Figure 2.2 *The XRD pattern of an ordinary glass plate.*

Many compounds, such us B_2O_3, SiO_2, and P_2O_5, readily form glasses by themselves and are called glass-formers or network formers [2,3]. There are some oxides, which are called as network modifiers, cannot form a glass by themselves but can form a glass as a mixture with network formers to certain content. Oxides of alkali metals or alkali-earth metals are typical network modifiers. When network modifiers are added to the glass they can modify the network, they break up the continuous network introducing dangling or nonbridging oxygens. There is another interesting class of oxides, known as intermediate oxides, such as Al_2O_3 and TiO_2, which have characteristic that fall between those of the network formers and network modifiers. They do not by themselves readily form a glass, but require the presence of small amount one or more additional compounds to form a glass. B_2O_3 is a well-known glass former and PbO can act both as glass former and network modifier.

2.3 Energy levels in Lanthanides

The energy levels of the lanthanides arise as a result of the interaction between the 4f electrons. The Hamiltonian that determines the energy levels can be written as [4,5]

$$H = H_{coloumb} + H_{es} + H_{so}$$

$$= -\frac{\eta^2}{2m}\sum_{i=1}^{n}\nabla_i^2 - \sum_{i=1}^{n}\frac{Z^* e^2}{r_i} + \sum_{i<j}^{n}\frac{e^2}{r_{ij}} + \sum_{i=1}^{n}\zeta(r_i)s_i.l_i \qquad (1)$$

where n is the number of f electrons, r_i is the distance of the ith electron from the nucleus, r_{ij} is the distance between the two electrons i and j, Z^* is the screened charge of the nucleus, and $\zeta(r_i)$ is the term for the spin orbit coupling.

The terms in the $H_{coloumb}$ represent the kinetic energy of the electrons and their coulomb interaction with the nucleus. Due to the spherical symmetry, the degeneracy within the configuration of 4f electrons is not removed because of this interaction. H_{es} represents the mutual coloumb interaction among the electrons. H_{so} represents the spin orbit coupling. These two interactions are responsible for the vivid energy level structure of the lanthanides. If the Spin – orbit term is weaker than the electrostatic term, it acts as a small perturbation on the energy levels obtained by the diagnolisation of H_{es}. Here the orbital angular momentum of the all the electrons are coupled to give $L = \sum l_i$. And the spin angular momentum as $S = \sum s_i$. Then the total angular momentum is coupled as $J=L+S$. And if the Spin-orbit coupling is stronger than the electrostatic interaction the j-j coupling scheme is used. In j-j coupling, orbital angular momentum and the spin angular momentum of the individual electrons is added to give the total angular momentum as $j_i = \sum(l_i + s_i)$. The total angular momentum is then taken as $J = \sum j_i$. For lanthanides both the interactions are of the same magnitude. The L-S coupling scheme is often used, but the best way to describe the energy levels is the intermediate coupling scheme. Here the Hamiltonian $H_{es}+H_{so}$ is calculated on a basis formed by a set of Russel-Sanders

eigenfunctions [6,7]. Spectroscopically lanthanides can be divided into two categories (a) the elements Lanthanum, Yttrium, Scandium and lutetium has closed shells and their first excited state occurs in the far ultraviolet. (b) The other elements from praseodymium to ytterbium, containing 2 to 13 electrons have their first excited state in the infrared. Generally, the energy levels of the lanthanides are given in Dieke's diagram, which is shown in Figure 2.3. The spectroscopic notation used to label the energy levels is $^{2s+1}L_J$.

When these elements are introduced into a glass or crystal host, it experiences an electrostatic filed known as the crystal field, which is produced by the charge distribution of the host. This field further lifts the degeneracy and we get a maximum of (2J+1) stark levels. The magnitude of the stark splitting is determined by the strength of the crystal field and the number by the symmetry of the environment. The splitting of the levels because of the spin-orbit coupling is of the order of 1000 cm^{-1} whereas for stark levels it is of the order of 100 cm^{-1}. For example, in Eu^{3+} the unperturbed levels are split as ^5D, ^7F and so on as a result of the electrostatic (H_{es}) term. The degeneracy is further lifted because of the spin-orbit coupling and ^5D is split into ^5D_k, k =0,1,2,3,4 and ^7F is further split as ^7F_k, k =0,12,3,4,5,6. The crystal field can further split each of these k levels into 2J+1 levels. The transition intensities and the selection rules governering the transitions in lanthanides are obtained from the Judd-Ofelt theory. The procedure for the calculation of the various spectroscopic properties using this theory is described in the following section.

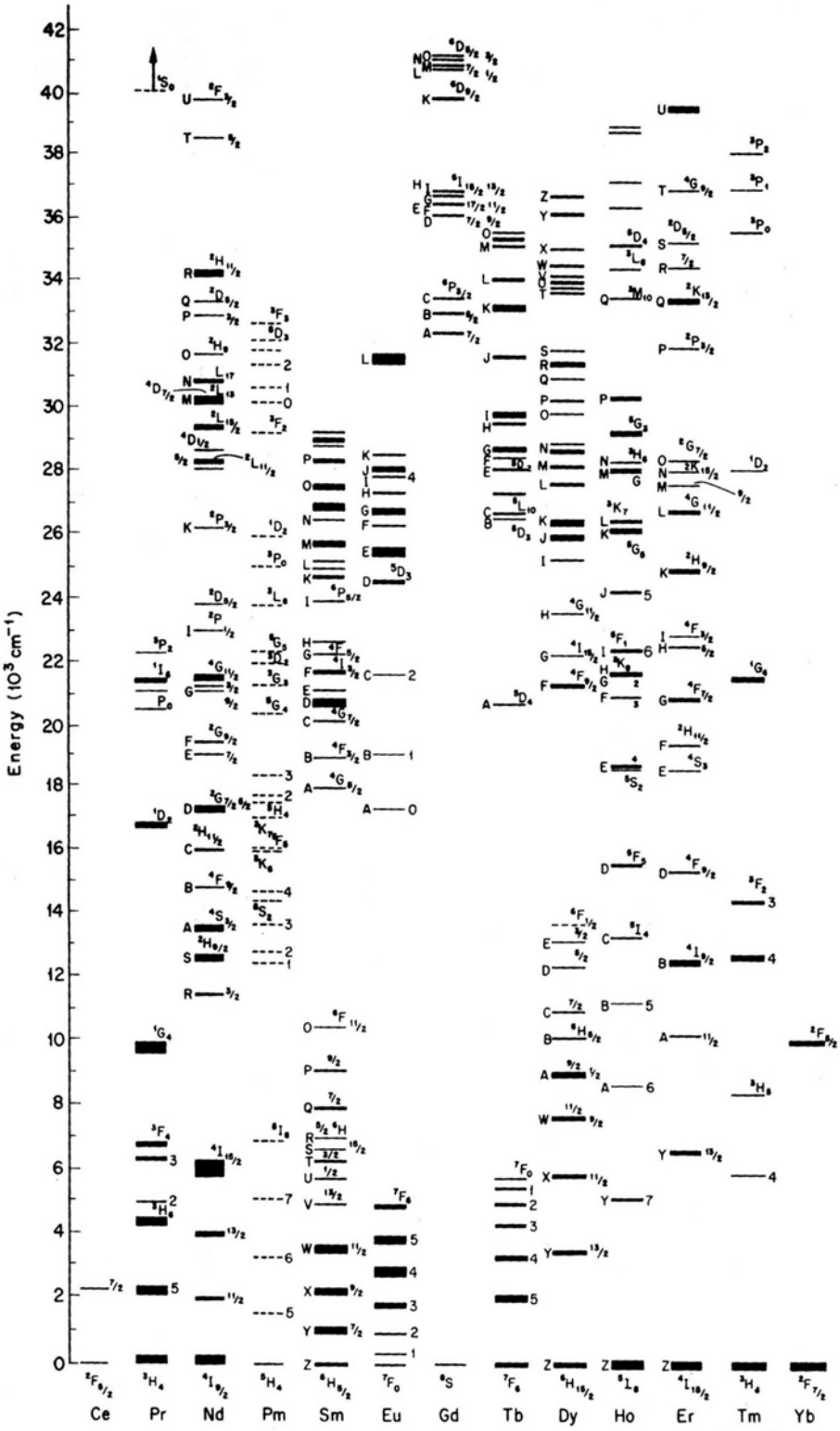

Figure. 2.3 *Energy level diagram of the lanthanide [8]*

2.4 Judd – Ofelt Theory

The oscillator strengths of the lanthanides generally are of the order of 10^{-5}-10^{-7} as compared to that of 0.65 in the case of Sodium D lines. This is because the majority of the transitions are induced electric dipole transitions. An electric dipole transition is the consequence of the interaction of the ion with the electric field vector through an electric dipole. The creation of an electric dipole supposes a linear movement of charge. Such a transition has an odd parity. The electric dipole operator has therefore odd transformation properties under inversion with respect to an inversion center. Intraconfigurational electric dipole transitions are forbidden by the laporte selection rule. Non - centrosymmertrical interactions allow the mixing of the electronic states of opposite parity i.e. the observed transitions here arise due to the admixture into the 4f configuration of opposite parity. Judd [9] and Ofelt [10] worked out the theoretical background for the calculation of the intensities of the forced electric dipole transitions for these elements. The absorption spectrum is used to calculate Judd-Ofelt parameters. Various radiative properties can be calculated using the Judd-Ofelt parameters. The procedure involves the calculation of the Judd-Ofelt parameters Ω_t and then calculate the various spectroscopic properties using these parameters. These are obtained by solving the equation for the oscillator strength, P

$$P = \left(\frac{8\pi^2 mc}{3h\lambda(2J+1)} \right) \frac{(n^2+2)^2}{9n} \sum_{t=2,4,6} \Omega_t \left\langle \Psi J \middle| U^t \middle| \Psi' J' \right\rangle^2 \qquad (2)$$

where Ω_t are the Judd-Ofelt parameters, J and J' are the total angular momentum of the initial and final states. $U^{(t)}$ are the doubly reduced matrix elements of the unit tensor operator for the corresponding transition. The reduced matrix elements of the unit tensor operators $U^{(t)}$ evaluated in the intermediated coupling scheme are almost insensitive to the ion environment. Hence values obtained for one host may be used for the other hosts. We have used the $U^{(t)}$ values given by Carnall *et al* [11]. Such an equation can be written for each of the transitions in the absorption spectra. The experimental oscillator strength of a transition from

ground state to a level centered at $\bar{\nu}$ is obtained by integrating the absorption centered about it,

$$P_{exp} = 4.32 \times 10^{-9} \int \varepsilon(\bar{\nu}) d\bar{\nu} \qquad (3)$$

The set of equations are solved by least squares procedure to obtain the Ω_t parameters. These parameters are used to calculate the theoretical oscillator strength by substituting back in the Eq. (2). The RMS is defined in terms of the observed and calculated strengths defined as

$$(P_{cal} - P_{obs})^2/(N-3) \qquad (4)$$

Here N is the number of transitions considered. The radiative transition probability between levels J and J' is calculated by

$$A(\Psi J, \Psi' J') = \left(\frac{64\pi^4 \nu^3}{3h(2J+1)}\right) n \left(\frac{n^2+2}{3}\right)^2 e^2 \sum_t \Omega_t \langle \Psi J | U^t | \Psi' J' \rangle^2 \qquad (5)$$

where the reduced matrix elements are now from the excited state to the lower levels. The total transition probability of the level J is

$$A_T(\Psi J) = \sum_{\Psi' J'} A(\Psi J, \Psi' J') \qquad (6)$$

where the sum runs over all the J' levels which have lower energy than that of J. The matrix elements have been taken from Carnall *et al* [12] work. The radiative lifetime is given as

$$\tau_R = \frac{1}{A_T} \qquad (7)$$

The branching ratio is defined as

$$\beta_R = \frac{A(\Psi J, \Psi' J')}{A_T(\Psi J)} \qquad (8)$$

The selection rules for these induced electric dipole transitions as derived from the Judd-Ofelt theory are [13]:

I. $\Delta L \leq 6$

$\Delta S = 0$

$\Delta J \leq 6$

II For an ion with even number of electrons:

$J = 0 \leftrightarrow J' = 0$ is forbidden

$J = 0 \leftrightarrow$ odd J' are weak

$J = 0 \leftrightarrow J' = 2, 4, 6$ are strong

For magnetic dipole transitions, free atom selection rules are still valid.

2. 5 Linewidth and the Lifetime

Homogeneous and inhomogeneous processes cause a broadening of the spectral line shapes of transitions [14]. The homogeneous broadening is an intrinsic property and arises from the finite lifetime of the initial state involved in the transition. The lifetime of a level is related to an uncertainty ΔE in its energy, by the Heisenberg uncertainty principle. The lifetime of an excited state is governed by the transition probabilities to all the lower energy levels. For the simple case of a two level system, the time evolution of the fluorescence signal is a single exponential decay.

$$I = I_0 \exp(-At) \qquad (9)$$

where the lifetime is defined as $\tau = A^{-1}$. When there are more than one lower levels, then the total transition probability is taken as the sum of the transition

probabilities to all the levels as in Eq. (6). When the nonradiative transitions are involved a separate term corresponding to that rate is added. The nonradiative transfers will be discussed in the next section. In an experiment, the population is taken to the excited state using a short pulse and lifetime is measured as the time at which the fluorescence intensity becomes 1/e of the initial intensity. In the presence of the nonradiative energy transfer the decay profile deviates from the single exponential nature. Lifetime broadening mechanisms cause a Lorentzian lineshape [15]. Among the relaxation mechanisms that can reduce the lifetime of a state, the radiative process is the less important, because most radiative decay times are much longer than the respective nonradiative decay times and the broadening results to be negligible with respect to the ones owed to other relaxation processes. The larger the number of processes, which depopulate the level, the shorter the lifetime, the broader the band transition. The principal sources of inhomogeneous broadening are the variations in the crystal field due to strains in crystals or due to configurational disorder in glass. The ions occupy sites whose environment is perturbed in different ways, and this gives rise to differences in the frequencies at which a given transition can occur. Hence the observed spectrum consists of a superposition of lines coming from ions at different sites. For an emission band of a rare-earth in a glass, the inhomogeneous broadening (full width at half maximum of about 100 cm^{-1}) is much larger than the homogeneous broadening at room temperature. Inhomogeneous broadened lines may have a Gaussian shape or the convolution of Gaussian and Lorentzian lineshapes, called Voigt profile. Another broadening mechanism can be considered to arise from the Stark splitting of the levels. The typical spectrum of a crystal is characterized by several narrow lines due to the transitions between the different Stark levels. In a glass these levels are inhomogeneously broadened, therefore, the transition lines overlap and appear to form one large transition and sometimes with a partly visible substructure.

2.6 Nonradiative relaxation

An excited atom can relax to the ground state radiatively or nonradiatively. In the radiative relaxation a photon is emitted while in the latter case the excited state goes to the ground state with the excitation of phonons. There can be nonradiative relaxation in an isolated ion as in fluorescence experiments, where the excited state decays nonradiatively to a lower excited state and from there decays radiatively to the ground state. The larger the energy gap between two levels, the greater is the probability of the radiative decay from the upper level, i.e. if the energy difference is small, the probability for the nonradiative decay increases. The lifetimes are affected by the nonradiative transfers and the total probability is written as

$$A = A_{rad} + A_{nr}$$

where A_{nr} is the nonradiative rate. Nonradiative decays also reduce the fluorescence intensity. An excited ion can also relax nonradiaively because of the presence of the other ions nearby, the second ion can either be of the different species or can be of the same species. The phonon cut off energy of a glass (the phonon of highest energy in the glass) also plays a crucial role in determining the extent of the nonradiative transfers. The probability of nonradiative transfer decreases with the more number of phonons being required to bridge the energy gap of the ion [16]. The following table lists the phonon cut off energies of some of the common glasses.

Table 5.1 *The highest phonon energies ($\eta\omega_{max}$) of some of the glasses.*

Glass	$\eta\omega_{max}$ (cm^{-1})
Tellurite	800
Germnate	900
Phospate	1300
Silicate	1400
Borate	1400

2.7 Applications of Rare-earths

Rare-earths play such an important in much of the modern optical technology based on photonics as the active constituent, it is not an over statement to say that this technology would not have been possible without them. The range of applications of the rare-earth doped materials is amazing. The best known application of the rare-earths is the Nd doped YAG and glass lasers [17,18]. This is a four level laser with $^4F_{3/2}$ as the upper lasing level and $^4I_{11/2}$ is the lower level. The lower level is 2000cm^{-1} above the ground state that makes it easier to achieve the population inversion. These lasers lase at 1.06 μm. The Nd : glass laser materials are primarily used as amplifiers for very large pulsed lasers. Lawrence Livermore National Laboratories NOVA laser and the recent National Ignition facility use the Nd: glass amplifier stages. The first fiber laser was also operated in Nd doped glass fiber [19]. Nd doped glasses are used by glassblowers for the protection of eyes. The present day communication primarily is at 1.53μm, hence this technology needs laser sources, amplifiers and detectors working at this wavelength. Er doped fiber amplifiers operate at this wavelength. Erbium-doped fiber amplifiers have enabled a one more step in the ever-expanding technology and continue to be the subject of many investigations [20-22]. Solid state lasers based on the phenomenon of up-conversion are promising for the violet/blue laser sources. Various rare-earths have been investigated for this purpose [23-27]. Rare-earths are the excellent candidates for the next generation of optical data storage and processing, allowing a dramatic increase in both storage density and processing speed. The phenomenon of hole burning has acquired a great importance because of the possible application to the data storage. Samarium and europium show a great promise and have been studied for this phenomenon [28-30]. Recently a quantum computer hardware model based on europium doped inorganic crystal has been proposed [31]. Europium also finds application as probes in the clinical diagnosis and drug screening [32,33]. Rare-earths are also used in the infrared quantum counters [34,35]. Laser frequency locking to rare-earth transitions has also shown tremendous possibilities for new laser sources that are ultra stable. Rare-earths ions also play a critical role in energy efficient luminescent materials such as phosphors for

fluorescent lamps, cathode ray tubes and plasma displays as both active emitters as well as sensitizing agents that increase efficiency. Terbium based materials are standard green lamp phosphors [36]. Divalent europium is the active center of many commercially available blue phosphors [37]. The trivalent europium is used for its red colour in the colour televisions. There is strong motivation to replace mercury containing fluorescent lamps with the more environmentally friendly alternatives and the rare-earths are a promising alternative. Perhaps, the list of applications of the rare-earths and the rare-earth doped crystals and glasses are infinite.

2.8 References

1. G. R. Desiraju, Nature, **423**, 485 (2003).
2. E. R. Elliott, *Physics of Amorphous materials* (Longman scientific technical) chapter 1.
3. A. G. Guy, *Introduction to material science* (Mc Graw-Hill, 1972), chapter5.
4. B.R. Judd, *Operator techniques in atomic spectroscopy* (McGraw – Hill Book Company Inc. 1963) Chap. 4.
5. W. M. Yen and P. M Selzer, *Laser spectroscopy of Solids* (Springer-Verlag, New York, 1981) Chapter1.
6. E. U. Condon and G. H. Shortley, *Theory of atomic spectra* (Cambridge University Press, 1977) Chapter XI.
7. H. Erying, J. Walter and G. E. Kimball, *Quantum Chemistry* (John Wiely and sons inc. New York, 1944).
8. K. N. R. Taylor and M. I. Darby, *Physics of Rare-earth solids*, (Champman & Hall, London).
9. B. R. Judd, Phys. Rev. **127**, 750 (1962).
10. G. S. Ofelt, J. Chem. Phys. **37**, 511 (1962).
11. W. T. Carnall, P.R. Fields and K. Rajnak, J. Chem. Phys. **49**, 4424 (1968).
12. W. T. Carnall, Argonne national Laboratory Report ANL-78-XX-95.

13. *Handbok on the Physics and Chemistry of rare-earths*, edited by K. A. Gschneidner and L. Eyring (Elsevier, North Holland, 1998).
14. L. Allen and J. H. Eberly, *Optical resonance and two level atoms* (John Wiely & sons, New York, 1975) chapter 1.
15. *Laser spectroscopy*, W. Demtroder (Springer-Verlag, 2003) chapter 3.
16. J. M. F. V. Dijk and M . F. H. Schuurmans, J. Chem. Phys. **78**, 5317 (1983).
17. W.F. Krupke, IEEE J. Quant. electronics, **10**, 450 (1974).
18. J. A. Caird, A. J. Ramponi and P. R. Staver, J. Opt. Soc. Am. B **8**, 1391 (1990).
19. W. T. Silfvast, *Laser Fundamentals* (Cambridge University Press, 1998). Chapter 14.
20. M. A. Mahdi, F. R. Adikan, P. Poopalan, S.Selvakenndy and H. Ahmad, Opt. Commun. **187**, 389 (2000).
21. S. Ohara, N. Sugimoto, K. Ochiai, H. Hayashi, Y. Fukasawa, T. Hirose, T.Nagashima and M. Keyes, Opt. Fiber Tech. **10**, 283 (2004).
22. C. Cheng, Opt. Laser Tech. **36**, 607 (2004).
23. L. E. E. de Araujo, A. S. L. Gomes, C. de. B. Araujo, Y.Messaddeq, A. Florez and A. Aegerter, Phys. Rev. B. **50**, 16219 (1994).
24. H. Higuchi, M. Takahashi, Y. Kawamoto, K. Kadono, T. Ohtsuki, N. Peyghambarian and N. Kitamura, J. Appl. Phys. **83**, 19 (1998).
25. G. S. Maciel, L. de S.Menezes, C.B. de Araujo and Y.Messaddeq, J. Appl. Phys. **85**, 6782 (1999).
26. H. T. Amorim, M. V. D. Vermelho, A. S. Gouveia, F. C. Cassanjes, S. L. J. Riberiro and Y. Messaddeq, J. Solid. Stat. Chem. **171**, 278 (2003).
27. C. H. Kam and S. Buddhudu, Solid. State Commun. **128**, 309 (2003).
28. M. Nogami, Y. Abe, K. Hirao and D. H. Cho, Appl. Phys. Lett**. 66**, 2952 (1995).
29. M. Nogami and Y. Abe Appl. Phys. Lett. **71**, 3465 (1997).
30. K. Fujita, K. Tanaka, K. Hirao and N.Soga, J. Opt. Soc. Am. B **15**, 2700 (1998).

31. N. Ohlsson, R. K. Mohan, and S. Kroll, Opt. Commun. **201**, 71 (2002).
32. P. R. Selvin, J. Jancarik, M. Li, and W. Hung, Inorg. Chem. **35**, 700 (1996).
33. J. Chen and P.R. Selvin, J. Photochem. PhotoBio. A **135**, 27 (2000).
34. M. R. Brown, W. A. Shand, Adv. Quant. Electron. ed. By D. W. Goodwin (Acedemic Press, New York, 1970).
35. W. Tian, R. S. Pandher and B. R. Reddy, J. Appl. Phys. **88**, 2191 (2000).
36. A. P. Magyar, A. J. Silversmith, K.S. Brewer and D. M. Boye, J. Lumin. **108**, 49 (2004).
37. M. V. Nazarov, D.Y. Jeon, J. H. Kang, E. J. Popovici, L.E. Muresan, M. V. Zamoyanskaya and B. S. Tsukerblat, Solid. State Commun. **131**, 307 (2004).

Chapter 3

Sample Preparation and Experimental Techniques

The first Section discusses about the preparation of the PbO-B_2O_3 glass being used for the studies in the thesis. Various experimental techniques used to characterize the glass such as X-ray diffraction, FTIR and differential scanning calorimetry are described. The techniques used for the characterization of the doped rare-earth, absorption and fluorescence are discussed. Details of the experimental setup for the measurement of the lifetime are discussed. The second section shows our attempts to measure the refractive index dispersion using white light Michelson Interferometer and the reflection techniques. A novel algorithm is also discussed for the measurement of the refractive index dispersion.

Section I:

3.1 Lead Borate Glass

The choice of the host material and the emitters is very critical in understanding the local field related issues. Glass preempts reorganization of the medium in the microenvironment of the metal ion. Therefore the bulk dielectric constant represents more satisfactorily the environment of the metal ion [1]. Glass is not only easy to prepare but also a reasonably good variation in the refractive indices can be achieved. A variety of glasses are available where the refractive index would be anywhere in the range of 1.4-2.5. One can therefore achieve a variation in the refractive index using a binary mix of two glass forming materials. Several glasses have been reported in the literature giving a good variation in the refractive index [2]. Borate is a well-known glass former and Lead can act as both former and modifier [3]. This binary glass system has been known to have a

very wide range of glass formation range of 20-80 mol% (of PbO) [4]. And it is also possible to make a 90 % [5,6] lead glass. Lead can also act as a glass former [7-9]. We have been able to make the glass system from 30 to 100 PbO. The 20% glass was very difficult to be formed. This large glass formation range can give a large variation of refractive index. PbO is a heavy material and B_2O_3 is a light material, and hence through relative variation of PbO and B_2O_3, a large variation in the refractive index can be achieved. Some of the recent studies indicate that lead-borate glass could be a good choice as a host material to achieve a flat gain for the dense wavelength division multiplexing applications [10]. In the next sections the method of preparation of the glass and the techniques used to characterize it and the rare-earths are described.

3.2 Glass Preparation

The glasses are prepared by the melt quench method. The stoichiometric quantities of the initial materials PbO, H_3BO_3 and rare-earth oxides are ground in an agate mortar under acetone for 20 minutes to ensure the formation of a homogenous mixture. The mixture taken in a silica crucible is subjected to three steps of heating, 1h at 200 ^{O}C, 2h at 500 ^{O}C and for 45 minutes at 800-1000 ^{O}C (depending on the composition), with high borate as well as high lead glasses needing the higher temperatures. The first two steps ensure a complete formation of B_2O_3 and also ensure that no trace of H_2O that is formed is left in the crucible. The third step of heating forms a clear melt. When a clear melt is formed it is quenched into a copper mould and pressed with another copper plate. The glass thus formed is subjected to annealing at 250 ^{O}C for 24 h. The glass at this stage is not suitable for the optical studies as the surfaces are not clear and parallel. To make it transparent the glass is polished. First it is ground either with emery paper or on a flat metallic surface with Alumina powder. In the second step, samples are polished on shemoy leather, which is mounted on a rotating motor. Cerium Oxide is used in this stage. The entire process of preparation of glass is summarized in Figure 3.1.

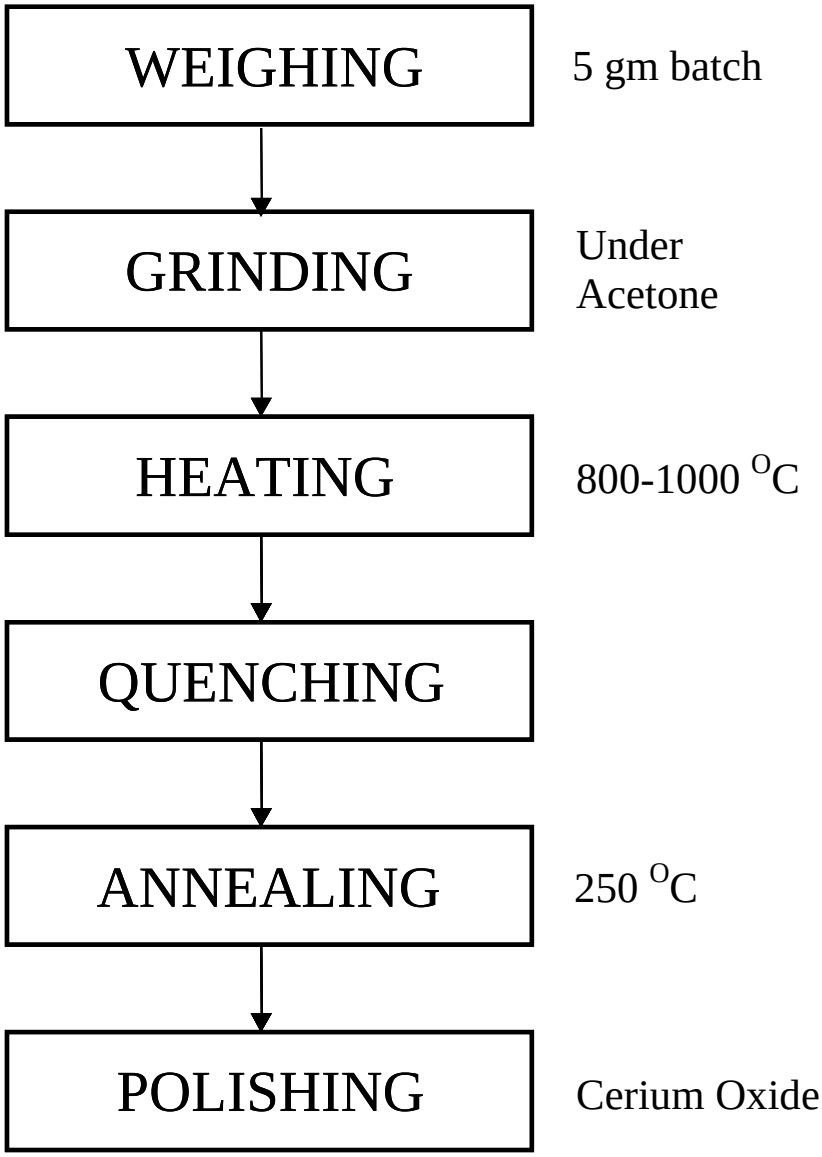

Figure 3.1 *The steps involved in the preparation of glass.*

The following glasses have been prepared –

1. (a) x PbO + (100-x) B_2O_3 : $1Ln^{3+}$, x=100,90,…30;
   (b) 60 PbO + 40 B_2O_3 : yLn^{3+}

   Ln= Eu and Tb

   y =0.1,0.5,1, 2.5(2) and 5

2. x PbO + (100-x) B_2O_3 : $1Eu^{3+}$+ y Nd^{3+} x=90, 80,…30 and
   y =0.05,0.1,0.25,0.5 and 1.
3. 60 PbO + 40 B_2O_3 : ySm^{3+}
   y =0.05, 0.1, 0.5, 0.75, 1, 1.5, 2, 3, 4, and 5

The samples in set 1 are investigated in chapter 4. This constitutes the transparent glass for the study of the nature of the cavity. In the set 1b, the concentration of the dopant is changed in order to examine its effect on the lifetimes. The sample sets 2 and 3 constitute the case where, apart from the dispersion, absorption is also present. These are used for the investigation to determine the magnitude of the radius of cavity. These studies are presented in chapter 5. In the sets 1 and 3, y is varied upto 5mol%. The 5-mol% Tb^{3+} is not transparent, but shows the characteristics of a glass.

3.3 Characterization of Sample

The measurement of the lifetimes and the refractive index of the glass are of the primary importance for the local field studies, but the complete information of the glass is essential. The complete characterization of the sample can be summarized as in the figure 3.2. The charterization of the glass includes the amorphous nature by x-ray diffraction, determination of glass transition temperature from differential scanning calorimetry and the determination of the phonon frequencies from the infrared spectrum and the refractive index, which is important for the present work. The absorption and fluorescence, including the lifetimes, are the measurements on the doped rare-earths.

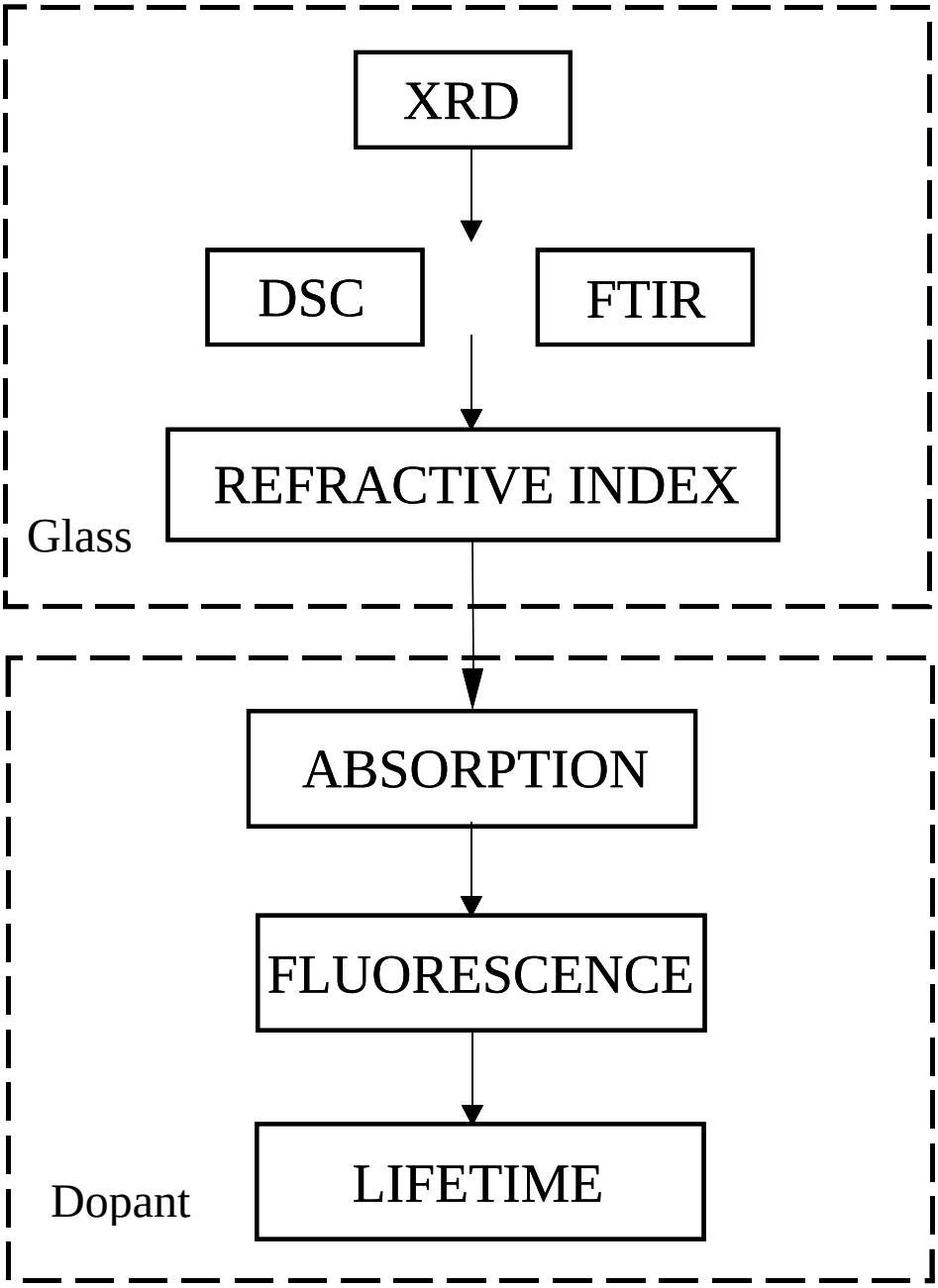

Figure 3.2 *Sample characterization*

3.3.1 X - ray Diffraction

The first thing to be ensued after making a glass is the amorphous nature of the sample. This is done by recording the X- ray diffraction (XRD). The XRD is recorded on Philips PW 1830 X-ray diffractometer. The XRD of glass is characterized by absence of any sharp peaks, which is an indication of the absence of any long-range order. The XRD for all the samples showed the characteristic spectrum as seen in Figure 3.3 for x=30.

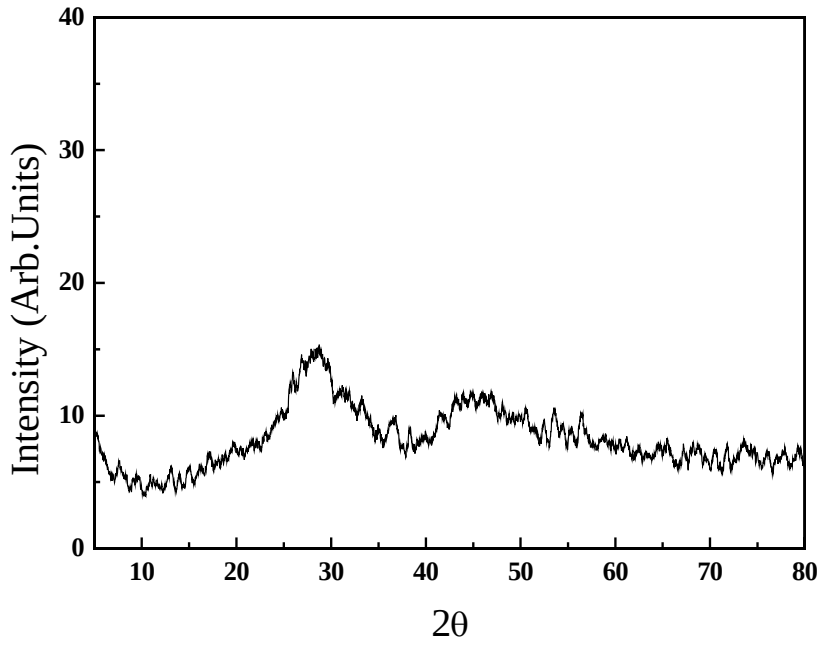

Figure 3.3 *The X ray diffraction of the 30Pbo+70B_2O_3 glass. The absence of sharp peaks shows the amorphous nature.*

3.3.2 Differential Scanning Calorimetry (DSC)

Glass is an amorphous solid, which exhibits a glass transition. Glass transition is a phenomenon where the material exhibits a more or less abrupt change in the derivative thermodynamic properties from crystal like to liquid-like values with the change in the temperature. The technique of DSC is used for the determination of the glass transition temperature (T_g). This technique involves heating the sample by gradually increasing the temperature at a constant rate and measuring the heat flow through the sample with respect to an empty reference.

The DSC was recorded on TA instruments DSC 2010 Differential Scanning Calorimeter. Figure 3.4 shows the DSC curve for one of the glass samples. The knowledge of the glass transition temperature helps in fixing the annealing temperature. Generally, the samples are annealed for a very short time at the glass transition temperature or for a very long time below the transition temperature. The process of annealing helps remove any strains that may be present in the sample. The glass transition temperatures are tabulated in table 1, which is given on page 38 of this chapter.

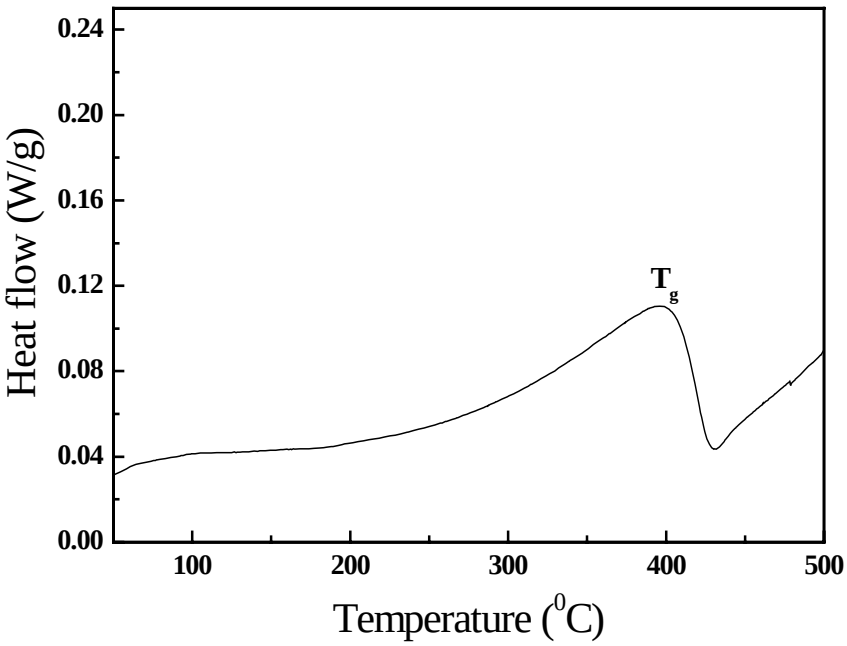

Figure 3.4 *The DSC curve of the 50 PbO+50B_2O_3 glass.*

3.3.3 FTIR

The vibrational modes of the glass can be identified by the Fourier transform infrared spectrum. The FTIR spectra are recorded using JASCO FT-IR 5300 spectrometer. For recording this spectrum, the sample is first ground into powder. Then it is mixed with KBr and a thin pellet is made which is used for the recording. As shown in figure 3.5, there are two strong absorption bands at 920 cm^{-1} and 1320 cm^{-1}. These are due to the B-O stretching modes. The weak

band around 700 cm^{-1} is due to the Pb-O bond [11]. The sharp band around 2400 cm^{-1} is not related to the sample. It is present even when the recording is done with KBr alone. The integrated area varies about 7% with the compositional variation of glass.

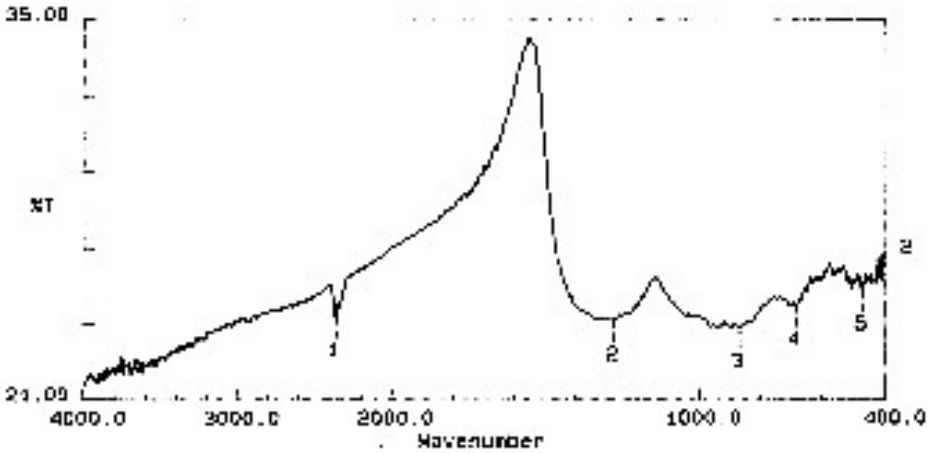

Figure 3. 5 *FTIR spectrum of 60PbO+40B_2O_3 sample.*

3.3.4 Refractive index

The refractive is measured using the Brewster's angle method with a He-Ne laser. The refractive index shows a linear relationship to the mol% as shown in the Figure 3.6. A linear fit yields the value for the refractive index for pure B_2O_3 glass as 1.49, which compares very well with that of the value reported [2]. The refractive index for x= 30 is 1.71 and for x=100 it is 2.2. This variation is what makes this system an ideal one for this experiment. A similar variation may also be obtained by taking different glasses for different refractive indices, but then there may complications arising out of change in the environment, whereas having the single system preempts this possibility. Section 3.4 gives the details of our efforts made in evaluating the refractive index dispersion. The lifetime measurements are made in the spectral region of 500 - 7 00 nm, and the refractive

index does not vary much in this region, the values measured using Brewster's angle method at 633 nm are used. We have developed the spectral interferometry technique to measure the exact value of the refractive index over wide spectral range for the analysis of the lifetime variation. Though the present thesis does not make use of the precision values, these techniques are developed with a view to improve the accuracy in our future experiments.

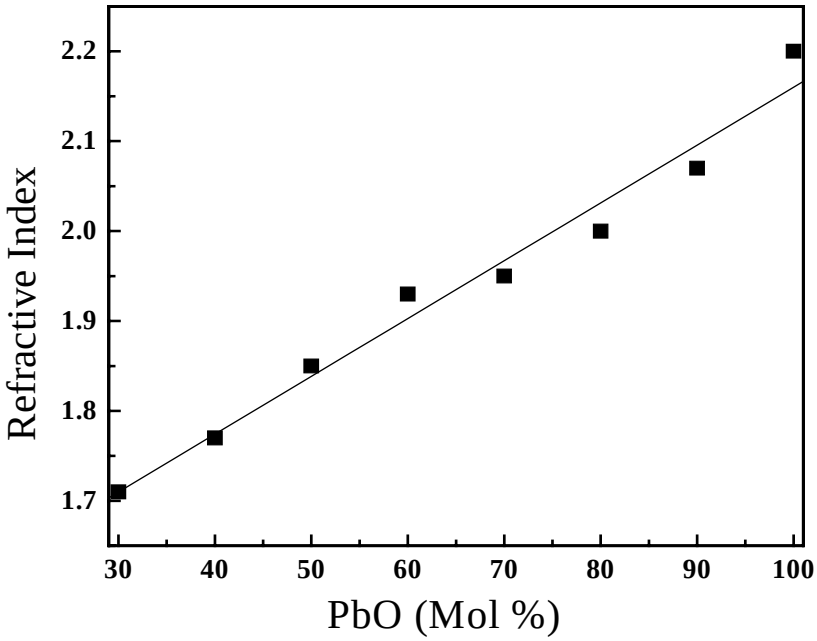

.

Figure 3.6 *Refractive index at 633 nm of PbO-B_2O_3 binary system plotted as a function of the mol% of PbO.*

3.3.5 Absorption

The absorption spectrum is recorded on a UV-VIS-NIR Shimadju 3010 spectrophotometer. The absorption spectra of rare-earths have bands from UV to IR regions. Sm^{3+} has strong absorption peaks in IR as compared to that of the visible region. Nd^{3+} has strong absorption peaks in Visible and near IR. While for Eu^{3+} and Tb^{3+} majority of the transitions occur between 350 to 500 nm. Some of the transitions in Eu^{3+} occurring near UV are forbidden within the framework of first order perturbation treatment of the Judd-Ofelt theory [12]. Hence they have very weak intensity. Particularly, in the lead-borate glass where the absorption

edge extends upto 425 nm it is very difficult to observe these transitions. The reduced matrix elements for most of the transitions for both Eu^{3+} and Tb^{3+} are in the order of 0.005 compared to the matrix elements for some of the strongest absorption peaks of rare-earths where they are of the order of 0.5. Figure 3.7 shows the absorption spectra of lead-borate glass. Column 3 in the table 3.1 gives the absorption edge of all the binary compositions of the lead-borate glass.

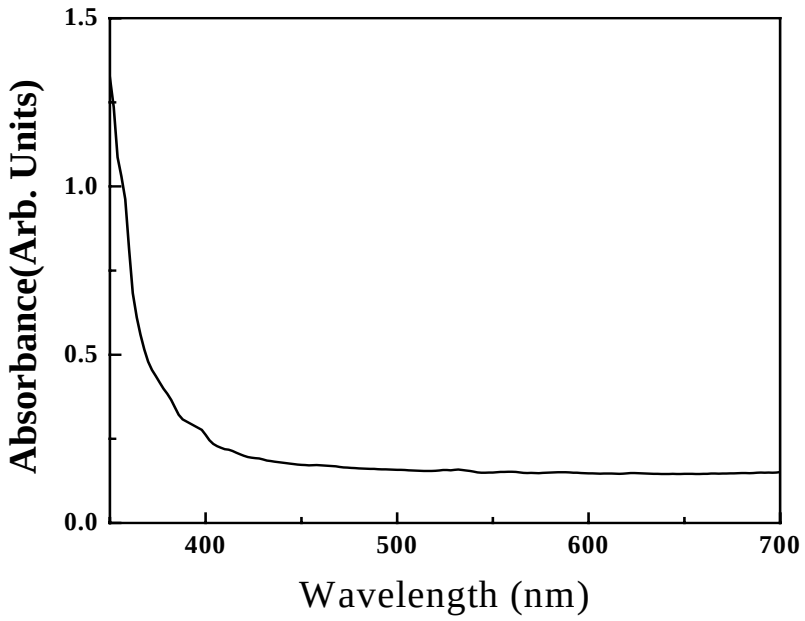

Figure 3.7 *Absorption spectrum of the Lead Borate glass.*

3.3.6 Fluorescence

The Fluorescence spectra are recorded on a Hitachi F-3010 fluorescence spectrometer. Lifetime measurements are done with the 6ns pulsed Nd: YAG laser. Second harmonic of the Nd : YAG laser is used as the pump source for the Raman shifter. Figure 3.8 shows the schematic of the Raman shifter used. The Raman cell is made of stainless steel and is 50 cm long. The input laser beam is focused into the Raman cell with a plano-convex lens of 30 cm focal length and is collimated back using another 30 cm plano-convex lens. The Stokes and anti-

Stokes lines are separated by means of a Pellin-Broca prism mounted on a rotating stage. The cell is filled with H_2 gas after evacuating it with a rotary pump. Since the vibration mode of H_2 is 4155 cm^{-1}, the first Stokes line for 532 nm is at 683 nm (14642 cm^{-1}) and the first anti-Stokes (AS_1) line at 436 nm (22952 cm^{-1}) and the second anti-Stokes (AS_2) is at 369 nm (27107 cm^{-1}). AS_1 and AS_2 are used for the excitation of Sm^{3+} and Tb^{3+} respectively. Second harmonic of the Nd : YAG laser is used for the excitation of Eu^{3+}. To record the lifetimes the light is first focused on to the sample using a 5 cm focal length lens. The lifetimes measured are of the order of a millisecond and the exciting source is 6 ns which instantaneously takes the atoms to the excited state. The repetition rate is 10 Hz, which means that the second pulse arrives after all the excited

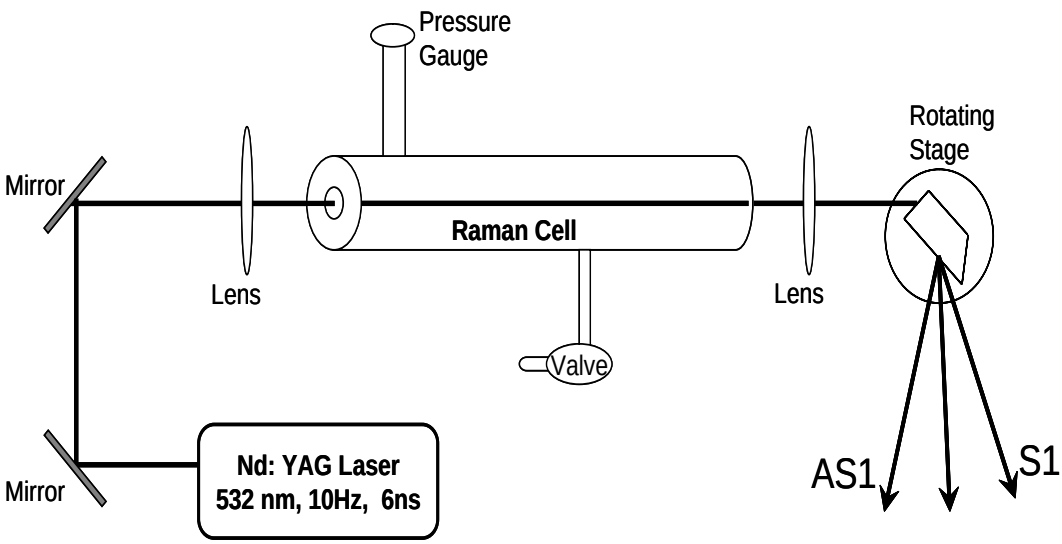

Figure. 3.8 *Raman shifted lines from a H_2 gas cell. S_1 and AS_1 are first Stokes and Anti-Stokes lines respectively.*

ions have decayed. The fluorescence is collected in the 90-degree geometry on to a 0.5 m Jobin - Vyon monochromator using two lenses of 6 and 10 cm focal length. Colour filters are used before the monochromator to cut off the pump wavelength and transmit only the fluorescence. The monochromator is connected to an EMI 9558 QB Photo Multiplier Tube. Figure 3.9 shows the setup for the

lifetime measurement. The PMT signal is viewed on a digital oscilloscope Tektronix TDS 220 and is grabbed using a CCD camera, which in turn is interfaced to a computer. Figure 3.10 shows a typical decay curve.

Table 3.1 *The glass transition temperature (T_g) and the cut-off wavelength ($\lambda_{cut\ off}$) for the PbO-B_2O_3 glass system.*

S. No.	PbO (mol%)	T_g (^0C)	$\lambda_{cut\ off}$ (nm)
1	30	478	428
2	40	457	415
3	50	403	425
4	60	350	416
5	70	357	420
6	80	356	400
7	90	381	375
8	100	427	-

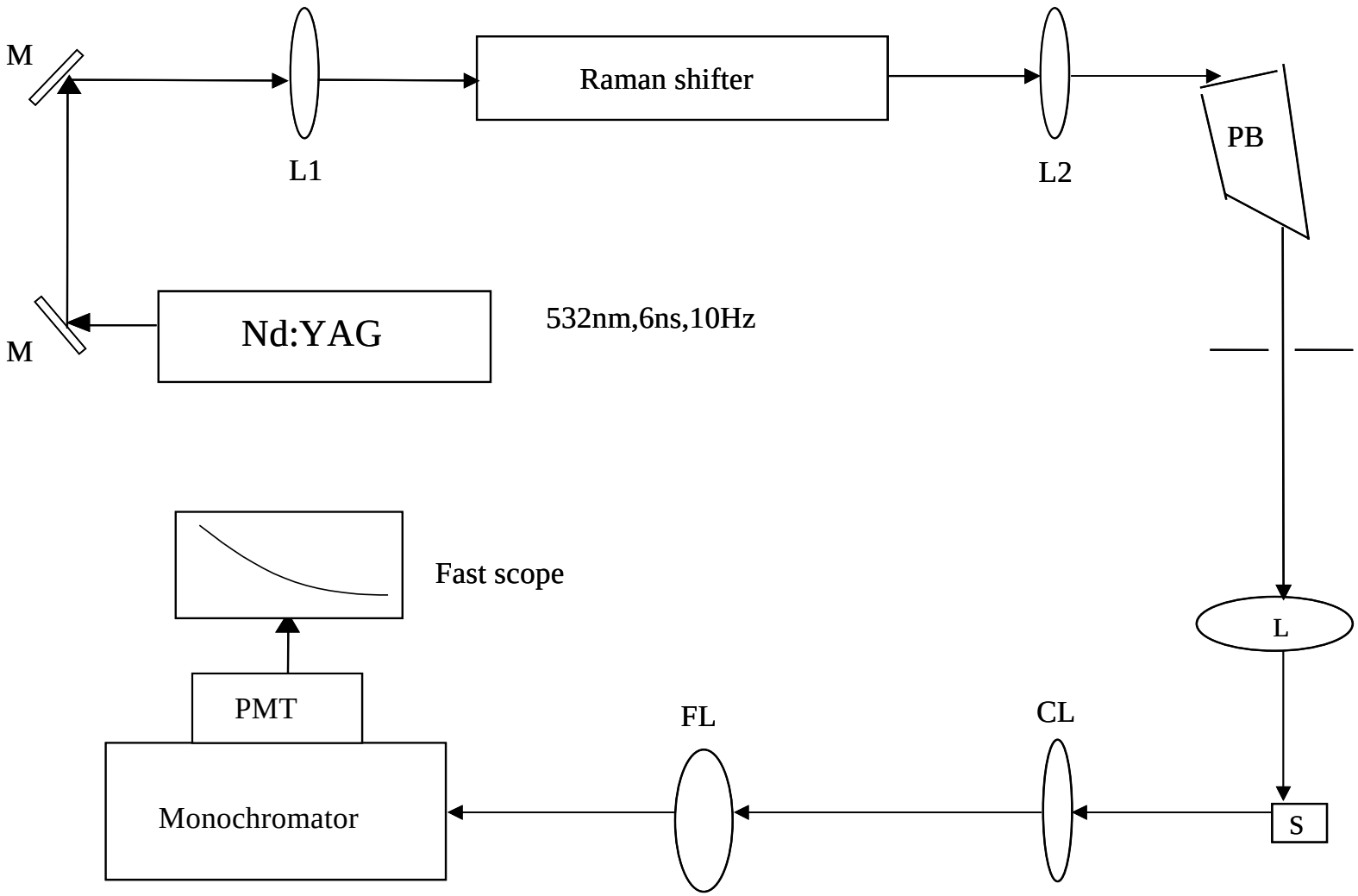

Figure 3. 9 *Schematic diagram of the fluorescence lifetime measurement setup. PB stands for Pellin Broca, L -Lens, S-Sample CL-Collimating Lens, FL –Focusing Lens, M - Mirror and PMT Photo Multiplier Tube.*

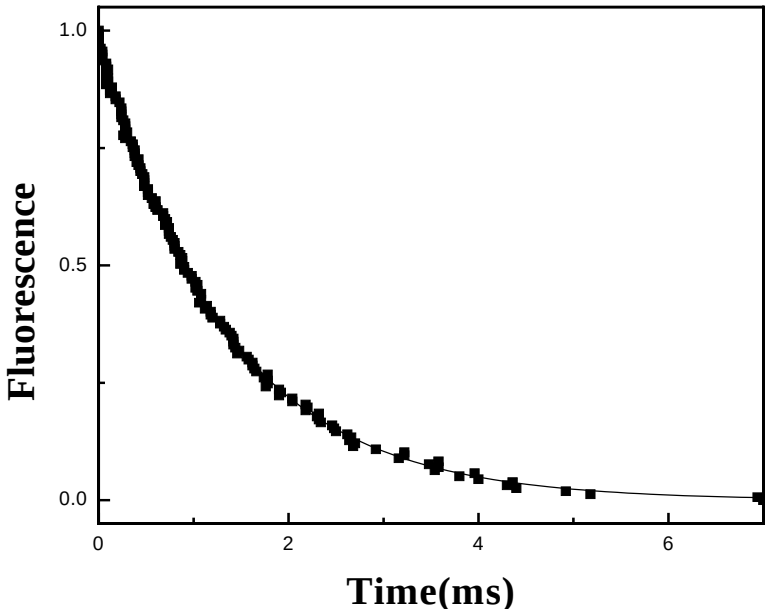

Figure. 3.10 *A typical fluorescence decay curve.*

Section II : Spectral Interferometry for the measurement of Refractive index

3.4 Spectral Interferometry

Spectral interferometry with a broad bandwidth white light source is a potential technique and has been applied to the measurement of the spectral phase introduced by optical fibers [13], differential refractive index of liquid samples [14,15], multimode reflectometers for ultra high spatial resolution [16], real time measurement of dispersion curves [17], polarization mode dispersion in optical fibers [18], group delay of dielectric laser mirrors [19], absolute distance [20] and simultaneous measurement of the refractive index and thickness of transparent materials[21,22].

The measurement of the refractive index and thickness using this technique can give high accuracy of the order of 10^{-5} as compared to other available techniques [23-27]. Single shot, real time, non-destructive measurement of the dispersion curve over the entire spectrum of the source is the highlight of the experiment. The versatility of the technique lies in its simplicity and the unlimited dynamic measurement range. The main advantage of spectral interferometry is that the whole spectrogram can be recorded in a single shot using a dispersing element like a prism or a grating and a CCD array detector. Small vibrations do not invalidate the information that can be obtained from the spectrogram, as most of the information is stored in the periodicity of the fringes and not in their contrast.

3.5 experimental set- up

A simple dispersion compensated Michelson interferometer is used in our measurements. As the work is done in the frequency domain, where the dispersive effect of material studied is of importance, it becomes necessary to compensate for the unequal material contribution due to optical components other than the sample, like the beam splitter and mirrors. Dispersion compensation between the interfering beams is achieved either by using a cube beam splitter or if a surface coated plate beam splitter is used, a compensating plate of the same

material should be kept in the appropriate arm of the MI through which the light beam travels less of the material. One of the mirrors is kept on a linear translation stage and by moving it, optimum number of spectral fringes within the region of interest can be obtained for any arbitrary value of a constant L_0 [28]. The flexibility in selecting the required path difference between the interfering beams makes it possible to extend the useful dynamic measurement range of the technique in measuring different thickness samples. This flexibility is also useful to observe the stationary fringe at any wavelength within the spectrum, where the group velocity between the two arms of the interferometer is compensated. The experimental set up is shown in figure 3.11. The source used is a 12W tungsten filament lamp. This lamp illuminates a pinhole which acts as the secondary source. Light beam emerging from the pinhole is collimated with a lens of focal length, f = 18 mm. An aperture of 1 mm diameter kept in the collimated beam uses only the spatially filtered central portion of the light. This beam of light is sent inside a standard, dispersion compensated Michelson interferometer (MI). The 50-50 cube beam splitter, amplitude divides the input light beam and sends it into the two arms of the interferometer. The two aluminum coated mirrors M_1 and M_2 reflect the two beams back into the same path and they interfere at the

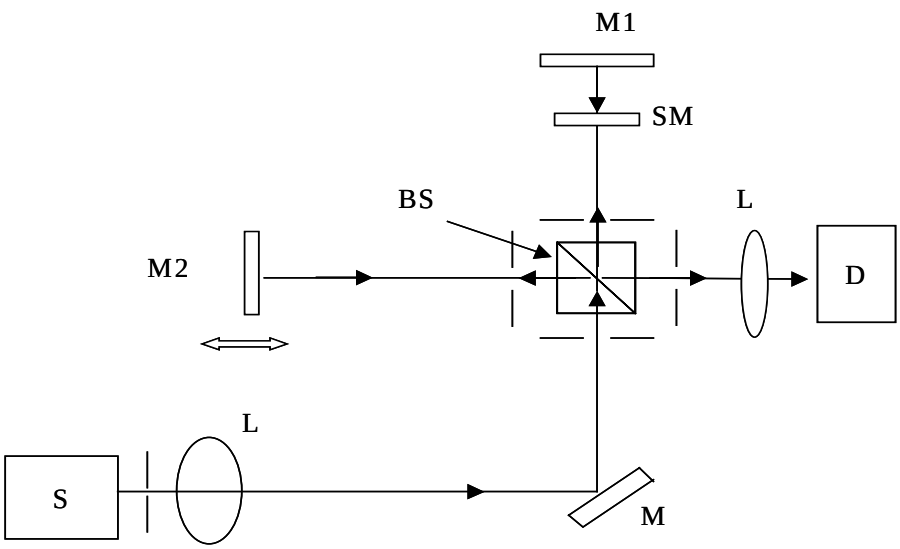

Figure 3.11 *Schematic diagram of White light Michelson interferometer. S-source ,L-lens, M,M1,M2-Mirrors, BS-beam splitter, SM – sample and D-detector*

same point in the beam splitter. The beams traverse a total length of L_1 and L_2 in the two arms of the MI. The mirror M_1 is kept fixed, while the other mirror M_2 is placed on a linear translation stage. One more aperture of the same diameter is kept at the exit of the interferometer to select only the central part of the superposed beams. Light emerging from the interferometer is detected using a CCD spectrometer (CVI SM -240). Thus the optical path difference between the two interfering beams because of the purely dispersive sample introduced in one of the arms, for each wavelength within the bandwidth of the light can be written as

$$\Delta(\lambda) = n(\lambda)2t - L_0 \tag{1}$$

where $n(\lambda)$ is the refractive index of the material introduced in the interferometer arms, 't' is its thickness and L_0 is an arbitrary path length introduced to get either the stationary fringe point within the region of the spectrum or to get well resolved spectral fringes within the region of observation. The explicit equation form for the refractive index as a function of wavelength for normal dispersive materials like glass and polymers which do not have any absorption in the visible region of the spectrum is given by the Cauchy's dispersion relation as

$$n(\lambda) = A + \frac{B}{\lambda^2} + \frac{C}{\lambda^4} \tag{2}$$

The constant L_0 can be chosen such that the total phase difference or the group dispersion between the two interfering beams becomes zero at some wavelength within the bandwidth of the spectrum, where one can see a broad fringe with the periodicity of the fringes changing on either side. Experimentally this is achieved by translating the mirror M_2 and visually observing the fringes. The resulting interferogram (S) is described by

$$\frac{S(\lambda)}{S_0(\lambda)} = \frac{1}{2}\left(1 + V(\lambda)\cos\left(2\pi\Delta(\lambda)/\lambda\right)\right) \qquad (3)$$

where S_0 s the lamp spectrum, V(λ) is the visibility. The sensitivity of this technique can be seen from figure 3.12, where for a small change in the parameter B, the interferogram shows noticeable differences.

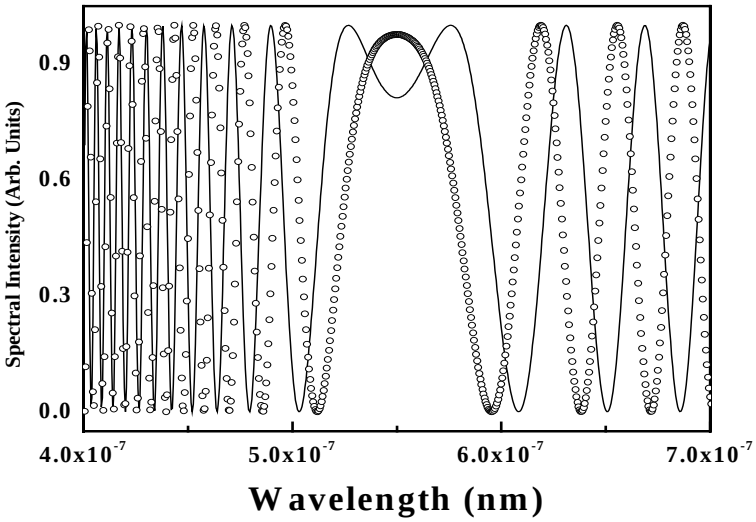

Figure 3.12*.The affect of the parameter b the fringe pattern. A=1.4524 C=1.839*10^{-31}m^{-4},t=0.002m.for B = 2e-15(line) and B = 2.1e-1 5 (circles). V(λ)has been taken as 1 for all the wavelengths.*

Figure 3.13 shows the interferogram recorded for an ordinary glass slide. The thickness of the slide is 1 mm. The data has been fitted to Eq.(3) using the Levenberg Marquard Non-linear least square program written in FORTRAN. The Visibility factor v(λ) has been taken to be equal to 1 for all the wavelengths. The constants obtained from the fit are A =1.452, B = 4.593×10^{-15} and C =1.129×10^{-28} with chi-squared =0.01. The refractive index is plotted in figure 3.14. From these values the refractive index at 633 nm is 1.464. If the thickness of the slide is taken as 1.02 mm the refractive index at 633 nm comes out to be 1.435. Therefore the value obtained with 1.02 mm is much closer to the value

derived through the Brewster's angle measurement (1.43). Though the value obtained by the Brewster's angle method is reliable, its accuracy is limited to second place because of the beam size and the surface scattering etc.

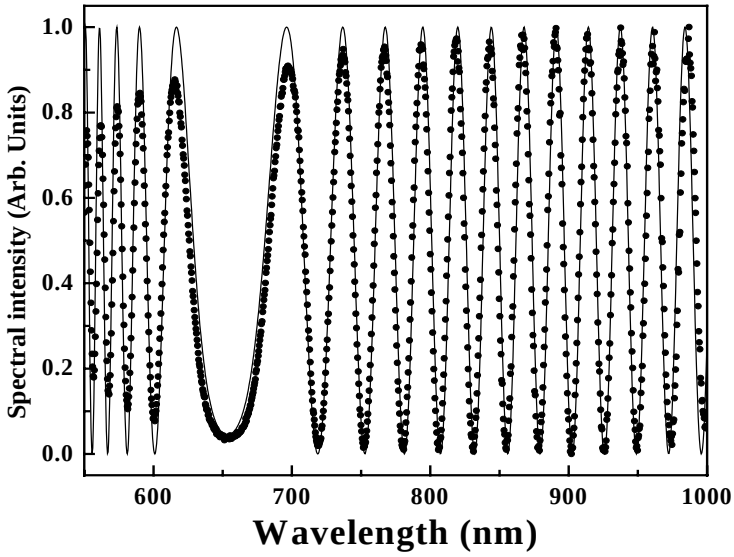

Figure 3.13 *Michelson interferogram for a glass slide (symbols) and the fit using Eq.(3) (solid line).*

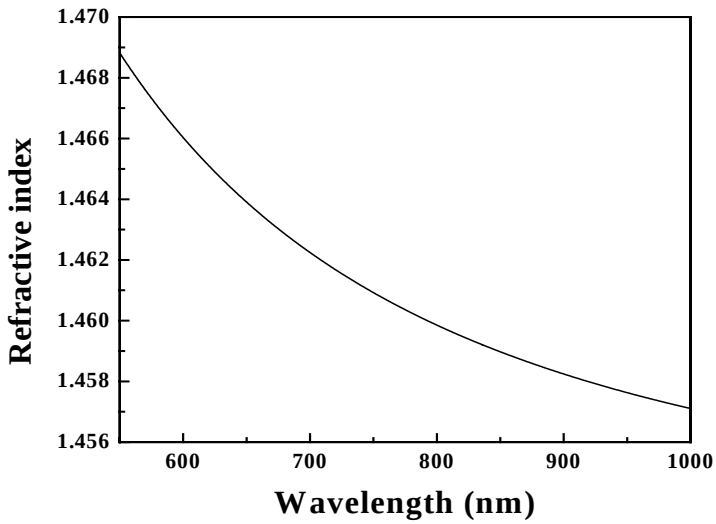

Figure 3.14 *Refractive index of the glass obtained from the fit.*

Therefore, though the interferometric technique is sensitive, it has an inherent ambiguity which has not been addressed by the previous workers. Present work is an attempt to remove this ambiguity by integrating two/three techniques (Michelson interferometer, reflection spectrum and a novel computational algorithm). The ambiguity arises from the phase term, which is product of the refractive index and thickness, which are the parameters to be measured. This can seen from figure 3.15, where the interferogram remains the same for two sets of parameters whose product is same. This ambiguity can be overcome by one of the following methods-

1. Measurement of the refractive index by another method, like Brewster's angle method and use that value for the analysis.
2. Measurement of the thickness using another method.
3. Performing another measurement that depends on the thickness or refractive index alone.
4. Mathematically, eliminating one of the parameters.

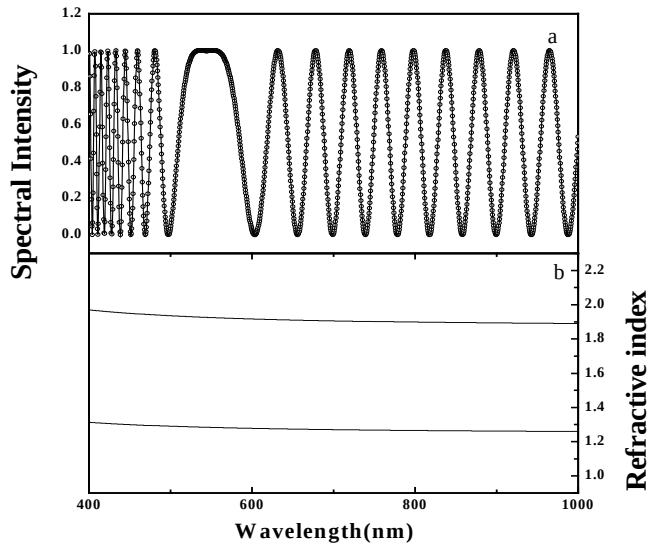

Figure 3.15 *(a) Michelson interferogram for two different sets of refractive indices and thickness (2 and 1.33 μm), (b) The refractive indices* $1.25+10^{-14}/\lambda^2+2\times10^{-29}/\lambda^4$ *and* $1.87+1.5\times10^{-14}/\lambda^2+3\times10^{-29}/\lambda^4$.

3.6 Reflection Spectrum

We demonstrate novel algorithms based on the methods 3 and 4. Reflection spectrum is a technique, which allows one to fix the thickness based on the number of fringes. Another advantage of using the reflection spectrum is that the measurement can be incorporated within the interferometer set up without the use of any additional equipment. For the white light falling normally on the sample of thickness, t, with refractive index n_1, coated on a substrate of refractive index n_2, the reflectance [29,30] is given as (figure.3.16)

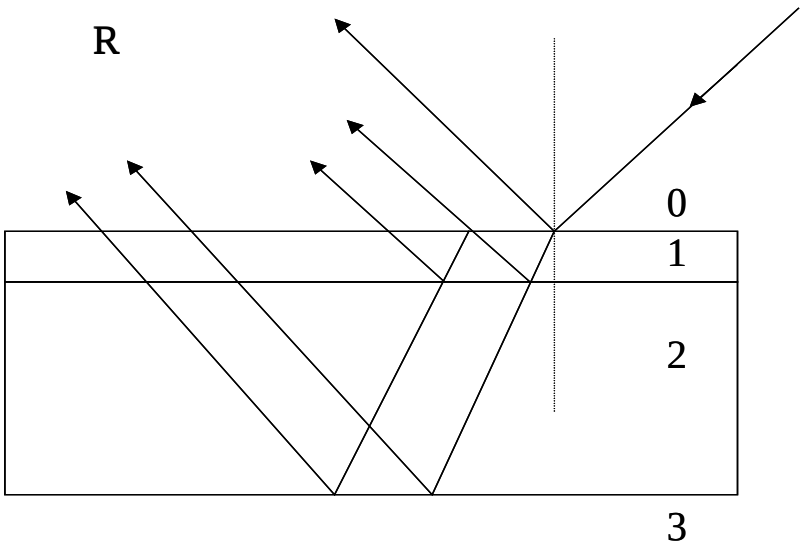

Figure 3.16 *Schematic diagram of the reflection geometry. 0 and 3 correspond to air, 1 is the sample and 2 is the substrate.As a guide to the eye oblique incidence is shown.*

$$R = R_{02} + \frac{T_{02} R_{23} T_{20}}{(1 - R_{23} R_{20})} \tag{4}$$

$$R_{02} = |r_{02}|^2 \qquad T_{02} = |t_{02}|^2 \frac{n_2}{n_0}$$

$$R_{20} = |r_{20}|^2 \qquad T_{20} = |t_{20}|^2 \frac{n_0}{n_2} \tag{5}$$

$$R_{23} = |r_{23}|^2$$

$$r_{02} = \frac{r_{01} + r_{12}e^{-i2\beta}}{1 + r_{01}r_{12}e^{-i2\beta}} \tag{6}$$

$$t_{02} = \frac{t_{01}t_{12}e^{-i\beta}}{1 + r_{01}r_{12}e^{-i2\beta}} \tag{7}$$

$$r_{20} = \frac{r_{21} + r_{10}e^{-i2\beta}}{1 + r_{21}r_{10}e^{-i2\beta}} \tag{8}$$

$$t_{20} = \frac{t_{21}t_{10}e^{-i\beta}}{1 + r_{21}r_{10}e^{-i2\beta}} \tag{9}$$

$$\beta = 2\pi(\frac{t}{\lambda})n_1 \tag{10}$$

$$r_{ij} = \frac{n_j - n_i}{n_i + n_j} \tag{11}$$

$$t_{ij} = \frac{2n_i}{n_i + n_j} \tag{12}$$

For i, j = 0,1,2,3 $\quad |i - j| = 1$

Here r_{ij} and t_{ij} are the reflection and the transmission coefficients at the i-j interface respectively. And n_1 is the refractive index of the sample, n_2 of the glass and $n_o = n_3 = 1$. Figure 3.17 shows the affect of the thickness on the reflection spectrum. The curves have been generated using Eq.(4). The

values used for the refractive index of the sample is $1.5+10^{-14}/\lambda^2+2\times10^{-29}/\lambda^4$ and for the substrate $1.452 + 4.59\times10^{-14}/\lambda^2 + 1.13\times 0^{-29}/\lambda^4$.

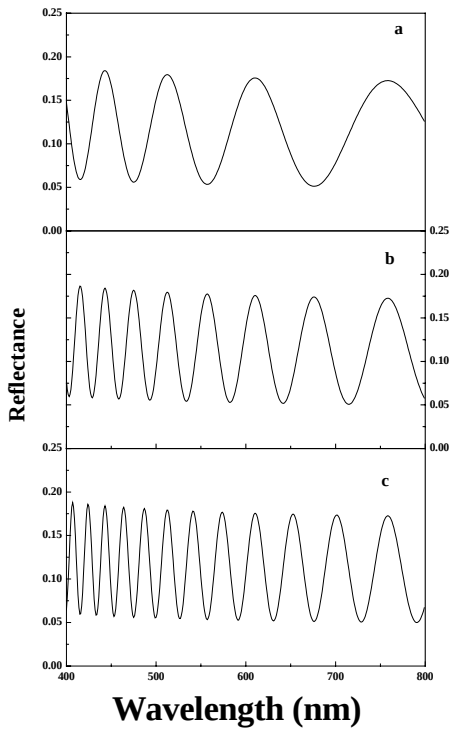

Figure 3.17 *The effect of thickness on the reflectance (a) 1 μm (b) 2μm (c) 3μm with refractive index* $1.5+10^{-14}/\lambda^2+2\times10^{-29}/\lambda^4$ *on a glass plate.*

From figure 3.17 we can see that the number of fringes depends on the thickness. Hence one can now use the Michelson interferogram and the reflection spectrum in tandem as the former is a sensitive technique and the latter gives a fairly good idea about thickness. The algorithm consists of first fitting the interferometer data. This fit yields the values of the refractive index and thickness, which are related to the actual values by a factor. If one uses these values to fit the reflection data, the scaling factor can be obtained. Then use this value to fit the interferometer data. Successive such iterations would lead to an accurate and unambiguous values for the refractive index as well as the thickness. The algorithm can be summed up as follows.

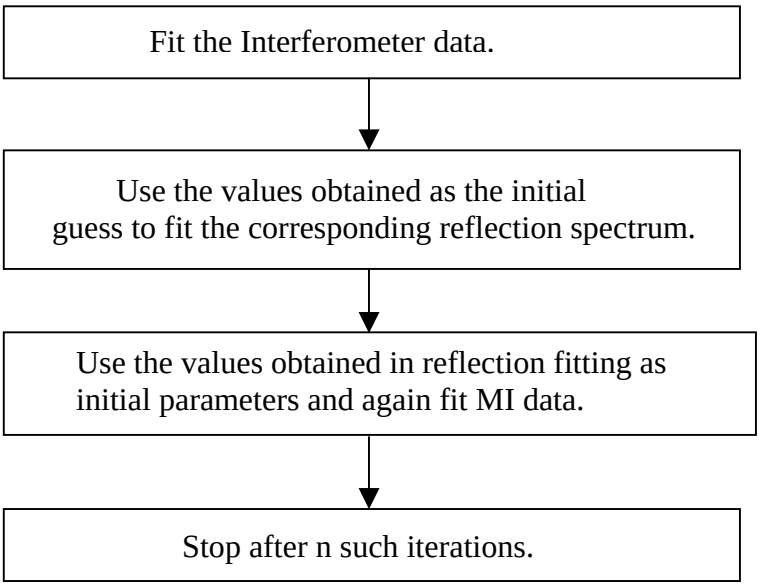

Figure 3.18 *Algorithm for the determination of the refractive index and the thickness using the Michelson interferometer and the reflection*

3.7 A Novel Algorithm

As pointed out in previous section, the ambiguity in the measurement arises from the occurrence of the refractive index and thickness as a product. This method consists of defining a merit function and then rewriting it in such a way as to make it dependent on only one of the parameters. Michelson interferometer (S) and the reflection (R) are functions of the refractive index n and the thickness t. One can perform N such measurements at different thicknesses and eliminate thickness to make the merit function dependent only on the refractive index [30]. Alternatively, one can keep the thickness constant and measure at different wavelengths so as to eliminate refractive index and make merit function dependent only on the thickness. The merit function is defined as

$$F = \sum_{i=1}^{N} f_i(n_i, t)$$

where

$$f_i(n_i, t) = \left(\frac{S_i - S(n_i, t)}{S_i}\right)^2 + \left(\frac{R_i - R(n_i, t)}{R_i}\right)^2$$

$$i = 1,2,\ldots\ldots N$$

Where R_i and S_i are the measured reflectance and the spectral intensity in the Michelson interferometer respectively at *i*th wavelength. The best agreement between the calculated and the measured values of R and S are obtained by minimizing the merit function F. The minimum of F should satisfy

$$\frac{\partial F}{\partial n} = 0, \qquad \frac{\partial F}{\partial t} = 0$$

$$\frac{\partial F}{\partial n_i} = \frac{\partial f_i}{\partial n_i}$$

$$= \frac{2(R(n_i,t) - R_i)}{R_i^2}\frac{\partial R}{\partial n_i} + \frac{2(S(n_i,t) - S_i)}{S_i^2}\frac{\partial S}{\partial n_i} = 0$$

For a given value of t, if we solve the equation for n_i^o

$$n_i^o = n_i^o(t, R_i, S_i)$$

With the above substitution, R and S can be written as

$$R^o = R^o(t, R_i, S_i)$$

$$S^o = S^o(t, R_i, S_i)$$

Now the merit function becomes

$$F = \sum_{i=1}^{N} f_i(t, R_i, S_i)$$

where

$$f_i(n_i, t) = \left(\frac{S_i - S(t, R_i, S_i)}{S_i}\right)^2 + \left(\frac{R_i - R(t, R_i, S_i)}{R_i}\right)^2$$

Now the merit function depends only on thickness. The fitting of the merit function can yield the correct value of the thickness. After the value of thickness is obtained, this can be used to fit the Michelson interferometer to obtain the value of the refractive index.

Though the interferometric and the reflection techniques were developed with a view to measure the refractive index dispersion, the refractive index used in the thesis was measured only at one wavelength (of He – Ne laser) using Brewster's angle method. Another reason for the refractive index measurement at only wavelength in the present work is because the strongest emission and absorption overlap in a very small spectral region and the change in the refractive index would be very small in this region of interest.

3.8 References

1. M. Ravi, A. Samanta, and T. P. Radhakrishnan, J. Phys. Chem. **98,** 9133 (1994).
2. *Handbook of Glass Data*, Part B, Edited by O. V. Mazurin, M. V. Streltsina and T. P. Shvaiko, (Elsvier, Amsterdam, 1985).
3. E. R. Elliott, *Physics of Amorphous materials* (Longman Scientific Tech.)
4. M. B. Saisudha and J. Ramakrishna, Phys. Rev. B **53**, 6168 (1996).
5. A. H. Harper, *Handbook of ceramics, glasses and diamonds* (Mc GRAW-HILL), Chapter 5.
6. Q. Chen, M. Ferraris, Y. Menke, D. Milanese and E. Monchiero, J. Non-Cryst. Solids, **324**, 1 (2003).
7. C. Dayanand, G. Bhikshamaiah and M. Salagram, Mater. Lett. **23**, 309 (1995).

8. M. B. Volf, *Chemical approach to glass: Glass science and* technology, Vol. 7 (Elsevier, Amsterdam, 1984).
9. K. J. Rao, B. G. Rao and S. R. Elliott, J. Mater. Sci. **20**, 1678 (1985).
10. Q. Chen, M. Ferraris, D. Milanese, Y. Menke, E. Monchiero and G. Perrone J. Non-Crys.Solids, **324**, 12 (2003).
11. N. Nachimuttu, research thesis *Optical properties of lanthnide ions doped in borate, phosphate and oxyfluride glasses* page 235 (1996).
12. R. D. Peacock, *Structure and bonding*, Vol.**22** (Springer-Verlag, 1975) page 116.
13. J. Piasecki, B. Colombeau, M. Vampouille, C. Froehly and J.A. Arnaud, Appl. Opt. **19**, 3749 (1980).
14. C. Sainz, J.E. Calatroni and G. Tribillon, Meas. Sci. Technol. **1**, 356 (1990).
15. A.L. Guerrero, C. Sainz, H. Perrin, R. Castell and J. Calatroni, Opt. laser Tech. **24**, 333 (1992).
16. N. Tan-no T. Ichimura, T. Funaba, N. Anndo and Y. Odagiri, Opt. Lett. **19**, 587 (1994).
17. C. Sainz, P. Jourdain, R. Escalona and J. Calatroni, Opt. Commun. **110**, 381 (1994).
18. X.D. Cao and D.D. Meyerhofer, Opt. Lett. **19**, 1837 (1994).
19. A.P. Kovacs, K. Osvay, Zs. Bor and R. Scipocs, Opt. Lett. **20**, 788 (1995).
20. U. Schnell, E. Zimmermann and R. Dandliker, J. Pure Appl. Opt. **4**, 643 (1995).
21. V. Nirmal Kumar and D. Narayana Rao, J. Opt. Soc. Am. B **12**, 1559 (1995).
22. V. Nirmal Kumar, Y. Chandrasekhar and D, Narayana Rao, Pramana, **47**, 163 (1996).
23. R.Ulrich and R. Torge, Appl. Opt. **12**, 2901 (1973).
24. W. E. Case, Appl. Opt. **22**, 832,(1983).
25. D. K. Qing, I. Yamaguchi, T. Okamoto and Y. Yamamoto, Opt. Lett. **25**, 914 (2000).
26. Murali Sastry, Bull. Mater. Sci. **23**,159 (2000).

27. M. Mulato, I. Chambouleyron, E. G. Birgin and J. M. Martinez, Appl. Phys. Lett. **77**, 2133 (2000).
28. H. Delbarre, C. Przygodzki, M. Tassou and D. Boucher, Appl. Phys. B **70**, 45 (2000).
29. R. M. A. Azzam and N. M. Bashara, *Ellipsometry and polarized light* (North-Hlland,Amstedam,1977)
30. Q. Bie, B. Cheong, M. Chung, Z. Lin, T.S. Lee, W. M. Kim and S. G. Kim, Jpn. J. Appl. Phys. **39**, 5139 (2000).

Chapter 4

Lifetimes in Transparent Dielectric

This chapter discusses the results of the measurement of lifetimes as a function of the refractive index (real) of the glass in order to see which of the local field models is applicable. In the first part of the chapter, the derivations for the local fields in a transparent dielectric for both the real and virtual cavities for a static field is presented. The experimental results on the measurement of the lifetimes of Eu^{3+} *and* Tb^{3+} *doped in the glass system x PbO+ (100-x)* B_2O_3 *are discussed.*

4.1 Introduction

The lifetime of an atom is determined by the electronic wavefunction of the atomic states involved together with the density of states and the electromagnetic field strength of the optical modes at the position of the atom. The spontaneous emission can be regarded as being stimulated by the vacuum fluctuations of the electromagnetic filed. The lifetime of an atom can be changed either changing the density of states or the field strength at the position of the atom. Placing it in a dielectric can change the field strength at the position of the atom. This change is a consequence of the local field. The radiative lifetimes of an atom in a dielectric, neglecting the local field effects has been predicted by Nienhius and Alkemade [1] as being inverse to the refractive index of the dielectric. But, in principle the atom couples to the microscopic vacuum fluctions. To incorporate the microscopic interactions, one needs to take into account the local filed effects. The approach is still macroscopic in nature, but the electric field at the radiating atom field is different from the macroscopic field. To describe the interaction of an atom with the electromagnetic field, Martin [2] proposed that the atom be considered as a charged conducting sphere surrounded by the continuous dielectric. A better model was introduced by Bell [3] by considering the atom as an ideal dipole in the center of a spherical cavity. Two

limiting cases for the cavity have been proposed in the literature - the real and the virtual cavity. In the former case, the cavity is empty (no dielectric) whereas in the latter, the cavity is filled with the dielectric of the same refractive index as the surrounding dielectric. The real cavity is also known as empty cavity. The virtual cavity is due to Lorentz [4] and is sometimes known as full cavity. The local field depends on the choice of the specific nature of the cavity. It is assumed the dimension of the cavity are larger than the dimensions of the emitter and smaller than the wavelengths involved. The next section gives the derivation for the relationship between the applied field and the local field strengths for both the cases of the real and the virtual cavities in the framework of the electrostatics.

4.1.1 Virtual cavity

In the virtual cavity case the dielectric is taken as continuous over the entire space including the center of the cavity. The electric field produced at the center of the sphere by atoms contained within the sphere will tend to cancel. The total field acting at the center of the cavity can be written as [5,6]

$$E_{loc} = E + \frac{4\pi}{3} P \qquad (1)$$

When the external field is applied the dipole moment is proportional to the local field. If there are N molecules with polarizability α, then the total dipole moment is

$$\begin{aligned} P &= Np \\ &= N\alpha E_{loc} \end{aligned} \qquad (2)$$

Where p is the polarizability of an individual atom. Using the expression for the local field from Eq.(1),

$$P = \frac{N\alpha}{1 - \frac{4\pi}{3} N\alpha} E \qquad (3)$$

Solving this equation for susceptibility χ using the relation $P = \chi E$

$$\chi = \frac{N\alpha}{1 - \frac{4\pi}{3} N\alpha} \tag{4}$$

In terms of the permittivity the relation can be written as

$$\frac{\varepsilon - 1}{4\pi} = \frac{N\alpha}{1 - \frac{4\pi}{3} N\alpha} \tag{5}$$

Rearranging the terms, and writing in the equation in terms of the χ again

$$\frac{\varepsilon - 1}{\varepsilon + 2} = \frac{4\pi}{3} N\alpha$$

$$\chi = \frac{\varepsilon + 2}{3} N\alpha \tag{6}$$

ε can be replaced by square of the refractive index ,i.e. $\varepsilon = n^2$

$$\chi = \frac{n^2 + 2}{3} N\alpha \tag{7}$$

The relation between E and E_{loc} can be obtained by rewriting the Eq.(1) and using Eq.(5)

$$E_{loc} = \frac{\chi}{N\alpha} E$$

and using Eq.(7)

$$E_{loc} = \frac{n^2 + 2}{3} E \tag{8}$$

4.1.2 Real Cavity

For the real cavity case the atom is at the center of an empty sphere surrounded by the dielectric i.e the refractive index inside the cavity is equal to one and outside it is some n. The solution of the Laplace equation gives the potential. Taking the center

of the sphere as the origin of the co ordinate system and the direction of the z-axis as the direction of the applied field vector the potential as ϕ can be written as [7]

Region of the sphere	Potential (ϕ)
Outside	$\phi_1 = \sum_{l=0}^{\infty}[A_l r^l + B_l r^{-(l+1)}]P_l(\cos\theta)$
Inside	$\phi_2 = \sum_{l=0}^{\infty}[C_l r^l + D_l r^{-(l+1)}]P_l(\cos\theta)$

(9)

The behavior of the field at the interface is governed by the boundary conditions and the conditions imply that the potential should satisfy

$$(\phi_1)_{r\to\infty} = -E\ z = -E\ r\cos\theta$$
$$(\phi_1)_{r=a} = (\phi_2)_{r=a}$$
$$.\varepsilon\left(\frac{\partial\phi_1}{\partial r}\right)_{r=a} = \left(\frac{\partial\phi_2}{\partial r}\right)_{r=a} \qquad (10)$$

Because of the first boundary condition and as a result of the fact that Legendre polynomials are linearly independent, all coefficients A_l s vanish except $A_1 = -E_0$. At the center ϕ_2 must not have a singularity and because of this, all coefficients D_l vanish. The potential now becomes

$$\phi_1 = \sum_{l=0}^{\infty} B_l r^{-(l+1)} P_l(\cos\theta) - E\ \cos\theta$$
$$\phi_2 = \sum_{l=0}^{\infty} C_l r^l P_l(\cos\theta) \qquad (11)$$

Applying the second and the third boundary condition all the coefficients B_n and C_n except for n=1 vanishes. And we get B_1 and C_1 as

$$C_1 = \frac{3\varepsilon}{2\varepsilon + 1} E$$

$$B_1 = -\frac{\varepsilon - 1}{2\varepsilon + 1} a^3 E \qquad (12)$$

Substituting back these in Eq.(11)we get

$$\phi_2 = -\frac{3\varepsilon}{2\varepsilon + 1} E\ z \qquad (13)$$

and the field now becomes

$$E_{local} = \left(\frac{3n^2}{2n^2 + 1} \right) E \qquad (14)$$

4.2 Lifetime and local field

When an atom or molecule is excited to its upper energy level it comes back to the ground state through the emission of a photon. According to the Fermi's golden rule, the transition probability, A, from a level 2 to 1 of an atom interacting with the electric field E is given by

$$A = \frac{2\pi}{\hbar} \left| \langle \psi_2 | \mu.E | \psi_1 \rangle \right|^2 \rho(E) \qquad (15)$$

If the atom is placed in a dielectric of refractive index n, then the electric field is to be taken as the total field the atom sees that is the local field, then the spontaneous emission probability is

$$A\ (n) = \frac{2\pi}{\hbar}\left|\langle\psi_2\,|\mu.(l(n)E)|\psi_1\rangle\right|^2 \rho(E_2)$$

$$A\ (n) = \frac{2\pi}{\hbar} l(n)^2 \left|\langle\psi_2\,|\mu.(E)|\psi_1\rangle\right|^2 \rho(E_2)$$

$$A(n) \propto l(n)^2\, A\ (0) \qquad (16)$$

Where A (0) is the spontaneous emission probability in the absence of the local field and l(n) is the local field correction factor. The local field effect is not only applicable to the static fields but is also shown to be relevant for the varying fields [8-14]. Combining the results obtained in section 2.2 for the real and virtual cavities and the above equation for the SEP, the lifetimes in the case for real and virtual cavity now becomes

$$\tau(n) = \frac{1}{n}\left[\frac{3\,n^2}{2n^2+1}\right]^{-2} \tau(0) \qquad (17)$$

$$\tau(n) = \frac{1}{n}\left[\frac{n^2+2}{3}\right]^{-2} \tau(0) \qquad (18)$$

These equations are written with the assumption that the radius of the cavity is larger than the dimensions of the atom and less than the wavelengths involved. Figure 4.1 shows the plot of local field correction factor (LFCF) vs the refractive index for both the cases of real and virtual cavities. For refractive index closer to 1 there is not much difference in the LFCF given by two models but in the region above 1.5 and above the difference is considerable.

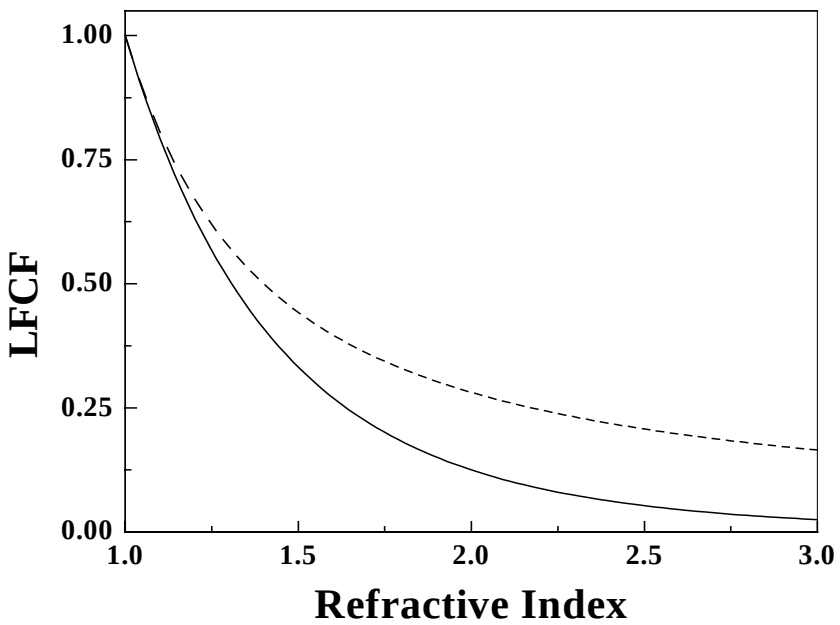

Figure 4.1 *The plot of local field correction factor LFCF as a function of refractive index. Solid line for the virtual cavity and the dashed line for the real cavity.*

4.3 Examples of Local Field Effect

The local fields not only leads to changes in the spontaneous emission lifetimes but also leads to some other interesting effects. In linear optics, the local field correction leads to effects like frequency shifts and in nonlinear optics an enhancement in the harmonic signal. The problem of frequency shifts in a two level atom has been studied both theoretically [15-17] and experimentally [18-20] where the dielectric constant is given by

$$\varepsilon = 1 + \frac{4\pi\rho\, p^2 / \hbar}{(\omega_0 - \omega_L) - \omega - i\gamma} \qquad (19)$$

where ω_L is the frequency shift with respect to the non interacting system. The third order susceptibility is written as [11]

$$\chi^{(3)} = L(\omega_4)L(\omega_3)L(\omega_2)L(\omega_1)N\gamma \qquad (20)$$

where γ is the molecular hyperpolarisability and L is the correction factor due to the local field. In the realm of nano world one encounters for a composite material the absorption coefficient [21]

$$\alpha = 9p\frac{\omega}{c}\frac{\varepsilon''}{(\varepsilon_m' + 2\varepsilon_d)^2 + \varepsilon_m''^2}\alpha_1(\omega) \qquad (21)$$

where p is the packing fraction and ε_m and ε_d are the dielectric constants of the metal nanoparticles and the dielectric respectively with single prime as the real and double prime as the imaginary parts.

4.4 Lifetimes in Europium

The 4f shell of Eu^{3+} contains six electrons. The ground state is $^7F_0$ and the ^7F multiplet has six other levels with j taking values upto six. ^5D is next multiplet containing five levels. The lowest of these levels is $^5D_0$ and is the fluorescing level. Figure 4.2 shows the excitation spectrum of Eu^{3+}. The $^7F_1$ level is very close the ground level and hence it is also thermally populated at room temperature and we can observe transitions from this level.

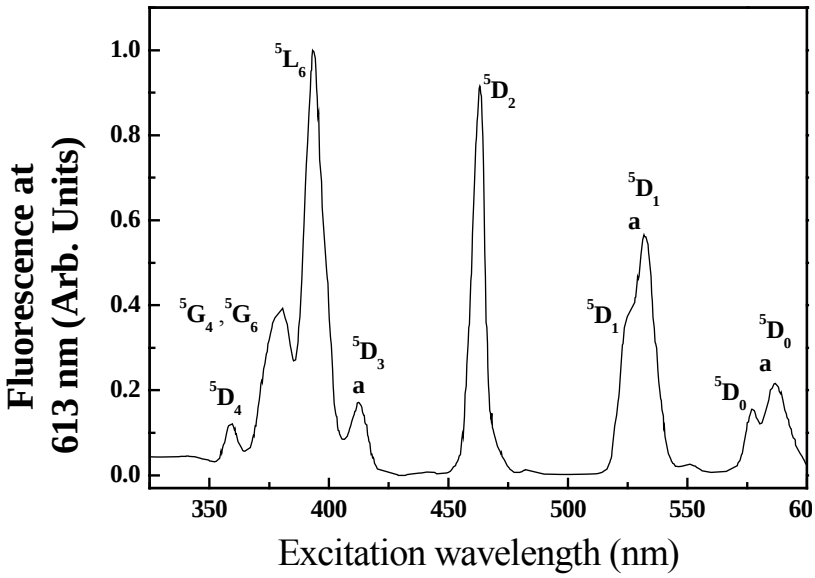

Figure 4.2 *Excitation spectrum of Eu^{3+} monitered at 613 nm normalized with the $^5L_6$ transition. The transitions marked (a) are from $^7F_1$ and the rest are from the ground state $^7F_0$.*

Generally, the fluorescence spectrum of Eu^{3+} is due to transitions from the ^5D_j multiplet to the ^7F_j multiplet. However, in oxide glasses the spectrum consists only the $^5D_0$-^7F_j transitions [22]. Figure 4.3 shows the emission spectrum of Eu^{3+} excited with 532 nm. The transitions to $^7F_{0,3,4}$ are very weak and most of the fluorescence branches to the other two levels. Table 4.1 gives the center wavelength, widths and the branching ratios obtained from the fluorescence spectrum. The lifetimes are measured at 613 nm, as the emission is strongest at this wavelength. The time evolution is a single exponential for all the compositions of the glasses as seen from a typical decay in figure 4.4.

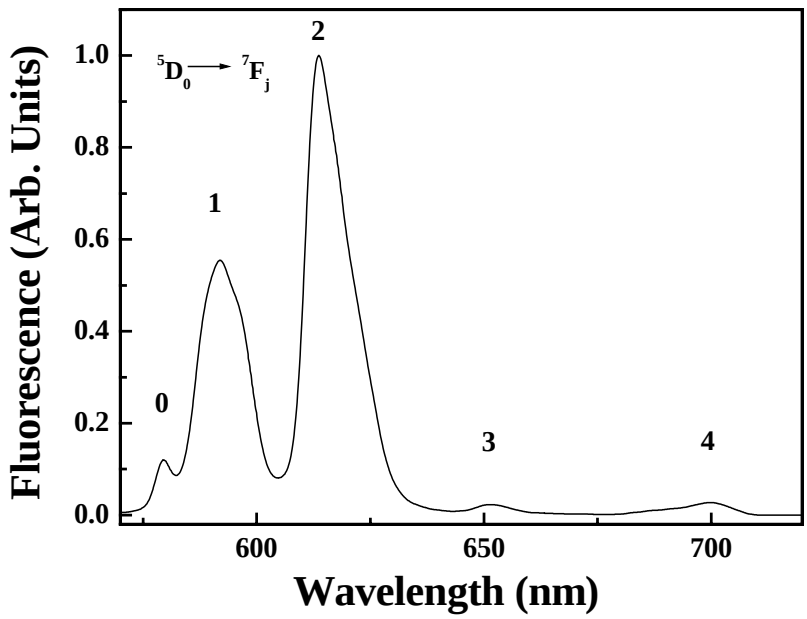

Figure 4.3 *Fluorescence spectrum of Eu^{3+} excited with 532 nm. The intensity is normalized to the intensity of $^7F_2$. The number on each band indicates the value of j.*

Table 4.1 *The Peak position, peak widths and the branching ratios from the fluorescence spectrum of* Eu^{3+}.

ransition from $^5D_0$ to ^7F_j	Peak position (nm)	Peak width (nm)	Branching ratio
0	578.6	8.96	0.05
1	593.4	9.90	0.30
2	613.0	9.50	0.56
3	650.0	-	0.07
4	700.0	-	0.02

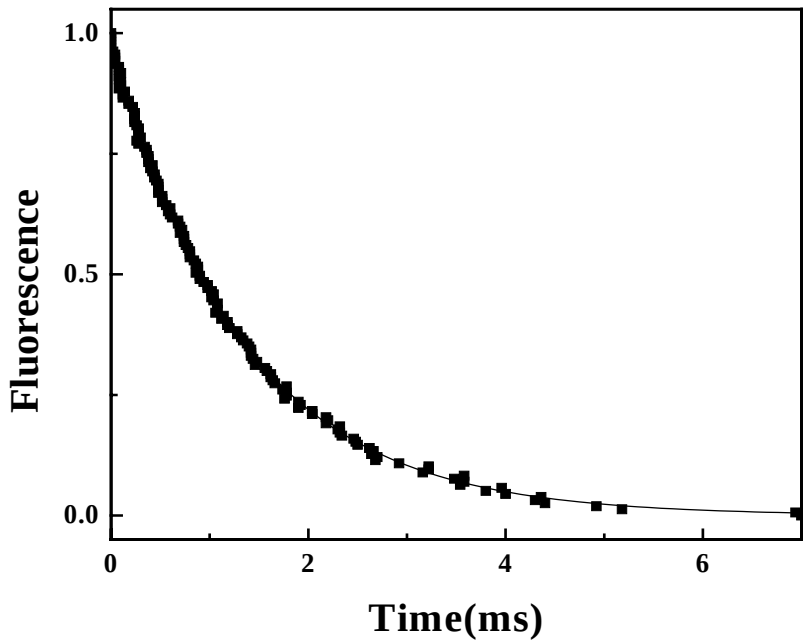

Figure 4.4 *A typical decay curve for the* Eu^{3+} *in* $60PbO+40B_2O_3$ *glass. Squares are the experimental data and the solid line is a fit to single exponential.*

The lifetimes are of the order of a millisecond. The quantum yield is close to unity as the contributions from the nonradiative decay can be neglected. The lowest of the excited state to the highest of the ground state energy difference is about 12500 cm^{-1} and the highest phonon energy of the glass is around 1300 cm^{-1}.

Any nonradiative decay through this channel needs about ten phonons, which makes the probability of this process very less [23,24]. The fluorescence intensity remains the same for all the compositions of glass, which also indicates the absence of the nonradiative transfers. If the quantum yeild is affected by the host, then the fluorescence intensity should be dependent of the host. The fluorescence intensity decreases by about 25% from the low refractive index to the high refractive index. This is an apparent decrease in the fluorescence yield. There can be two important reasons for this decrease in the intensity. First, the Fresnel reflection is more for the high refractive index glass as compared to that of the low refractive index. Hence, even though we use a constant excitation power the high refractive index glass sees less of it compared to that of the low refractive index glass. Also the collected fluorescence intensity is less by same amount for the high refractive index glass. For a constant pump intensity, considering the Fresnel reflection, the actual pump intensity becomes 0.93 for n=1.7 and 0.86 for n=2.2, that means a drop of about 7%. Considering the loss at the collection side also, we can expect a drop of about 14% for high refractive index glass compared to that of low refractive index in the fluorescence signal. The second reason for the decrease of the fluorescence can arise from the concentration of the Eu^{3+} ions, as it is lower in the high refractive index glass. The concentration is of the order of 3.85×10^{-20} /cm^{-3} for 40 PbO and 3.25×10^{-20} /cm^{-3} for 90 PbO glass. This is so because the initial amount of Eu^{3+} taken for the preparation is not based on the knowledge of the density of the glass. Hence this factor can also contribute to the decrease in the fluorescence intensity.

Another cause for the quenching of the fluorescence can arise from the interaction among the Eu^{3+} ions. In order to examine this aspect, fluorescence intensities and the lifetimes are measured as a function of the concentration of the Eu^{3+} in the glass system $60PbO+40B_2O_3$. Figure 4.5 shows the fluorescence spectra with different concentrations of the Eu^{3+}. The fluorescence intensity increased with the concentration (Figure 4.5 inset). The branching ratios remain-

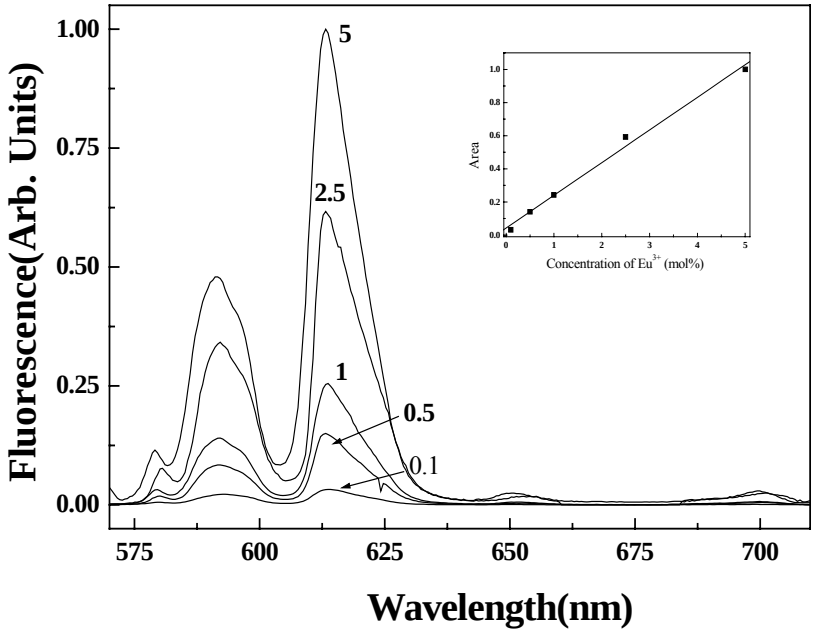

Figure 4.5 *The fluorescence spectra of the $60PbO+40B_2O_3:yEu^{3+}$. The value of y is indicated on each curve. The inset shows the area under the $^7F_2$ band (solid squares) and the solid line is the linear fit.*

-ed the same for all the concentrations of Eu^{3+}. The lifetimes do not show any drastic change with the concentration of Eu^{3+} as shown in figure 4.6. Hence, the observed lifetimes can be attributed to radiative decay. Lifetimes decrease with

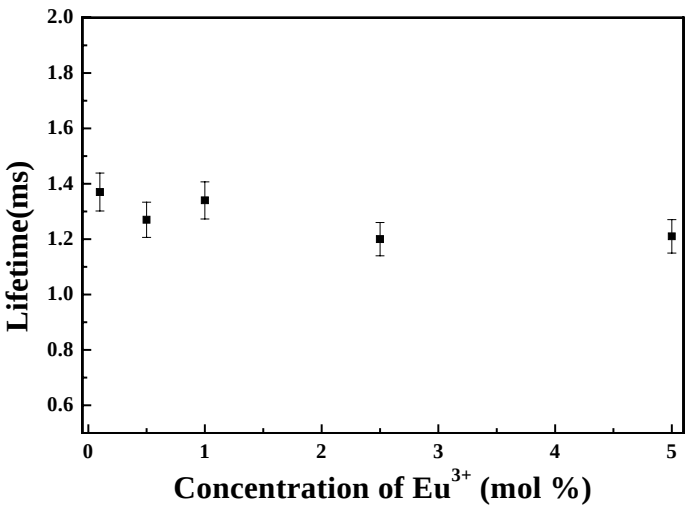

Figure 4.6 *The Eu^{3+} lifetimes as a function of the concentration.*

the increase of the refractive index. Hence the quenching effects can be neglected and the quantum yield is almost unity. The measured lifetimes can be entirely attributed to the radiative decay and the change in the lifetimes with refractive index to the local field. The lifetimes are plotted as a function of the refractive index in the figure 4.7. The lifetimes decrease with the increase of the refractive index. An error of 5% is introduced based on the measurements on three different sets of samples. The data has been fitted to Eqs.(17) and (18) by floating the free space lifetime. The least square fitting is performed in Microcal Origin 6. From the fitting, the free space lifetime for virtual and real cavities is obtained as 8.92 ms and 4.57ms respectively. The virtual cavity fit not only gives a poor fit but also leads to a very high value for the free space lifetime. In figure 4.7 the dashed line is the virtual cavity fit and the solid line is the real cavity fit. It can be clearly seen that the data agrees well with the real cavity model.

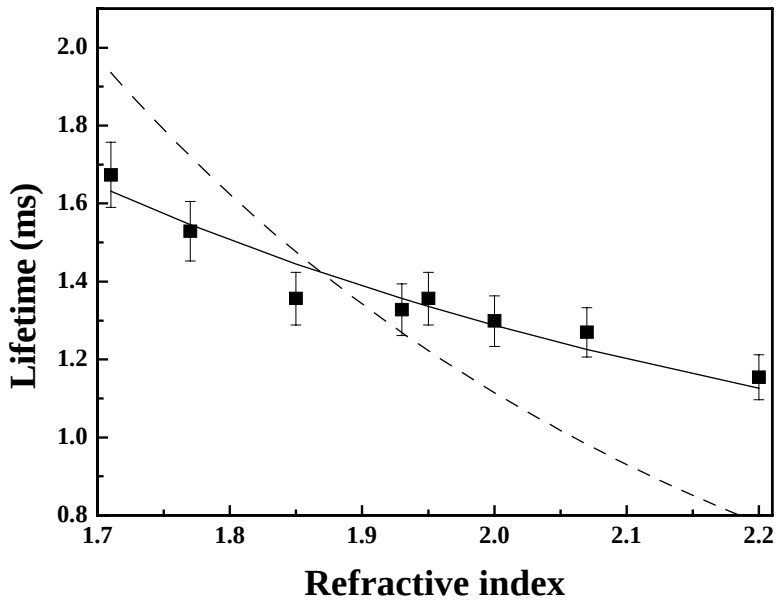

Figure 4.7 *The plot for the refractive index vs the lifetime. Solid squares are the experimental data. The dashed line is the fit for the virtual cavity model and the solid for the real cavity.*

4.5 Lifetimes in Terbium

Spectroscopically, Tb^{3+} is very much similar to the Eu^{3+}. While Eu^{3+} has one less electron than the half filled f shell, Tb^{3+} has one more with eight electrons in the f shell. The ground state is $^7F_6$ and $^5D_4$ is the fluorescing level. Figure 4.8 shows the excitation spectrum of Tb^{3+} monitored at 546 nm.

The fluorescence spectrum, shown in figure 4.9, consists of four strong bands corresponding to the to the transition $^5D_4$ to ^7F_j, j=3,4,5,6**.** The strongest emission corresponds to that of j equal to 5 centered at 546 nm. About 90 % of the fluorescence branches to the transitions corresponding to j = 5 and 6. Table 4.2

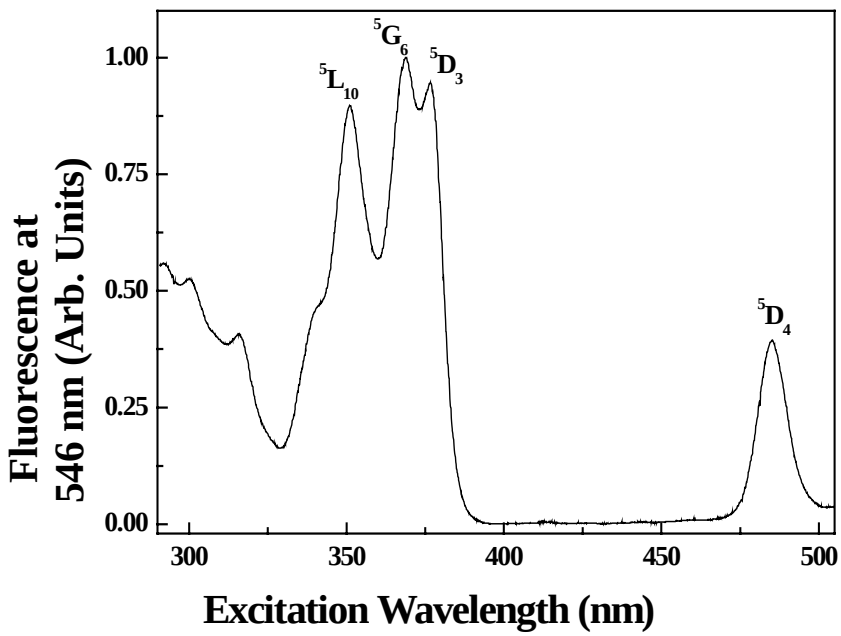

Figure 4.8 *Excitation spectrum of Tb^{3+} monitored at 546 nm. Intensity normalized to $^5G_6$ transition.*

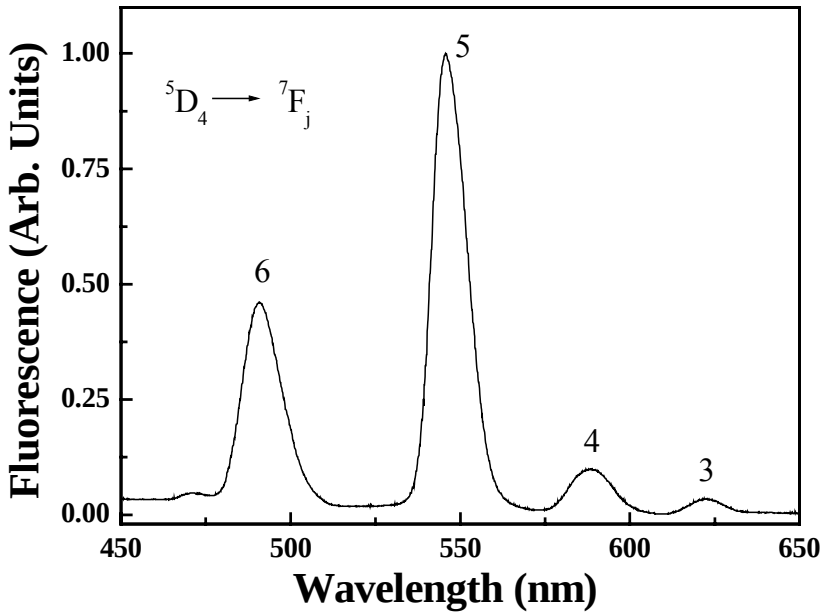

Figure 4.9 *The Fluorescence spectrum of Tb^{3+} excited with 395nm.The intensity is normalized to the $^7F_5$ transition.*

gives the peak position, peak width and the branching ratios for Tb^{3+}. Similar arguments as for that of Eu^{3+} apply for the quantum yield. The separation of the fluorescing level to the highest excited state here is about 15000 cm^{-1} which means the host does not contribute to the nonradiative decay. The concentration

Table 4.2 *The Peak position, peak widths and the branching ratios from the fluorescence spectrum of Tb^{3+}*

Transition from $^5D_4$ to ^7F_j	Peak position (nm)	Peak width (nm)	Branching ratio
6	491	12.56	0.32
5	546	10.20	0.59
4	589	12.83	0.07
3	623	10.90	0.02

quenching effects are also absent as can be seen from the fluorescence intensity increases linearly with the concentration of Tb^{3+} as seen in the figure 4.10 and the branching ratios are also independent of the concentration. The lifetimes remain

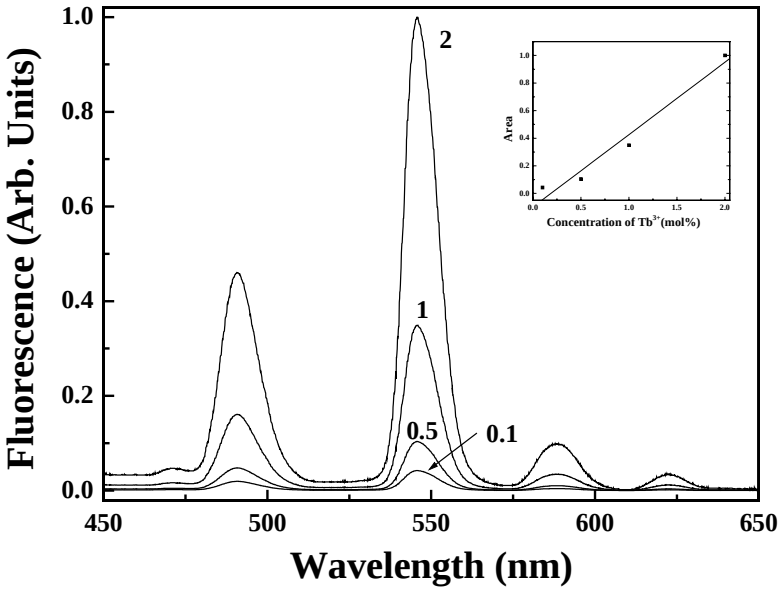

Figure 4.10 *The fluorescence spectra of the $60PbO+40B_2O_3$: yTb^{3+}. The value of y is indicated on each curve. The inset shows the area under the $^7F_5$ band (solid squares) and the solid line is the linear fit.*

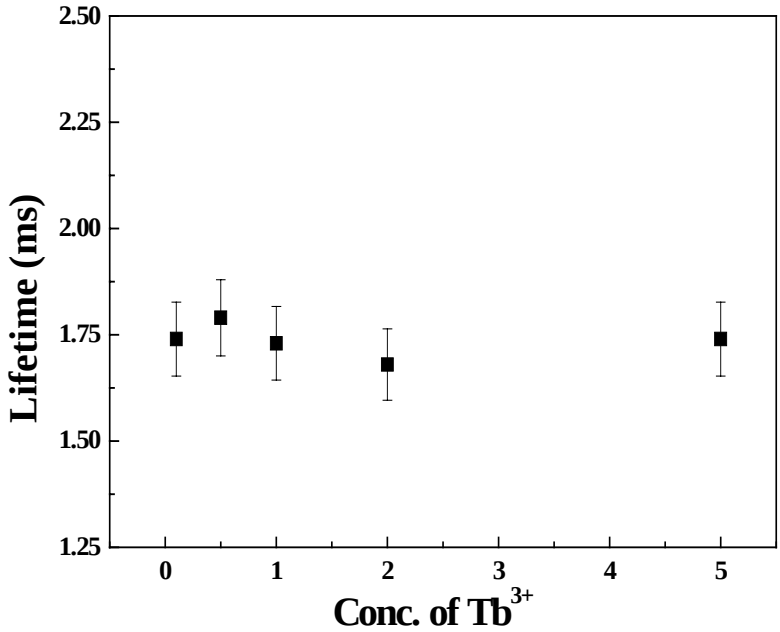

Figure 4.11 *The Tb^{3+} lifetimes as a function of the concentration.*

the same as a function of the concentration as seen in figure 4.11. The lifetimes are measured at 546 nm by exciting the samples with the second anti-Stokes line from the Raman cell at 369 nm. The decay are single exponential for all the samples. A typical decay curve is shown in figure 4.12.

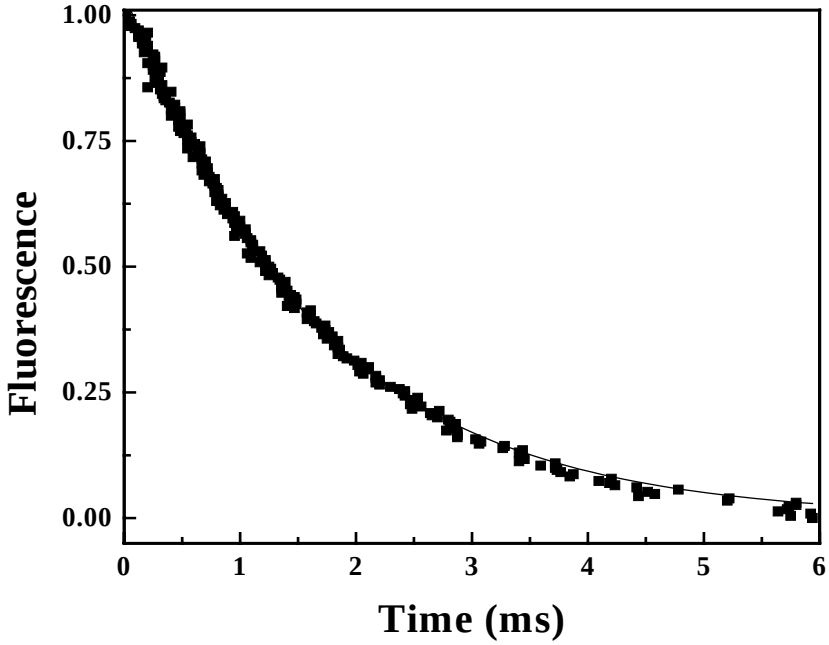

Figure 12 *A Typical decay curve for the Tb^{3+} in $60PbO+40B_2O_3$ glass. Squares are the experimental data and the solid line is the fit to single exponential.*

The lifetimes as a function of the refractive index are plotted in the figure 4.13. The data agrees very well with the real cavity model as expected. The free space lifetime obtained after fitting is 11.10 ms for the virtual cavity and 5.68 ms for the real cavity. The dashed line is the fit to the virtual cavity and the solid line is the fit for the real cavity.

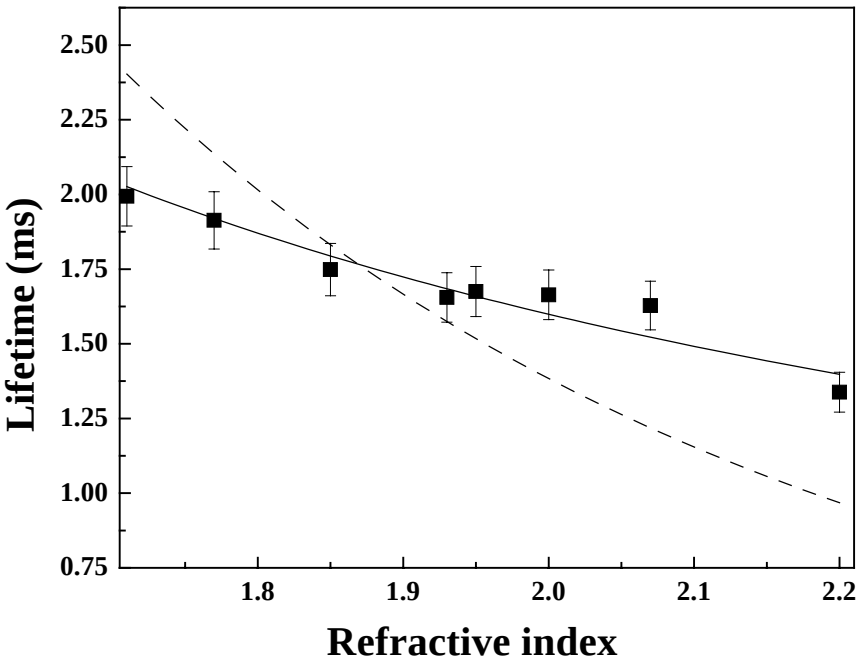

Figure 4.13 *The lifetime as a function of the refractive index for Tb^{3+}. The solid squares are the experimental data. The dashed line is the fit for the virtual cavity model and the solid for the real cavity.*

The study of the lifetimes of the Eu^{3+} and Tb^{3+} clearly show that the real cavity model gives an accurate and consistent description of the lifetimes in transparent dielectrics. The question as to why this model is applicable can be easily understood by considering the more general equation for the spontaneous emission probability of an emitter in a cavity of radius a inside a dielectric of polarisability α [25]

$$A(n) = A(0)\ \frac{9n^5}{[2n^2 + 1 - (2\alpha / a^3)(n^2 - 1)]^2} \qquad (22)$$

This is a more general case as both the real and the virtual cavity equations can derived starting from this equation. The real cavity case is straightforward, if the second term in the denominator goes to zero then the equation for the real cavity follows. This is possible either the radius is large or the polarizability is small.

For the case of the virtual cavity, the average polarizability within the cavity should be equal to that of the surrounding medium.

$$\frac{3\alpha}{4\pi a^3} = N_{diel}\alpha_{diel} \tag{23}$$

where N_{diel} and α_{diel} are the number density and the polarizability of the constituents of the dielectrics. N_{diel} and α_{diel} are related to the refractive index of the dielectric through the Clausius-Mossotti relation as

$$\frac{4\pi N_{diel}\alpha_{diel}}{3} = \frac{n^2 - 1}{n^2 + 2} \tag{24}$$

substituting this equation back gives the equation for the virtual cavity. The polarizability of the rare-earths is in the order of 10^{-24} cm^3 [26]. In order that the second term in the denominator become significant the value of a should be of the order of the 1Å, which is too small to be expected. The value of '*a*' is of the order of a nanometer, which will be evaluated in the next chapter. So as a result the real cavity model can be expected. The question of applicability of the particular model is dealt in terms of substitutional and interstitial [27,28] atoms and it was shown that the real cavity model applies for the substitutional atoms and the virtual cavity for the interstitial atoms. It was also shown that for a disordered system the substitutional case occurs prevalently for the impurity atoms.

4.6 Conclusion

The lifetimes of Eu^{3+} and Tb^{3+} are measured as a function of the refractive index in order to investigate which local field model is appropriate for the description of the lifetimes in a dielectric. The contributions from the nonradiative decay, in these ions, can be neglected because of the large separation of the energy levels. The fluorescence measurements are performed as a function of the concentration of the dopants. The fluorescence intensity increases linearly

with the concentration. The lifetimes remain unaffected by the concentration. The measured lifetimes are radiative, and the change in the lifetimes with refractive index is due to the local field effects. The lifetimes as a function of the refractive index are fitted to the equations for the two local field models. The real cavity model fits the data very well.

4.7 References

1. G. Nienhuis and C. Th. J. Alkemade, Physica, **81C**, 181 (1976).
2. A. Martin, Phil. Mag. **8**, 550 (1929).
3. R. P. Bell, Trans. Farady Soc. **27**, 797 (1931).
4. M. Born and E. Wolf, *Principles of Optics*, (Cambridge University Press, Cambridge 1999), chapter 2.
5. R. W. Boyd, *Nonlinear Optics* (Academic press inc. 1992) chapter 3.
6. J. D. Jackson, *Classical Electrodynamics*, (John Wiely & Sons, New York, 1962) chapter 4.
7. C. J. F. Bottcher, *Theory of Electric Polarization*, (Elsevier, Amsterdam, 1973) chapter 2.
8. J. Knoester and S. Mukamel, Phys. Rev. A **40**, 7065 (1989).
9. J. P. Dowling and C. M. Bowden, Phys. Rev. Lett. **70**, 1421 (1993).
10. A. S. Manka, J. P. Dowling, C. M. Bowden, and M. Fleischhauer, Phys. Rev. Lett. **73**, 1789 (1994).
11. J. J. Maki, M. S. Malcuit, J. E. Sipe, and R. W. Boyd, Phys. Rev. Lett. **67**, 972 (1991).
12. P. W. Milonni, J. Mod. Opt. **42**, 1991 (1995).
13. M. E. Crenshaw and C. M. Bowden, Phys. Rev. Lett. **85**, 1851 (2000).
14. R. J. Glauber and M. Lewenstien, Phys. Rev. A, **43**, 467 (1991).
15. R. Friedberg, S. R. Hartmann and J. J. Manassah, Phys. Rep. **C7**, 101 (1973).
16. R. Friedberg, S. R. Hartmann and J. J. Manassah, Phys. Rev. A **39**, 93 (1989).

17. R. Friedberg, S. R. Hartmann and J. J. Manassah, Opt. Commun. **75**, 263 (1990).
18. V.A. Sautenkov, H. V. Kampen, E.R. Eliel and J. P. Woerdman, Phys. Rev. Lett. **77**, 3327 (1996).
19. H. V. Kampen, V.A. Sautenkov, C.J. C. Smeets, E. R. Eliel and J. P. Woerdman, Phys. Rev. A **59**, 271 (1999).
20. S. T. Cundiff, Laser phys. **12**, 1073 (2002).
21. F. Hache, D. Ricard and C. Flyzanis, J. Opt. Soc. B **12**, 1647 (1986).
22. V. V. R. K. Kumar, A. K. Bhatnagar and R. Jagannathan, J. Phys. D **34**, 1563 (2001).
23. J. M. F. V. Dijk and M . F. H. Schuurmans, J. Chem. Phys. **78**, 5317 (1983).
24. A. J. Kenyon, Prog. in Quant. Electron. **26**, 225 (2002).
25. G. L. J. A. Rikken and Y. A. R. R. Kessener, Phys. Rev. Lett. **74,** 880 (1995).
26. A. F. Wells, Structural *Inorganic chemistry* (Calderon press, Oxford, 1975) page 267.
27. P. de. Vries and Ad Lagendijk, Phys. Rev. Lett. **81**,1381 (1998).
28. F. J. P Schuurmans, P. de. Vries and Ad Lagendijk, Phys. Lett. A **264**, 472 (2000).

Chapter 5

Lifetimes in Absorbing Dielectric

The term absorbing dielectric here refers to the environment of the fluorescing ion which gives rise to the nonradiative energy transfer of excited energy. Two different systems involving the process of energy transfer have been investigated. The first system is Eu^{3+}- Nd^{3+} co-doped binary glass. The affect of Nd^{3+} on the lifetimes of Eu^{3+} has been studied. The second system is the Sm^{3+} doped glass. The interaction among the Sm^{3+} ions leads to the shortening of its lifetimes. The lifetimes depend on the refractive index (real and imaginary) and the radius of the cavity. The data has been analyzed to obtain the radius of the cavity.

5.1 Energy Transfer between Rare-earths

An excited atom can relax to the ground state radiatively or non-radiatively. In the former, a photon is emitted while in the latter case the excited state looses its energy without the emission of a photon. The results of the previous chapter were that of radiative decay. Usually, the excited atom decays promptly by means of nonradiative transitions to a lower excited state, and then decays to the ground state. For example, in the previous chapter, Eu^{3+} is excited to $^5D_1$ from where it undergoes a nonradiative transfer to the fluorescing level $^5D_0$. Larger the energy gap between the states, the greater is the probability of the radiative decay, i.e. if the energy difference is small, the probability of the nonradiative decay increases. As a guide, it is generally held that if the energy gap between the lowest excited state and the highest of the ground states is ten times or more than the highest phonon ($\hbar\omega_{\max}$) of the material then the contribution of multiphonon relaxation will be negligible. If it is between four to ten phonons the probability is small

and if it less than four the probability is high [1-2]. The highest frequency vibrations for the lead-borate glass is observed around 1300 cm^{-1}. The nonradiative energy transfer can occur involving a pair of ions. In the process of energy transfer involving two rare-earth ions, the ion that transfers the energy is known as the donor or sensitizer and the one that accepts is known as the acceptor or the activator. The energy transfer in turn can be either radiative or nonradiative. The radiative transfer is trivial case of absorption by acceptor the light emitted by the donor. This process depends on the geometry of the experiment and can be corrected by exactly measuring the absorption and the emission characteristics of the ions involved. In this process, only the fluorescence intensity of the donor decreases while the lifetimes are not affected. This is sometimes referred to as inner filter effect. In the nonradiative energy transfer the donor decays without the emission of a photon. This process results in the decrease of the fluorescence intensity as well as the lifetimes of the donor. Figure 5.1 gives the schematic diagram of the decay of the excited state of an atom. The nonradiative decay can occur among a pair of ions of the same type i.e. both the donor and the acceptor are of the same type. When the concentration is low, the rare-earths are evenly distributed in the glass matrix and there is no interaction among the ions. But when the concentration is increased the inrteratomic distance decreases and the ions start interacting. This leads to the phenomenon known as concentration quenching. In concentration quenching both the fluorescence intensity and the lifetimes are reduced with respect to the low concentration values. There are mainly three types of interactions [1] among the same rare-earths – (a) Co - operative upconversion, (b) Energy migration and (c) cross relaxation. Co - operative upconversion relies on the two interacting ions being in the metastable state. In this process, the donor in the metastable state decaying to the ground state couples to the acceptor such that the acceptor goes from the metastable state to a higher level as shown in figure 5.2a. In energy migration, the donor is in the excited state and the acceptor is in the ground state. The donor decays to the ground state and thereby promoting the nearby acceptor into the excited state. The probability of nonradiative decay increases with

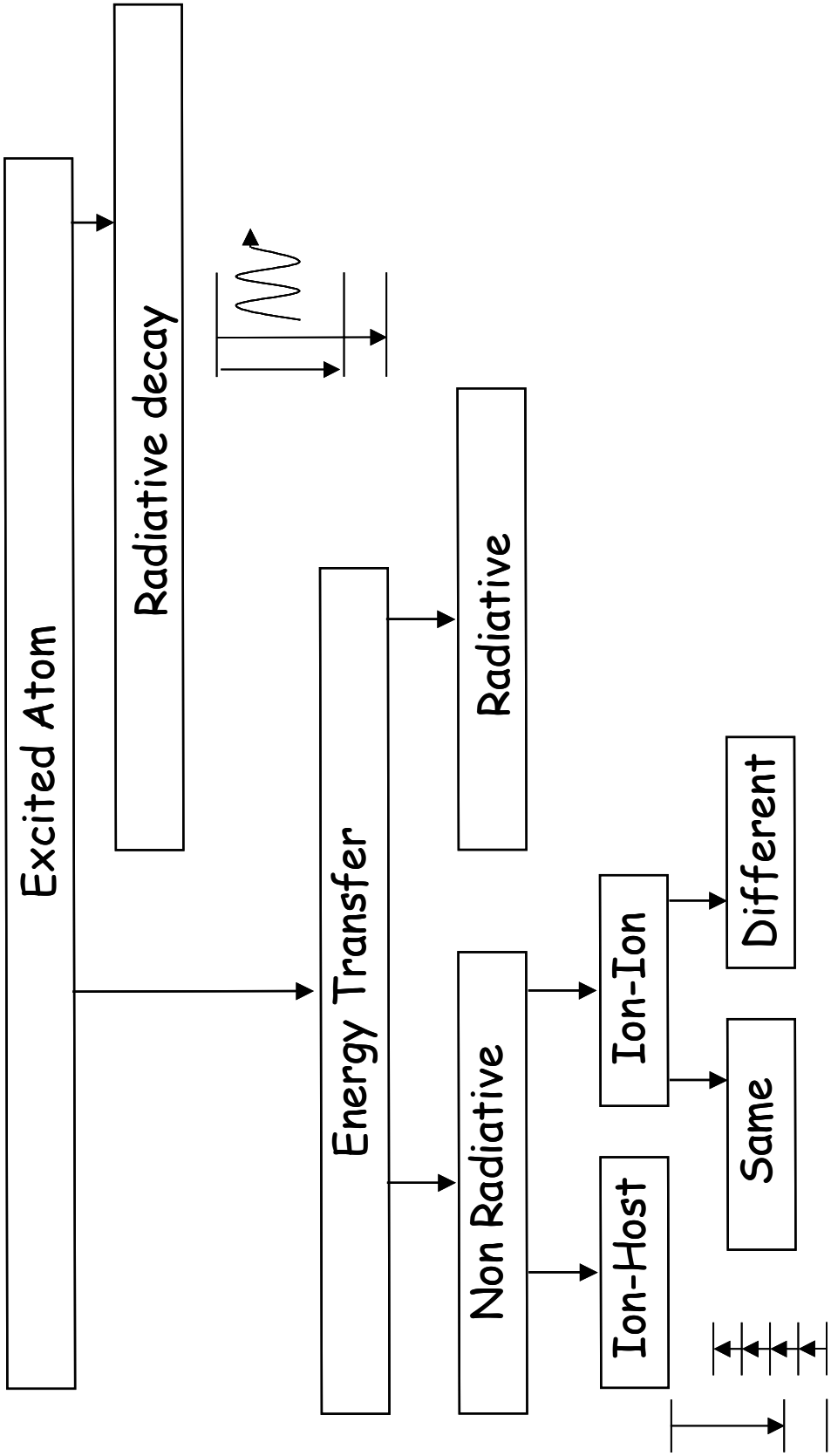

Figure. 5.1 Various processes responsible for the de-excitation of an excited atom.

successive such transfers. Figure 5.2b depicts the process of the energy migration. Cross relaxation (Figure 5.2c) is process in which the donor decaying from a highly excited state promotes the acceptor from the ground state to the metastable state. The energy transfer can occur between two different rare-earths [3-7]. Some of the processes are depicted in figure 5.3. In figure 5.3a the donor decaying from excited to the ground state can promote the acceptor from state 1 to the state 3 if the state 1 is populated. This scheme is used in the IR detection, i.e. if there is a fluorescence [8] from 3 to 0 of the acceptor, it implies the presence of the IR radiation at the wavelength of 0 to 1. In figure 5.3b successive transitions from the donor transfers the energy to the acceptor promoting it to level 2 [9,10]. Also it is possible that the energy from two ions is transferred to a single third ion promoting it to the excited state [11,12] as shown in figure 5.3c. The energy transfer between and to the rare-earths finds wide application in sensitizing solid state and glass lasers [13,14], infrared quantum [15] counters as well as the infrared to the visible converters [16,17].

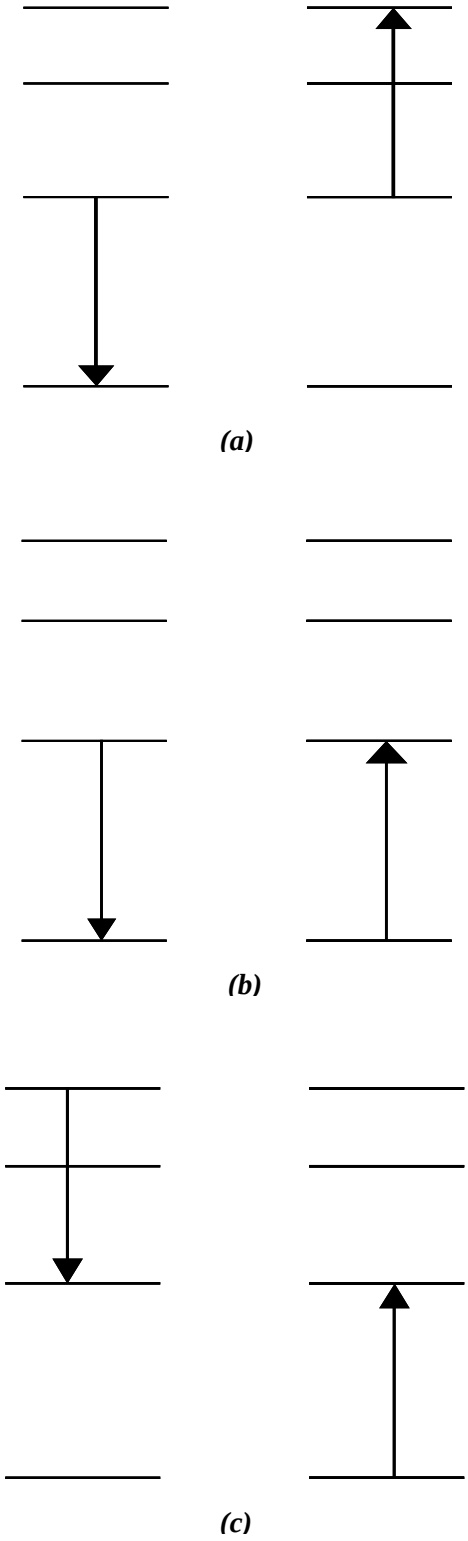

Figure 5.2 *(a) Co-operative upconversion, (b) Energy Migration and (c) Cross relaxation*

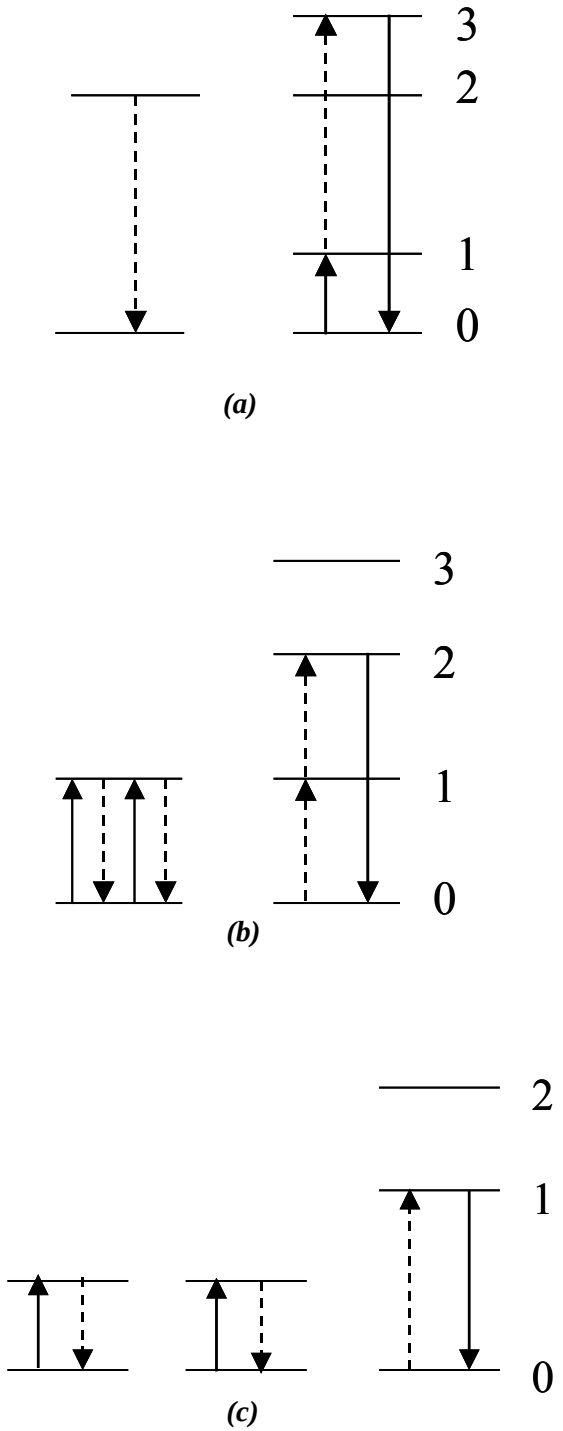

Figure 5.3 *Interactions between two different types of ions. Dashed line represents the energy transfer.*

The energy transfer depends on the concentration of the acceptors. Hence in order to probe these effects, the fluorescence needs to be studied as a function of the concentration of the donors. For a resonant energy transfer the rate of transfer is given as [18]

$$A = \frac{2\pi}{\hbar}\left|\left\langle \Psi_D, \Psi_A^* \middle| H \middle| \Psi_D^*, \Psi_D \right\rangle\right|^2 \int g_F(E) g_A(E) dE \quad (1)$$

where Ψ_D *and* Ψ_D^* are the ground and excited states of the donor and Ψ_A *and* Ψ_A^* are the ground and excited states of the acceptor; the integral is over the normalized emission band shape of the donor and the absorption of the acceptor in which the transitions D to D^* and A^* to A are represented by the lineshape functions g_F (E) and g_A (E) respectively. H is the Hamiltonian describing the interaction between the donor and the acceptor. The Hamiltonian may contain terms describing the different types of interactions- electric dipole-dipole ($\sim R^{-6}$), electric dipole-quadrapole ($\sim R^{-8}$) and electric quadrapole - quadrapole ($\sim R^{-10}$), where R is the distance between the ions. The energy transfer probabilities can be calculated from the donor fluorescence intensities as a function of the acceptor concentration or the lifetimes of the donors as a function of the concentration of the acceptors. The transfer probabilities can be calculated by measurement of the lifetimes of donor in the presence and the absence of the acceptors as [19]

$$P_{da} = \frac{1}{\tau} - \frac{1}{\tau_0} \quad (2)$$

where τ_0 is the lifetime of the pure donor and τ is the lifetime in the presence of the acceptor. The nature of the interaction among the ions can be deduced from the transfer probability. For the dipole-dipole interaction, the transfer probability follows a linear relationship to the square of the sum of the donor and the acceptor concentrations.

In the quantum electrodynamic approach to the problem, the problem is treated in terms of the quantized electromagnetic equations. And the total decay rate is written as

$$A = A^{\perp} + A''$$

Where $A^{\perp}$ is associated with the transverse decay rate and A'' to the longitudinal decay rate. A classical treatment of the spontaneous emission leads to the local field correction factor for a real cavity as [20,21]

$$l(n) = \left| \left(\frac{3n^2}{(2n^2+1)} \right) \right|^{-2} \tag{4}$$

for an atom in dielectric of refractive index $n(\omega) = \sqrt{\varepsilon} = \eta(\omega) + i\kappa(\omega)$. This equation however does not take into account the fluctuating component of the polarization associated with the absorption losses. Scheel *et al* performed the complete calculation including the fluctuating component of the polarization and the spontaneous emission rate derived by them leads to transverse decay rate has the form [22]

$$\begin{aligned} \frac{A}{A_0} = \quad & \frac{9\varepsilon_I(\omega_A)}{|2\varepsilon(\omega_A)+1|^2}\left(\frac{c}{\omega_A R}\right)^3 + \\ & \frac{9\varepsilon_I(\omega_A)[28|\varepsilon(\omega_A)|^2 + 12\varepsilon_R(\omega_A)+1]}{|2\varepsilon(\omega_A)+1|^4}\left(\frac{c}{\omega_A R}\right) + \\ & \frac{9\eta(\omega_A)}{|2\varepsilon(\omega_A+1)|^4}[4|\varepsilon(\omega_A)|^4 + 4\varepsilon_R|\varepsilon(\omega_A)|^2 + \varepsilon_R{}^2(\omega_A) \quad \varepsilon_I{}^2(\omega_A)] \\ & \frac{9\kappa(\omega_A)}{|2\varepsilon(\omega_A+1)|^4}[4|\varepsilon(\omega_A)|^2 + 2\varepsilon_R(\omega_A)] + O(R) \end{aligned} \tag{5}$$

$$\varepsilon_R = \eta^2 - \kappa^2 \text{ and } \varepsilon_I = 2\eta\kappa$$

Unlike the earlier works where the transverse decay rate was attributed to the radiative decay and the longitudinal rate to the nonradiative decay, here the longitudinal decay rate is essentially zero. The transverse decay rate contains R

dependent terms. The radius independent terms may be interpreted as contribution of the far field that gives rise to the radiative decay rate. The R dependent terms are a contribution of the near field that gives rise to the nonradiative decay. In particular, the terms proportional to R^{-3} can be regarded as being the rate of the dipole-dipole energy transfer from the atom to the medium. When $\varepsilon_I \rightarrow 0$ the R independent term is the leading term, and the equation reduces to that of transparent dielectric. In this equation, all the parameters except for the radius of the cavity are measurable. Therefore this enables us insight into an estimate of the radius of the cavity around the fluorescing ion. The following section describes the experimental results on the lifetimes of Eu^{3+} and Sm^{3+}. The imaginary part of the refractive index is calculated from the absorption spectra. The data has been analyzed using the Eq.(5) in order to obtain the value for the radius of the cavity. The value obtained for radius is determined only up to some factor as not only the radius but also the scaling factors of the absorption - assisted terms are undetermined in this model.

5.2 Eu^{3+} - Nd^{3+} system

As mentioned in the previous section, for an efficient energy transfer to occur, the absorption level of the dielectric should be as close as possible to the fluorescing level of the donor i.e. the energy difference between the donor's fluorescing level and the acceptor's energy level should be as small as possible. In other words, the levels should be matched. Among all the rare-earths, Nd^{3+} has the closest matched level to the fluorescing level $^5D_0$ of Eu^{3+}. This makes Nd^{3+} a good candidate to dope it with Eu^{3+} for this experiment. In Eu^{3+}- Nd^{3+} system, Eu^{3+} acts as a donor and Nd^{3+} as an acceptor. The glass together with the Nd^{3+} can be considered as the 'absorbing dielectric'. Preferably, the acceptor should not have any absorption at the pump wavelength used for the excitation of the donor. And if the absorption is present, the acceptor should not fluoresce in the region of interest of donor's fluorescence. Energy transfer studies involving Nd^{3+} have been widely studied as an acceptor in the fluorescence sensitization experiments because of its wide usage as a lasing ion. Both, the d-block elements

[23-25] and rare-earths including Eu^{3+} [26-28] have been investigated as the donor in these studies. As seen in figure 5.4, Nd^{3+} has a strong absorption centered a round 582nm, which is in resonance with the fluorescing level, $^5D_0$ of Eu^{3+}. The ground state of Nd^{3+} is $^4I_{9/2}$. The peak at 582 nm corresponds to the transition to the level ($^4G_{5/2,}$ $^2G_{7/2}$). Nd^{3+} also has also small absorption due to the

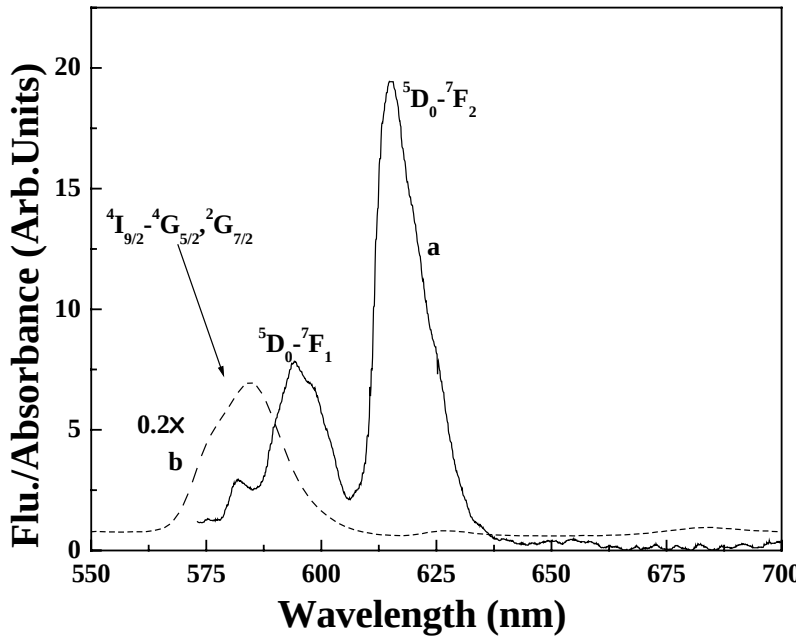

Figure. 5.4 *Fluorescence spectrum (solid line) of Eu^{3+} and the absorption spectrum (dashed line) of Nd^{3+}.*

energy level $^4G_{7/2}$ centered at 528 nm which extends to 532 nm i.e. the excitation wavelength used. But, the lifetime of this level is much smaller than the lifetimes of Eu^{3+} and hence decays very fast. So, virtually this is equivalent to having no absorption as far as the energy transfer process is concerned. The entire process of energy transfer involving these ions can be summed up as follows (figure 5.5)-

1. The excitation wavelength at 532 nm populates $^5D_1$ of Eu^{3+} and $^4G_{7/2}$ of Nd^{3+}.
2. Nd^{3+} undergoes nonradiative relaxation to the lower levels. And Eu^{3+} relaxes to $^5D_0$ nonradiatively.

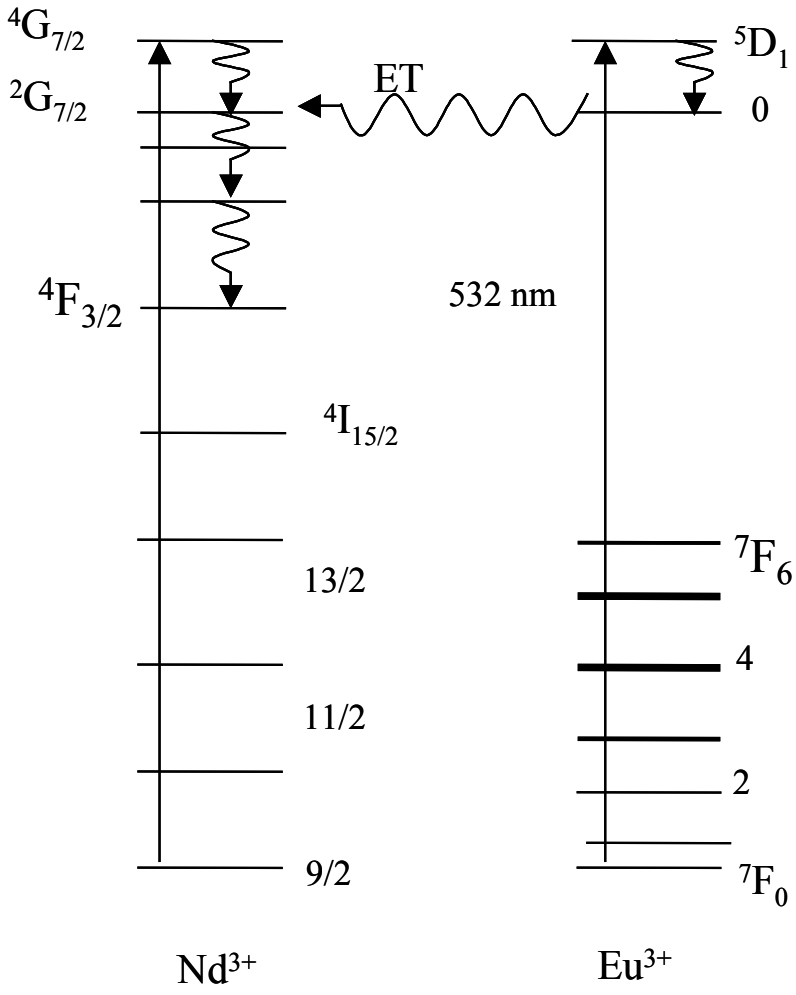

Figure 5.5 *The representative energy level diagram of Nd^{3+} and Eu^{3+}. The wavy line represents the non-radiative decay and ET is the energy transfer*

3. Eu^{3+}, in addition to the radiative decay of $^5D_0$ to ^7F_j, also transfers energy to ($^4G_{5/2}$, $^2G_{7/2}$) of Nd^{3+}.

4. $^4G_{5/2}$, $^2G_{7/2}$ of Nd^{3+}decays nonradiatively to lower levels.

The concentration of Nd^{3+} was gradually increased in the glass system xPbO + (100-x) B_2O_3 : $1Eu^{3+}$. The concentration of PbO was varied in steps of 10 from 30

to 90. The concentration of Nd^{3+} was varied from 0.05 to 1 mol%, and 0.1,0.25, 0.5 mol% being the intermediate concentrations. A total of seven sets of samples have been prepared with five different concentrations of the Nd^{3+}. A particular value of x corresponds to one real refractive index and the increasing content of Nd^{3+} corresponds to increasing value of the kappa. As the peak around 582 nm is responsible for the energy transfer, the values of κ have been obtained by taking the area under this peak from the absorption spectrum of Nd^{3+}. The value of κ are in the order 0.5×10^{-6} for lowest Nd^{3+} concentration and 9.5×10^{-6} for the highest Nd^{3+}.

The fluorescence intensity measurements show that the overall intensity decreases when the concentration of Nd^{3+} increases. Figure 5.6 shows the fluorescence of Eu^{3+} in $70PbO+30B_2O_3$ glass with different concentrations of Nd^{3+}. The spectra are normalized to the peak intensity of the strongest emission at 613 nm for the sample without Nd^{3+}. Inset of the figure shows the area under the 613 nm peaks as a function of the Nd^{3+} concentration. In addition to the quenching of Eu^{3+} by the Nd^{3+}, the partial absorption of the excitation energy

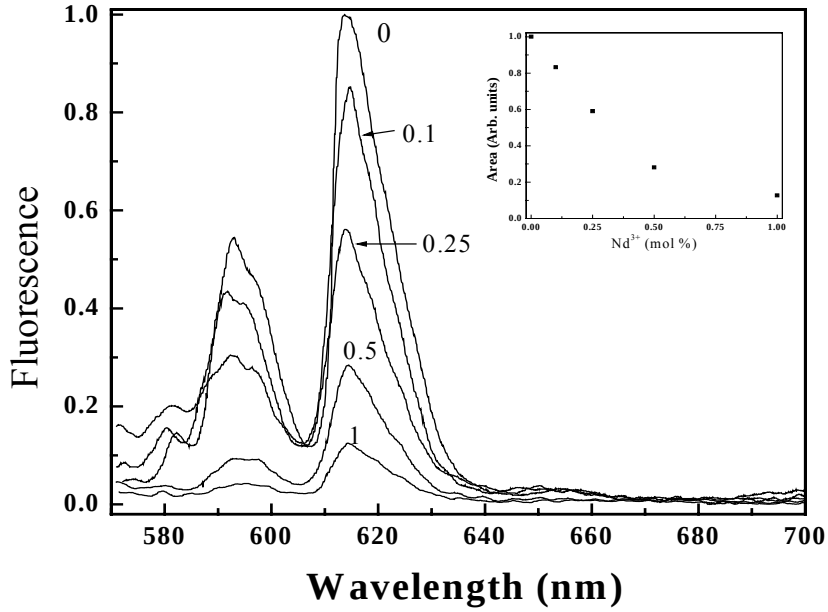

Figure 5.6 *Fluorescence spectrum of Eu^{3+} in the presence of varying amounts of Nd^{3+}. Number on each curve denotes the Nd^{3+} concentration. Inset shows the area under the peak centered at 613 nm.*

(532 nm) by Nd^{3+} itself could also be responsible for the decrease in the fluorescence intensity. There is no reverse energy transfer- i.e. from Nd^{3+} to Eu^{3+}. The excitation spectrum of Eu^{3+}, both in the absence and in the presence of Nd^{3+} are identical. The measured lifetimes also decrease with the increasing concentration of Nd^{3+}. The change in the measured lifetimes can be attributed to the energy transfer from Eu^{3+} to Nd^{3+}. As seen in figure 5.7 the decays show a deviation from the single exponential nature for higher Nd^{3+} concentrations.

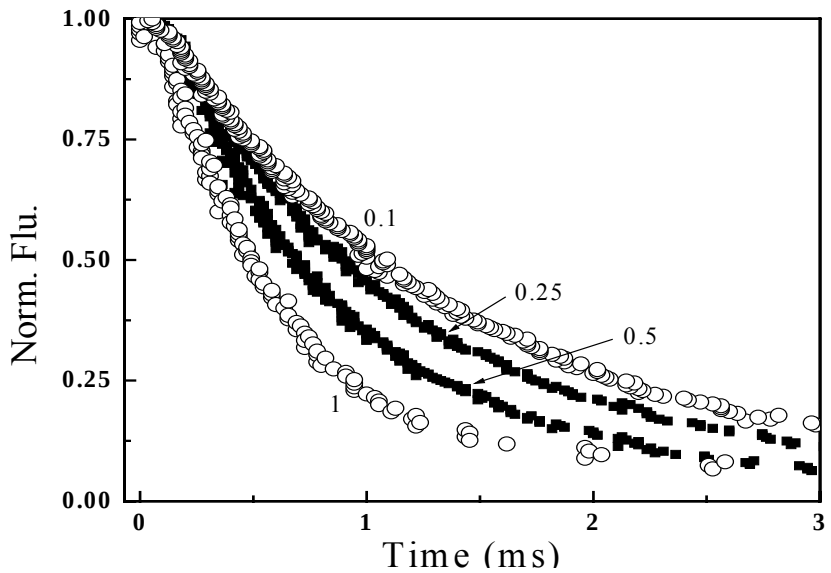

Figure 5.7 *Fluorescence decay curves of Eu^{3+} in the presence of varying amounts of Nd^{3+}.*

The lifetimes for all the samples have been taken to be as those obtained by a single exponential fit. The decrease in the lifetimes is a consequence of the energy transfer. The nature of this energy transfer is dipole-dipole interaction. This can be seen in figure 5.8. In the figure the transfer probability is plotted as a function of the square of the sum concentrations of Eu^{3+} and Nd^{3+}. The straight line indicates that the energy transfer is dipole-dipole in nature.

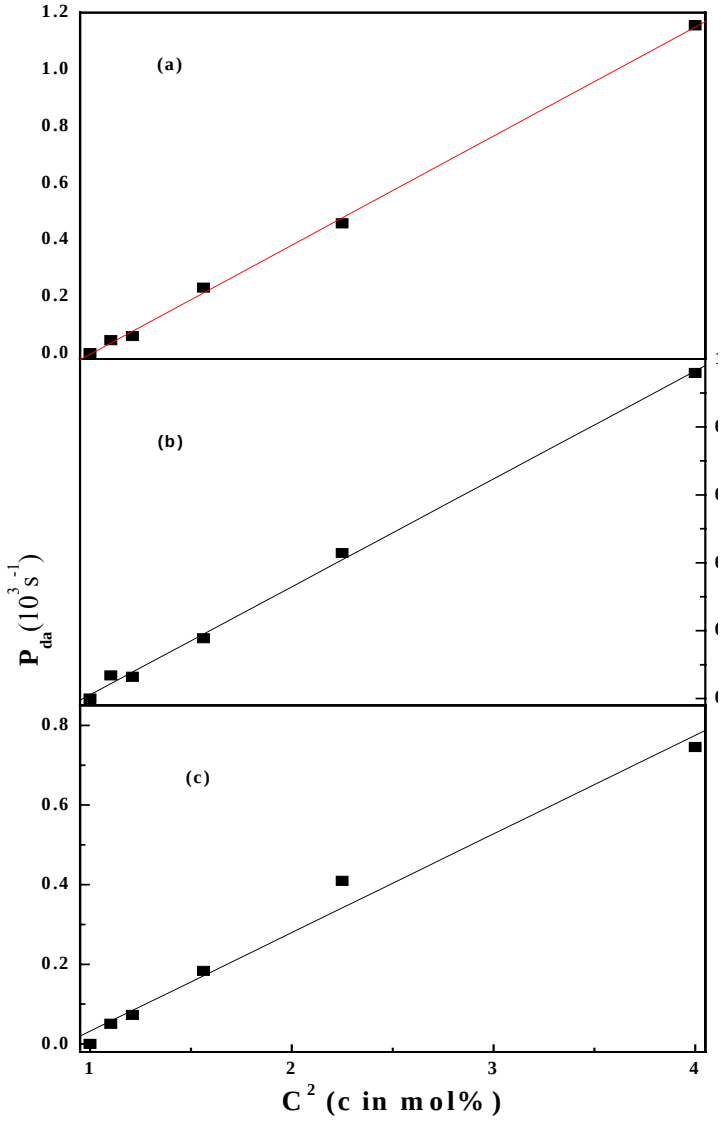

Figure 5.8 *Transfer probability as a function of the square of the concentration in (a) 40PbO (b) 60PbO and (c) 80PbO glass. Linear dependence shows the dipole-dipole interaction.*

The data has been fitted using Eq.(5). The data can be viewed in two different ways – (i) Fixing the real part of the refractive index and plotting the lifetimes as a function of the imaginary part (ii) fixing the imaginary part and plotting the lifetimes as a function of the real part. In other words, for a fixed composition of glass, lifetimes as function of Nd^{3+} concentration or for a fixed value of Nd^{3+} concentration lifetimes as a function of the composition of the glass. The lifetimes depend on both the real and imaginary parts of the refractive

index and R. The refractive index can be measured, whereas the R cannot be measured directly. Therefore the analysis of this data enables the determination of R. First, the data has been fitted by plotting lifetimes as a function of the imaginary part of refractive index. All the seven sets of data have been analyzed individually using the Eq.(5). There are four parameters in the equation – refractive index (real and imaginary), free space lifetime and the parameter R. The values η and κ have been assigned the measured values. The imaginary part shows a decrease as one goes from lower value of real refractive index to the higher value because of the decrease of number of Nd^{3+} ions. The other two parameters, R and the free space lifetime can be floated. The analysis of the lifetimes in a transparent dielectric in the previous chapter yielded the value of the free space lifetime to 4.57 ms. So that leaves R as the parameter that needs to be fixed. In figure 5.9 the lifetimes of Eu^{3+} as a function of the absorption with different real part of the refractive index and the fittings using the equation are shown. The least square fit yielded the value to be 1 ± 0.05nm for R. The experiments involving energy transfer from one rare-earth to another have shown that the multipolar interactions can occur over the distances of 2 nm [29].

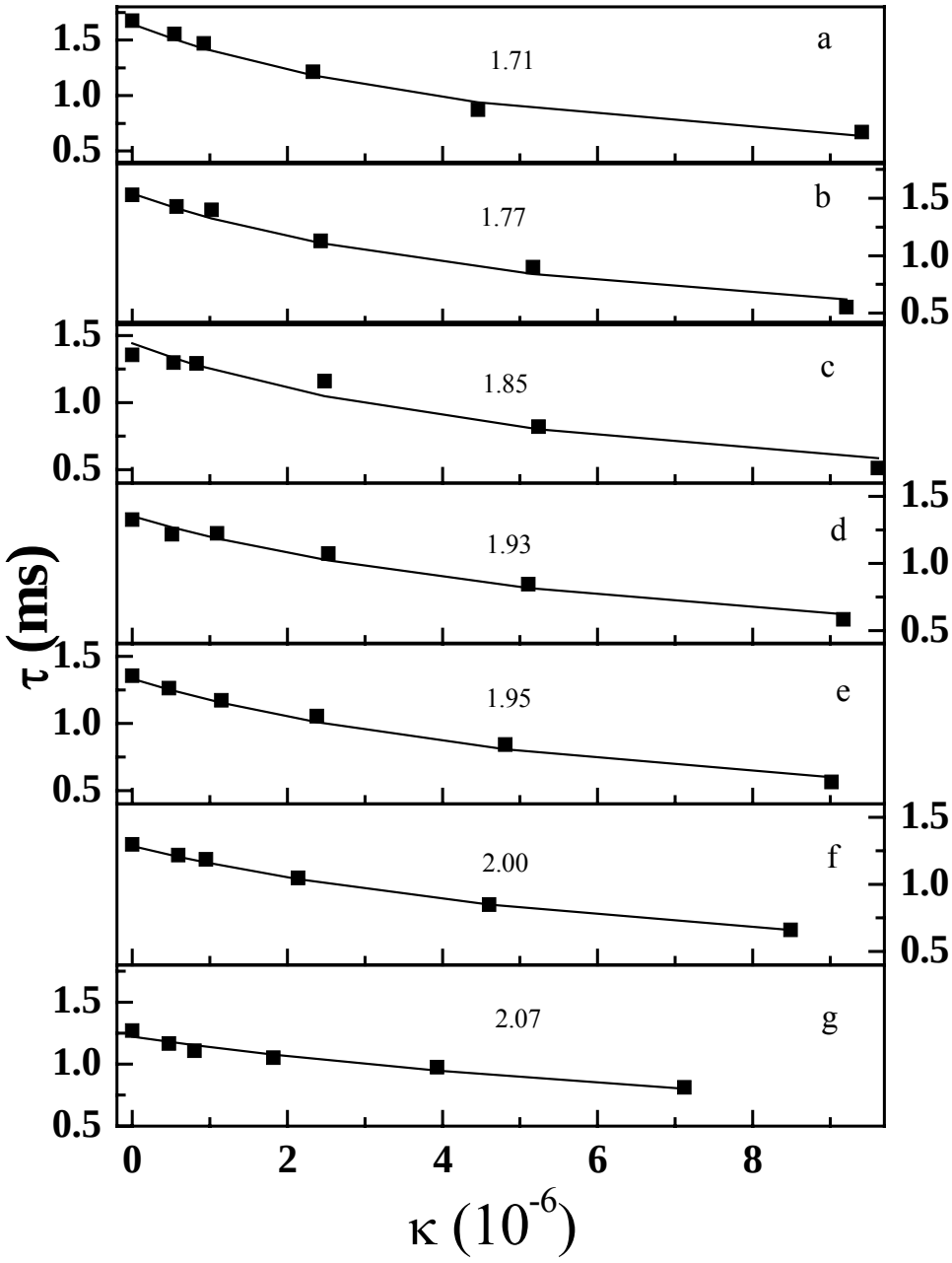

Figure 5.9 *Lifetimes as a function of the imaginary refractive index at different real refractive index indicated on each curve. The value of R (in nm) obtained from the fit (a) 1.05 (b)1.01 (c)0.97(d)0.97 (e) 0.94(f)0.97(g)1.04*

Having obtained the value of R at each real refractive index, next, the lifetimes are plotted as a function of the real refractive index for fixed imaginary part. Now, R has been taken from the above analysis and the free space lifetime has

been floated. Figure 5.10 shows the plot of the experimental lifetimes and the theoretical fit with real part of the refractive index as the independent axis. The free space lifetime obtained from the fit changed only slightly as compared to 4.57 ms. The values of the free space lifetime are tabulated in table 5.1.

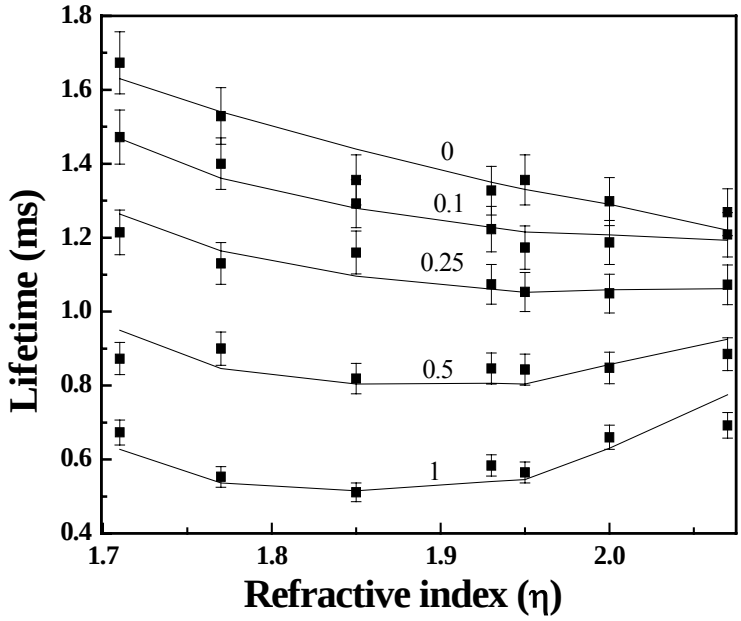

Figure 5.10 *Lifetimes as a function of the real refractive index. The numbers on the curve indicate the concentration of the* Nd^{3+} *concentration.*

Table 5.1 *Free space lifetime,* $\tau(0)$ *obtained in the fitting.*

Nd^{3+} (mol %)	τ (0) (ms)
0.05	4.60
0.1	4.70
0.25	4.75
0.5	4.52
1	4.20

5.3 Concentration quenching in Sm^{3+}

The decay in Sm^{3+} is reported to involve different mechanisms [30-33]. Samarium containing glasses have received relatively less attention than the other rare-earth ions despite many features of interest. For example, it is a promising ion for the spectral hole burning applications. Therefore it would be great importance to study the lifetimes of this ion. Sm^{3+} ion has five electrons in the f shell. The ground state is $^6H_{5/2}$. Though Sm^{3+} is stable ionic state, but is also known to exist as Sm^{2+}. This ion has strong absorption in the IR (low energy) compared to its absorption in the visible (high energy) region as shown in figure 5.11.

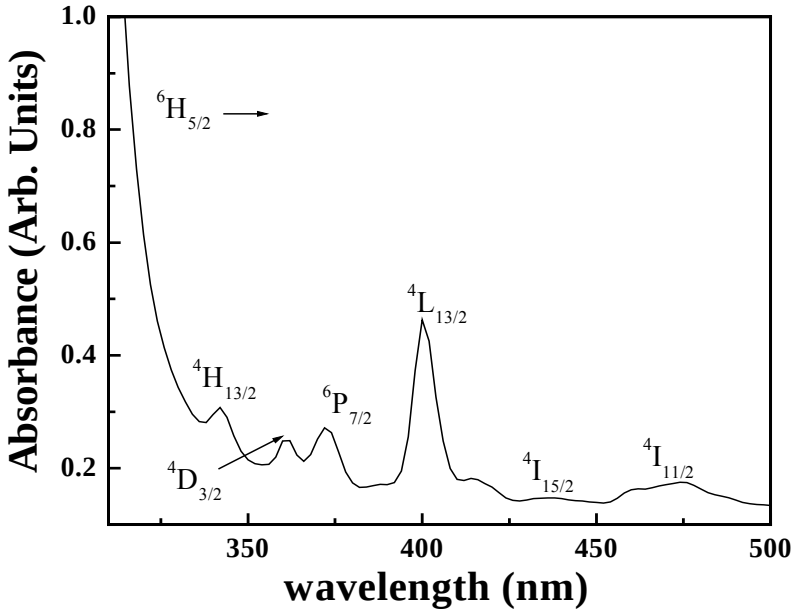

Figure 5.11a *High energy absorption spectrum of* Sm^{3+}.

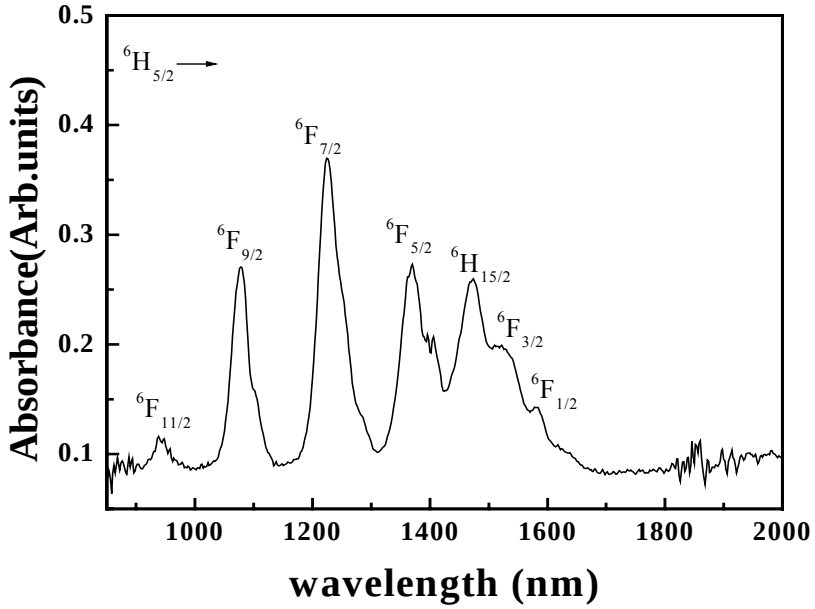

Figure 5.11b *Low energy absorption spectrum of* Sm^{3+}.

When excited with the pump light of 435 nm, $^4I_{15/2}$ is populated and from there it decays nonradiative to $^4G_{5/2}$. The level $^4G_{5/2}$, is the fluorescing level. Figure 5.12 shows the fluorescence spectrum of Sm^{3+}. In the visible region, the fluorescence spectrum consists of three strong bands corresponding to transitions

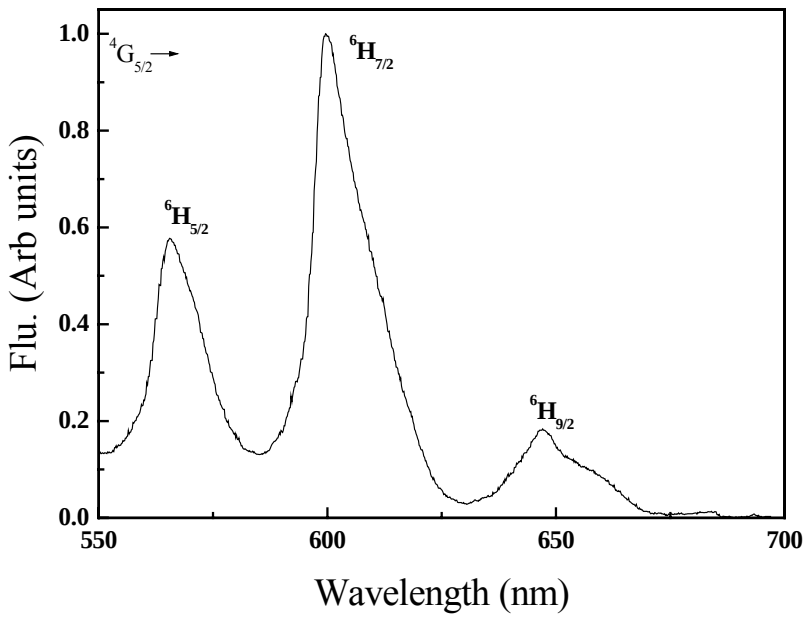

Figure 5.12 *Fluorescence spectrum of* Sm^{3+} *excited with 435 nm. The intensity has been normalized to* $^6H_{7/2}$ *transition.*

$^6H_{5/2}$ (565 nm), $^6H_{7/2}$ (600 nm) and $^6H_{9/2}$ (650 nm). The quantum yield of the fluorescence is small owing to the smaller energy gap (~7000 cm^{-1}) between $^4G_{5/2}$ and the next lower level, $^6F_{11/2}$ and as well as the concentration quenching effects. Quantum yield can be calculated using the lifetime calculated from the Judd-Ofelt theory as

$$Q = \frac{\tau_{meas}}{\tau} \qquad (7)$$

where τ is the lifetime calculated using the Judd-Ofelt theory and τ_{meas} is the measured lifetime. The calculated values of the branching ratios and the quantum

Table 5.2 *The center wavelength (λ), experimental branching ratio (β_{exp}), branching ratio from J-O theory (β_{cal}), lifetime calculated from J-O theory (τ) and the quantum yield.*

Transition from $^4G_{5/2}$ to ^6H_j	λ (nm)	β_{exp}	β_{cal}
5/2	565	0.32	0.26
7/2	600	0.59	0.33
9/2	650	0.09	0.26
τ (ms)	2.15		
Q	0.44		

yield agree well with the reported values [34,35] and are given in table 5.2 for 1 mol% doping. In the calculation of the lifetimes, the transitions $^6F_{11/2}$ and $^6F_{1/2}$ have not been included, as the reduced matrix elements are not available, which leads to higher lifetimes and smaller value for the quantum yield. Because of the large number of closely spaced energy levels, cross relaxation of the $^4G_{5/2}$ (17,730 cm^{-1}) becomes more probable. The transitions from $^4G_{5/2}$ to $^6F_{11/2}$ (7130 cm^{-1}), $^6F_{9/2}$ (8470 cm^{-1}), $^6F_{7/2}$ (9570 cm^{-1}) and $^6F_{5/2}$ (10,440 cm^{-1}) are closely matched with the absorption bands $^6F_{5/2}$, $^6F_{7/2}$, $^6F_{9/2}$, and $^6F_{11/2}$ respectively [36].

The samples 60PbO + $40B_2O_3$: y Sm^{3+}have been studied. y is varied in the range of 0.05 to 5 mol%. Figure 5.13 shows the absorption coefficient with varying amounts of Sm^{3+}. The fluorescence intensity increased for concentrations upto 0.5 mol%. and then it showed a monotonic decrease. Figure 5.14 shows the area under the fluorescence peak centered at 600 nm as a function of the Sm^{3+}

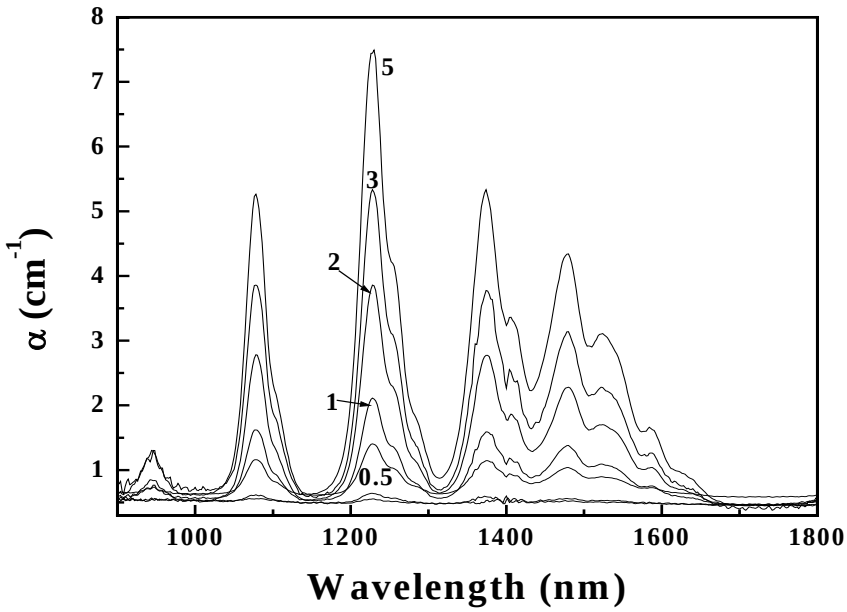

Figure 5.13 *Absorption coefficient of 60PbO + $40B_2O_3$: ySm^{3+}. The number on the figures denote the value of Sm^{3+}concentration.*

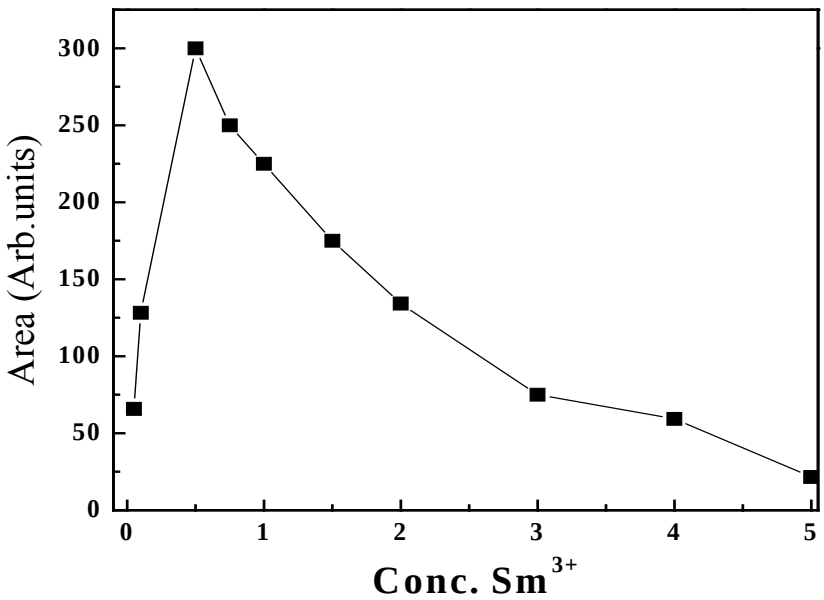

Figure 5.14 *Area under the fluorescence peak centered at 600 nm for the system 60PbO + $40B_2O_3$: ySm^{3+}.*

concentration. This implies that the interaction among the ions is absent upto 0.5mo%. The ions start interacting for the concentrations above 0.5 mol%. The lifetimes are measured at the 600 nm as the fluorescence is maximum at this wavelength. The lifetime remained same at about 1.3 ms for concentrations upto 0.5mol% and decreased monotonically thereafter with the increase in the concentration of the Sm^{3+}. This further verifies that the ions start interacting above the concentration of 0.5 mol%. Figure 5.15 shows the plot of the lifetimes as a function of the concentration of Sm^{3+}. Various interactions have been

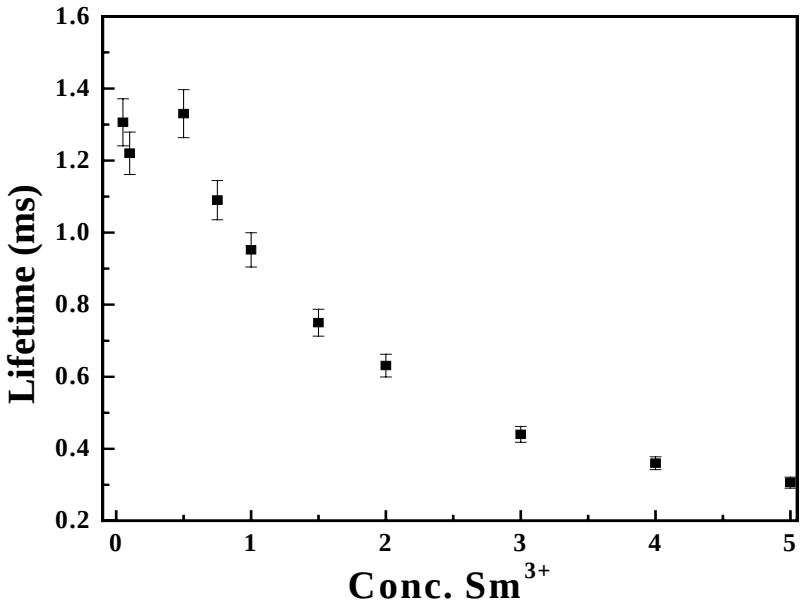

Figure 5.15 *The lifetimes as a function of the concentrations of Sm^{3+}.*

reported to be responsible for the ion-ion relaxation in Sm^{3+} that leads to the quenching of the fluorescence. The plot of the square of the concentration and the transfer probability shows that for concentrations upto 3 mol % the dipole – dipole interaction is more probable as it shows a linear dependence in this region. For the higher concentrations deviations are observed as the decay could be more complex. Figure 5.16 shows the linear region of the plot of the transfer probability as a function of the concentration squared. As the interaction governing here is dipole-dipole, Eq.(5) can be used for the analysis. The imaginary part of the refractive index is calculated as the area under the peaks corresponding to the transitions which are shown to participate in the ion-ion

relaxation. The free space lifetime has been obtained using Judd-Oflet theory. The oscillator strengths are calculated from the absorption spectra and refractive index is set to one for the evaluation of the free space lifetime. The analysis yielded the free space lifetime to be 8 ms. As in the case of Eu^{3+}- Nd^{3+} analysis of

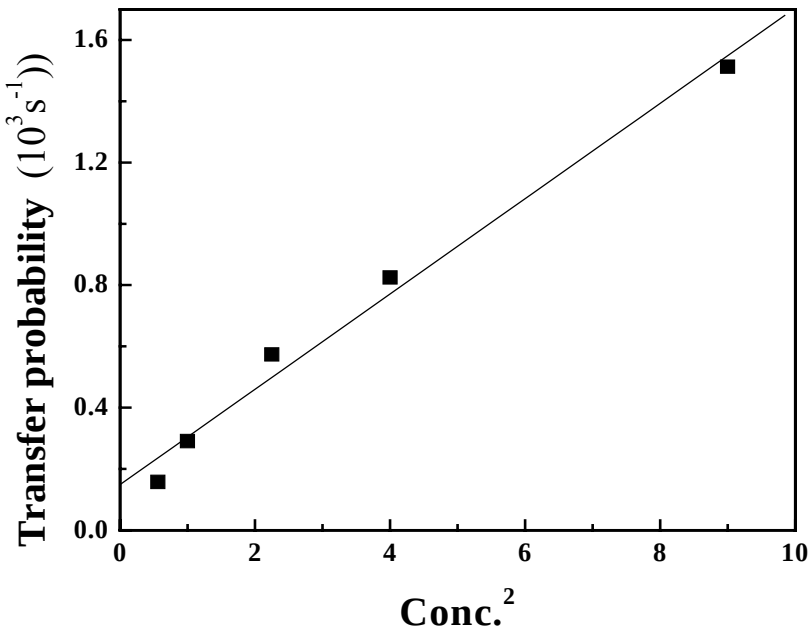

Figure 5. 16 *Transfer probability as a function of the concentration squared.*

.

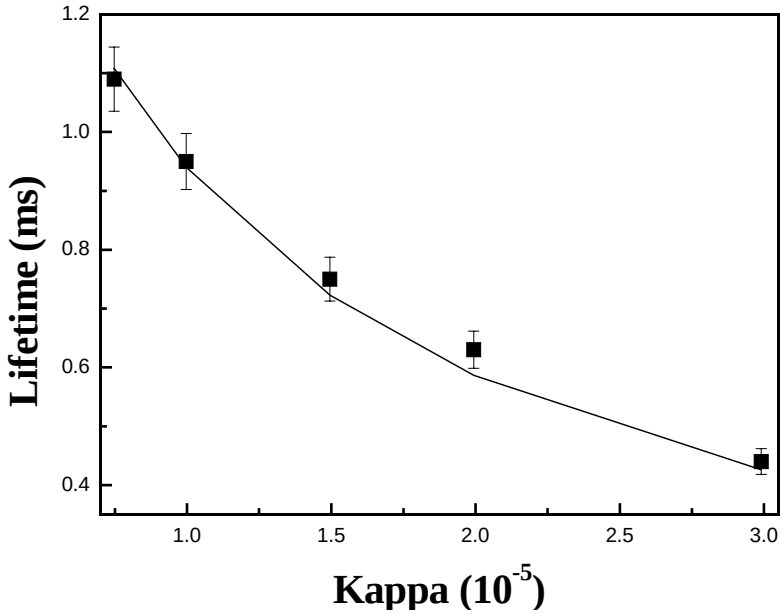

Figure 5.17 *A Fit using Eq.(5). Solid line is the fit to the experimental data (squares).*

the data using the Eq.(5) (Figure 5.17), the radius of the cavity has been floated. The analysis of the lifetimes using the equation gives the value o R to be of 1.48 nm.

5.4 Conclusion

The lifetimes are measured in the presence of absorption. The lifetimes of Eu^{3+} are measured as a function of the absorption introduced by the presence of Nd^{3+}. The fluorescence intensity and the lifetimes of Eu^{3+} decrease with the increase of Nd^{3+}. The dipole-dipole interaction is responsible for the energy transfer from Eu^{3+} to Nd^{3+}. The data has been analyzed using the theoretical equation derived by Schell *et al*. The analysis yielded the value of 1 nm for the parameter that is related to the radius of the cavity. In the second system, the fluorescence of Sm^{3+} is studied as a function of its concentration. Cross relaxation leads to concentration quenching. The fluorescence intensity increases upto 0.5mol% and then it decreases with the concentration. The lifetimes do not change for concentrations upto 0.5 mol% and decrease with the concentration for higher concentrations. The analysis using the theoretical equations gave the value for the parameter related to the radius of the cavity to be 1.48 nm.

5.5 References

1. A. J. Kenyon, Prog. in Quant. Electron. **26**, 225 (2002).
2. M. D. Shinn, W.A. Sibley, M.G. Drexhage and R. N. Brown, Phys. Rev. B **27**, 6635 (1983).
3. E. Nakazawa and S. Shinoya, J. Chem. Phys, **47**, 3211 (1967).
4. S. Parke and E. Cole, Phys. & Chem. glasses, **12**, 125 (1971).
5. J. C Joshi, B. C. Joshi, N. C. Pandey, R. Belwal and J. Joshi, J. Solid. Stat. Chem. **22**, 439 (1977).
6. B. C. Joshi and U. C. Pandey, J. Phys. Chem. Solids **50**, 599 (1989).
7. K. C. Sobha and K. J. Rao, J. Phys. Chem. Solids, **57**, 1263 (1996).
8. M. R. Brown and W. A. Shand, *Adv. Quant. Electron.* (Academic Press, New York, 1970).

9. M. F. Auzel, Compt. Rend. **262**, 1016 (1966).
10. V. V. Ovsyankin and P. P. Feofilov, Sov. Phys. JETP Lett. **3**, 317 (1966).
11. B. M. Antipenko, A.V. Dmitruk, V.S. Zubkova, G. O. Karapetyan and A. A. Mak, *Luminesence of Crystals, Molecules and Solutions* (Plenum Press, New York, 1973).
12. F. W. Ostermayer and L. G. Van Uitert, Phys. Rev. B **1**, 4208 (1970).
13. M. J. Weber J. Appl. Phys. **44**, 4058 (1973).
14. Z. J. Kiss and Duncan, Appl. Phys. Lett. **5**, 200 (1964).
15. W. Tian, R. S. Pandher and B. R. Reddy, J. Appl. Phys. **88**, 2191 (2000).
16. H. T. Amorim, M. V. D. Vermelho, A. S. Gouveia, F. C. Cassanjes, S. L. J. Riberiro and Y. Messaddeq, J. Solid Stat. Chem. **171**, 278 (2003).
17. C. H. Kam and S. Buddhudu, Solid. State Commun. **128**, 309 (2003).
18. D. L. Dexter, J. Chem. Phys. **21**, 836 (1953).
19. M. Inokuti and F. Hirayama, J. Chem. Phys. **43**, 1978 (1965).
20. S. M. Barnett, B. Hunter and R. Loudon, Phys. Rev. Lett. **68**, 3698 (1992).
21. S. M. Barnett, B. Hunter, R. Loudon and Matloob, J. Phys. B **29**, 3763 (1996).
22. S. Scheel, L. knoll, and D. G. Welsch, Phys. Rev. A **60,** 4094 (1999).
23. S. Shionoya and E. Nakazawa, App. Phys. Lett. 6, 117 (1965).
24. R. Balda, M. Sanz, J. Fernandez and J. M. F. Navarro, J. Opt. Soc. Am.B **17**, 1671 (2000).
25. P. R. Ehrmann, J. H. Campbell, T. I. Suratwala, J.S. Hayden, D. Krashkevich and K. Takeuchi, J. Non-Cryst. Solids, **263 &264**,251(2000).
26. N. Kraustsky and H.W. Moos, Phys. Rev. B **8**,1010 (1973).
27. C. Lurin, C. Parent, L. Flem and P. Hagenmuller,Phys. Chem.. Solids **46**,1083 (1985).
28. S. Murakami, M. Herren, M. Morita, S. Ohkubo and T. Suzuki, J. Lumin. **66&67**, 294 (1996).
29. R. Reisfeld and L. Boehm, J. Solid. Stat. Chem. **4**, 417 (1972).
30. J. D. Axe and P. F. Weller, J. Chem. Phys. **40**, 3066 (1964).
31. L. G. Van Uitert and L. F. Jhonson, J. Chem. Phys. **44**,3514 (1966).

32. R. Reisfeld, A. Bornstein and L. Boehm, J. Solid. Stat. Chem. **14**, 14 (1975).
33. V. Rodriguez, I. R. Martin, R. Alcala and R.Cases, J. Lumin.**55**, 23(1992).
34. P. Nachimuthu, R. Jagannathan, V. Nirmal Kumar and D. Narayana rao, J. Non Crys. Solids, **217**,215 (1997).
35. M. B. Saisudha and J. Ramakrishna, Phys. Rev. B **53**, 6168 (1996).
36. A. K. Agarwal, N. C. Lohani, T. C. Pant and K. C. Pant, J. Solid. State Chem. **54**, 219 (1984).

Chapter 6

Conclusion and Future Scope

In conclusion, the lifetimes of rare-earths doped in the binary glass system $PbO-B_2O_3$ have been studied to investigate the local field effects. The spontaneous lifetimes in a dielectric are determined by the refractive index and this enables one to tailor the lifetimes. The measurement of the lifetimes as function of the refractive index helps in determining which of the local field models to be used for the description of the spontaneous emission lifetimes in a dielectric. And the measurement of lifetimes in the presence of absorption enables one to estimate the radius of the cavity.

The lifetimes of Eu^{3+} and Tb^{3+} are measured as a function of the refractive index in order to investigate which local field model is appropriate for the description of the lifetimes in a dielectric. The contributions from the nonradiative decay, in these ions, can be neglected because of the large separation of the energy levels. The fluorescence measurements are performed as a function of the concentration of the dopants. The fluorescence intensity increases linearly with the concentration. The lifetimes remain unaffected by the concentration. The measured lifetimes are radiative, and the change in the lifetimes with refractive index is due to the local field effects. The lifetimes as a function of the refractive index are fitted to the equations for the two local field models. The real cavity model fits the data very well.

The lifetimes are measured in the presence of absorption. The lifetimes of Eu^{3+} are measured as a function of the absorption introduced by the presence of Nd^{3+}. The fluorescence intensity and the lifetimes of Eu^{3+} decrease with the increase of Nd^{3+}. The dipole-dipole interaction is responsible for the energy transfer from Eu^{3+} to Nd^{3+}. The data has been analyzed using the theoretical equation derived by Schell *et al*. The analysis yielded the value of 1 nm for the

parameter that is related to the radius of the cavity. In the second system, the fluorescence of Sm^{3+} is studied as a function of concentration. Cross-relaxation leads to quenching of fluorescence. The fluorescence intensity increases upto 0.5mol% and then it decreases with the concentration. The lifetimes do not change for concentrations upto 0.5 mol% and decrease with the concentration for higher concentrations. The analysis using the theoretical equations gave the value for the parameter related to the radius of the cavity to be 1.48 nm.

There is a tremendous scope for exciting work, both theoretical and experiments, in this direction. One of the interesting questions that need to be addressed is, aporori how to determine which local field model is relevant in a given situation. In this regard, the theoretical predictions based on the interstitial and substitutional impurities can be a good starting point. Another interesting question would be the case of cavity being non-spherical. It has been shown in this thesis that for the amorphous materials the real cavity model is appropriate for the description of the lifetimes. In order to investigate the question of the applicability of the virtual cavity, what are the kinds of the systems one needs to choose? There are many issues relating to the absorbing dielectric that are not yet addressed. Is the value of the radius obtained through the method described in this thesis absolute or does it needs to be scaled as noted by Scheel *et al?* And if it needs to be scaled – how does one obtain that scaling factor? In order to tailor the lifetimes, apart from the refractive index, one needs have the precise knowledge of the radius of the cavity? Does the value of this radius depend on the fluorescing ion or the dielectric or both? In order to answer these questions, more experiments in this direction involving different combinations of the rare-earths in different dielectric hosts would be of immense interest. In general, the coupling between the donor and acceptor can be multipolar in nature. In such a situation, what is the equation to be used for the description of lifetimes is an interesting problem, theoretically.

It is proposed to carry out many interesting experiments involving the rare-earths and rare-earth doped materials, by way of controlling the refractive

index and thereby controlling the local fields. Some of these experiments envisaged include the fabrication of the waveguides at telecommunication wavelength, hole burning and upconversion materials.

Work is under way to fabricate waveguides using the sol-gel method and as well as using the femto second channeling of the bulk glasses. The photosensitivity of glass enables devices to be fabricated by use of optical exposure techniques. One can fabricate waveguides by focusing and scanning light beams and one can prototype different structures simply by altering the scanning patterns. UV exposure techniques have been used extensively to fabricate glass waveguide devices. However, the types of material that can be processed with UV light are restricted and structures can be fabricated only on the surface because of the shallow penetration of UV light. The ability to fabricate three-dimensional structures would greatly increase integration densities as well as enable greater flexibility in device design and fabrication. Nonlinear ultrashort pulse material processing especially powerful for photonic devices in glass. Unlike UV photosensitive exposure techniques that involve linear absorption, material processing with high-intensity, near-infrared, ultrashort pulses involves nonlinear multiphoton absorption. The modification of material properties, such as refractive index change and cavity generation, is possible on a micrometer scale over a wide range of glass types without the need for linear absorption. The mechanisms of nonlinear laser fabrication in glass suggests that index changes are mediated by densification from local melting and rapid quenching after optical breakdown. The detailed physical nature of the process is under investigation by many groups. In contrast with linear absorption, nonlinear interactions allow subsurface processing inside bulk material. By tightly focusing the incident laser beam, one can produce highly localized structures with micrometer- scale dimensions in both the transverse and the longitudinal directions. One can write devices by simply scanning the incident beam over the substrate.

There is a great interest in the use of upconversion materials for efficient conversion of infrared radiation into visible light. This phenomenon has applications in many areas, such as upconversion lasing and two-photon fluorescence imaging. The operation of upconversion is also useful for the detection of infrared radiation by changing it to visible range where detectors are more efficient. Stepwise excited state absorption and energy transfer can be very efficient mechanisms for upconversion fluorescence in rare-earth-doped materials. The upconversion efficiency of rare-earth-doped materials at room temperature however has been found to very low, mainly due to quenching of emitting levels by nonradiative processes. By controlling the excited state dynamics with a judiciously selected local environment, one can reduce the quenching to produce efficient upconversion. The processing of materials to control the local environment of intermolecular interactions and local fields play an important role in producing rare-earth materials with highly efficient upconversion.

Eu^{3+} and Sm^{3+} glasses have attracted a great interest as a potential material for spectral hole burning applications. The phenomenon is not understood well. It would be interesting to see how the local environment is responsible for this phenomenon. All these studies should enable a better understanding of the interaction of the light with the matter and the role of the local environment.

Publications

In refereed journals:

1. "Measurement of local field effects of the host on the lifetimes of embedded emitters", **G. Manoj Kumar**, D. Narayana Rao, and G. S. Agarwal, Phys. Rev. Lett. **91,** 203903 (2003).
2. "Experimental studies of spontaneous emission from dopants in an absorbing dielectric", **G. Manoj Kumar**, D. Narayana Rao, and G. S. Agarwal, Opt. Lett. **30**, 732 (2005).
3. "Self-Quenching of Spontaneous Emission in Sm^{3+} Doped Lead-Borate Glass", **G. Manoj Kumar**, B. N. Shivakiran Bhaktha and D. Narayana Rao, Accepted for publication in Opt. Mater.
4. "A Review Article on the local field effects on the spontaneous emission probability" **G. Manoj Kumar**, D. Narayana Rao, Suneel Singh and G. S. Agarwal (Manuscript under preparation)

Conferences: (International / National)

1. "Unambiguous measurement of refractive index and thickness of thin film using transmission and reflection spectra", **G. Manoj Kumar** and D. Narayana Rao, Proc. National Laser Symposium-2000.
2. "Effect of composition on the covalency of Pr^{3+} doped B_2O_3-TeO_2 glass", **G. Manoj Kumar,** V. V. Ravikanth Kumar and D. Narayana Rao, Proc. National Laser Symposium-2001.
3. "The affect of the Local Field on the lifetimes of the Tb^{3+} doped in a bi nary glass system",**G. Manoj Kumar**, Sai Satosh Kumar, Suneel Singh and D. Narayana Rao, Presented at XXX Optical Society Of India Symposium on Optics and Opto-Electronics 2005.
4. "Energy Transfer from Eu^{3+} to Nd^{3+} in light of the Local Field Effects", **G. Manoj Kumar**, K. Koteswara Rao, M. Vittal and D. Narayana Rao, Proc. of National Laser Symposium-2005.
5. "Self quenching of Spontaneous emission in Sm^{3+} doped Lead Borate glass",**G. Manoj Kumar**, *B N Shivkiran Bhakta* and D. Narayana Rao, *presented* at the first workshop on rare-earths, May 2-5, held at University of Trento, Italy.
6. "Tailoring spontaneous emission lifetimes of rare - earths", *D. Narayana Rao*, **G. Manoj Kumar**, Suneel Singh and G. S. Agarwal, *Presented* at the International conference on 'Frontiers in Optics' held in September 2005.